Probing the role of environment and HI content in galaxy evolution: a multi-wavelength study of isolated and paired galaxies

Jamie Bok

January 2021

BKXJAM001

A thesis submitted in fulfilment for the
degree of Doctor of Philosophy
in
Astronomy

Department of Astronomy
UNIVERSITY OF CAPE TOWN

Supervisors: Prof. Thomas Jarrett, Dr Rosalind Skelton, A/Prof. Michelle Cluver, A/Prof. Sarah Blyth

Abstract

This thesis records a detailed examination of the impact of the merger-pair galaxy environment on both the neutral hydrogen (HI) and mid-infrared (MIR) properties of galaxies in the nearby Universe. Making use of publicly available HI profiles from the ALFALFA survey I construct the first statistically significant samples of close-pair galaxies (348 HI -optical and 282 HI - HI pairs), and contrast their HI content and star formation (SF) properties with a statistically significant HI sub-sample of isolated galaxies (544 galaxies) from the AMIGA project (Analysis of the interstellar Medium in Isolated GAlaxies; Verdes-Montenegro et al. (2005)). I present the first study of pairs using *WISE* data, and specifically examine their location on the MIR star-formation rate-stellar mass sequence (SFR-$M_\star$), or star-forming main sequence (SFMS), as a way to study how the close-pair environment influences the build up of galaxy stellar mass via SF. I also present the first MIR SFMS for isolated galaxies from the AMIGA catalogue to serve as the precedent for secular evolution. I derive an HI scaling relation for isolated galaxies using *WISE* stellar masses, and thereby establish a baseline predictor of HI content that can be used to assess the impact of environment on HI content when compared with samples of galaxies in different environments. I use this updated relation to determine the HI deficiency of both my paired and isolated galaxies, and invoke galaxy morphology (visual and MIR bulge-to-total ratios), the AMIGA isolation parameters η (local number density) and Q (tidal influence), star formation efficiency (SFE), and HI profile asymmetries to more closely inspect how these properties might be additionally driving the observed differences between the deficiency distributions of these two samples, as well as SFMS location. I also provide an analysis of the quantified HI profile asymmetries of my pair and isolated galaxy samples, exploring not only the prevalence of asymmetry in HI profiles, but also the possibility of using HI profile asymmetries to trace merger activity. I find enhanced profile asymmetries in my pair sample, and propose that high profile asymmetries may be used to infer merger activity/identify close galaxy pairs at high redshifts, in lieu of the typically used 2D HI maps we have for galaxies at low and intermediate redshifts, which are currently still limited. What my thesis shows is that although we have a plethora of data available (and coming), the key is to optimise how we use it, both in the questions we pose, and in understanding its limitations. We currently have large data-sets of HI profiles in the local Universe, which, when incorporated into a cohesive multi-

wavelength study, provide important clues as to how HI forms, influences, and is processed in galaxies. These are the studies informing our theories for galaxy evolution, providing the incentive for superior telescopes (e.g. SKA), and ultimately guiding our decision-making in how to proceed in our ongoing endeavour to understand our Universe.

Acknowledgements

I would like to express immense gratitude to my incredible team of supervisors, who have not only provided invaluable and expert professional guidance, but who have always treated me with kindness and compassion. Their support has been unwavering and sincere, and crucial to my success. Michelle, Tom, Ros, and Sarah- thank you for being stellar supervisors, and for always going above and beyond your professional duties to ensure my all round well-being. I one day hope to pay my privilege forward and provide such support to the next generation of astronomers. To my Spanish and British collaborators, Lourdes and Mike, thank you for being the absolute best introduction to collaboration for me. Your comments and input have always been so insightful, and it has been a true pleasure to have worked with you so closely.

For funding my PhD I thank the SAAO and Tom Jarrett. Your continued financial support has made my dream of becoming Dr. Bok possible! I am so incredibly grateful for all the opportunities and professional development you have afforded me through your financial assistance. To Roslyn Daniels at UCT, Linda Tobin and Valencia Cloete at the SAAO- thank you for taking such good care of me at your respective institutes. Your assistance throughout my postgraduate career has been invaluable, and I so appreciate your genuinely kind and helpful demeanors, which have always made it easy for me to reach out to you.

A special thank you goes to Naomi, who has been undeniably crucial to the advancement of my academic career right from the beginning. I look back fondly on the many, many, late nights we spent working together on assignments and studying for tests and exams during our undergraduate, honours, and masters programs. And even though you chose stars to explore the evolution of our Universe when I chose to galaxies, my PhD success has still been inextricably linked to your professional, and to a greater extent, personal friendship. Thank you.

To Mom and Dad, thank you for prioritising my education right from the beginning, and providing the best possible foundation for me to build a life that I am truly happy in. To my son, Sam, my primary anti-collaborator, thank you for sleeping occasionally. I will never forget the mercy you showed me by sometimes sleeping for 45 minutes straight. My love and gratitude

for you is infinite my darling boy, thank you for summoning the best of me.

And finally, to my best friend, partner, and father to my son, Arnold- I don't even know how to quantify the profoundly positive impact you have had in shaping the human being I am today. For never giving up on me, for always seeing the best in me, for your patience, tolerance, forgiveness, and your exemplary example for how to navigate life with integrity (for me and Sam), I thank you from the bottom of my heart.

Declaration of Authorship

The work presented in this thesis is my own, conducted under the supervision of Prof. Thomas Jarrett, Dr. Rosalind Skelton, A/Prof. Michelle Cluver, A/Prof. Sarah Blyth, with collaborative contributions from Michael Gordon Jones, Lourdes Verdes-Montenegro, and Ed Elson. This thesis contains research that has been published or submitted for publication:

Chapter 2: J. Bok, S.-L. Blyth, D. G. Gilbank, and E. C. Elson, "*Enhanced HI profile asymmetries in close galaxy pairs*", 2019, MNRAS 484, 582-594.
I am the primary author and researcher of this chapter, which has been published in the Monthly Notices of the Royal Astronomical Society Journal. I wrote all sections of the paper excluding a paragraph written by E. C. Elson, who estimated the relative amount of contaminant flux in the HI profiles using simulations, and presented his findings in the discussion.

Chapter 3: J. Bok, R.E. Skelton, M.E. Cluver, T.H. Jarrett, M.G. Jones, and L. Verdes-Montenegro, "*HI study of isolated and pair galaxies: the MIR SFR-Mstar sequence*", 2020, MNRAS 499, 3193–3213.
This chapter has also been published in the Monthly Notices of the Royal Astronomical Society Journal, and makes use of WISE data provided by T.H. Jarrett, and an HI scaling relation provided by M.G. Jones. Excluding 2 paragraphs written by T.H. Jarrett and M.G. Jones, and appendices A and B, I wrote all sections of this paper, for which I am first author and primary researcher.

Chapter 4: J. Bok, M.E. Cluver, T.H. Jarrett, R.E. Skelton, M.G. Jones, and L. Verdes-Montenegro, "*Decoding HI deficiency distribution of isolated and paired galaxies*"
This chapter will be submitted to the Monthly Notices of the Royal Astronomical Society Journal with myself as first author, and primary researcher. I make use of AMIGA isolation parameters (η and Q) provided by M.G. Jones, and wrote all sections of the paper myself.

Each of these chapters contain all the necessary information and can be read independently.

I confirm that I have been granted permission by the University of Cape Town's Doctoral Degrees Board to include the following publication(s) in my PhD thesis, and where co-authorships are involved, my co-authors have agreed that I may include the publication(s):

Chapter 2: J. Bok, S.-L. Blyth, D. G. Gilbank, and E. C. Elson, "Enhanced HI profile asymmetries in close galaxy pairs", 2019, MNRAS 484, 582-594.

Chapter 3: J. Bok, R.E. Skelton, M.E. Cluver, T.H. Jarrett, M.G. Jones, and L. Verdes-Montenegro, "HI study of isolated and pair galaxies: the MIR SFR-Mstar sequence", 2020, MNRAS 499, 3193–3213.

Chapter 4: J. Bok, M.E. Cluver, T.H. Jarrett, R.E. Skelton, M.G. Jones, and L. Verdes-Montenegro, "*Decoding the HI deficiency distribution of isolated and paired galaxies*", due to be submitted to MNRAS.

SIGNATURE: Signed by candidate **DATE:** 18 MARCH 2021

STUDENT NAME: Jamie Bok **STUDENT NUMBER:** BKXJAM001

Plagiarism Declaration

I, Jamie Bok, know the meaning of plagiarism and declare that all of the work in the document, save for that which is properly acknowledged, is my own.

Contents

List of Figures

List of Tables

Chapter 1

Introduction

The origin story for the remarkable diversity of galaxy properties is an ever-evolving, in-progress, global effort, with thousands of astronomers across the world contributing their insights. Piece by piece the skies are being mapped, and moments in time probed. With each new sample our understanding of how the Universe works advances. We have come to realise that galaxy environment is an important piece of the puzzle, with numerous galaxy properties (colour, morphology, star formation, for example) trending with density of environment (e.g., galaxies per Mpc^3) according to observations across the electromagnetic spectrum. Simulations ever advancing in sophistication suggest the links between galaxy environment and galaxy properties are causal, and offer plausible pathways to observations (Mihos & Hernquist 1996, Abadi et al. 1999, Borgani & Kravtsov 2011, Steinhauser et al. 2016, Hani et al. 2018, Moreno et al. 2020). Bearing in mind that stars are birthed within molecular clouds, more recently, observations and simulations have pointed to neutral hydrogen (HI) as playing a vital role in both the formation and evolution of galaxies as the primary raw fuel for star formation (Acosta-Pulido et al. 2015). Observations of HI have largely been limited to the low redshift Universe up until relatively recently. However, what we have uncovered about HI in the Local Universe has provided the necessary incentive to build the next generation of radio telescopes.

Major advances in the observing capability of HI are underway as the Square Kilometer Array (SKA) project comes to fruition. Soon we will be able to probe HI out to high redshifts ($z > \sim 1$), and with greatly improved resolution at intermediate and low redshifts, with surveys such as WALLABY (Koribalski et al. 2020), DINGO (Rhee 2020), LADUMA (Holwerda et al. 2011), MIGHTEE (Maddox et al. 2021), and MHONGOOSE (de Blok et al. 2017). With SKA1-MID we will be able to resolve individual clouds of HI in the local Universe, and probe the intergalactic medium (IGM)/intragroup medium in unprecedented detail. Our burning questions for how galaxies accrete and deplete their gas supplies (processes fundamental to galaxy evolution)

are expected to be observationally addressed. In preparation for the large volumes of incoming data, the work of astronomers has been to maximize the utility of data readily available to inform our next steps.

This thesis is a record of my personal and original contribution to the communal library of Astronomy, and documents my journey from conducting pilot SKA science with integrated HI profile asymmetries, to exploring galaxy evolution on the *WISE* mid-infrared (MIR) galaxy star-forming main sequence (SFMS) as a function of both HI content and local environment. With isolated galaxies serving as my baseline for secular evolution, I investigate first the impact of a single nearby neighbour on HI content, namely the close pair galaxy environment (predicted by simulations to significantly impact the gas content in galaxies), and subsequently extend my analysis to include more densely populated environments.

In chapter 2, I present an investigation into the viability of using asymmetries measured in HI profiles to trace merger activity by contrasting the HI profile asymmetry distributions of a close pair galaxy sample and a sample of isolated galaxies (both drawn from the ALFALFA α_{40} catalogue). In chapter 3 I revise my close pair sample to comprise specifically of gas-rich pairs from the α_{70} catalogue, and draw from the HI science sample of Jones et al. (2018), an HI subset of the AMIGA isolated galaxy sample (Analysis of the interstellar Medium of Isolated GAlaxies; Verdes-Montenegro et al. (2005)) to serve as my control sample of isolated galaxies (see §1.5 for details of the AMIGA project). I contrast these samples on the MIR SFMS using *WISE* stellar masses and SFRs, and study their HI properties (gas fraction and HI deficiency derived from their integrated HI profile masses) as a third dimension on the SFMS. In addition, I present an updated HI scaling relation for AMIGA galaxies to provide a baseline predictor of HI content in the absence of interaction, and use this relation to calculate the HI deficiencies of my sample galaxies. I study the scatter of my paired and isolated galaxies as a function of both gas fraction and HI deficiency, and propose 'quenching' scenarios for the sub-populations of quiescent/low star-forming galaxies in my pair sample by referring to their gas properties and MIR bulge-to-total (B/T) ratios (a proxy for morphology).

In chapter 4 I further explore potential pathways to my findings in chapter 3 by quantifying the close pair environment using the AMIGA isolation parameters η and Q, conducting a visual galaxy morphology classification, and computing star formation efficiencies (SFEs). I also present the HI profile asymmetries of the chapter 3 pair sample as a function of η and Q, as well as HI deficiency. Ultimately this thesis demonstrates that publicly and readily available data in the optical (SDSS; Abazajian et al. (2009)), radio (ALFALFA; Giovanelli et al. (2005)), and mid-infrared (*WISE*; Wright et al. (2010)), when incorporated into a cohesive multi-wavelength

study, has enormous utility in characterizing the nature of our Universe. In this introductory chapter I present the setting in which HI science is proving crucial to our understanding of how galaxies form and evolve, as well as the significant impact galaxy environment (isolated, paired, grouped, cluster) has on the HI properties of galaxies, as the context for my published works in chapters 2, 3, and in-progress publication in chapter 4.

1.1 Neutral Atomic Hydrogen: Revealing Reservoirs and their Removal

Since elemental hydrogen is the reservoir from which molecular hydrogen manifests, neutral hydrogen (HI) can be thought of as the raw fuel for star formation (SF), and is thus crucial to both galaxy formation, and evolution. Identifying and understanding processes that both supply and remove HI to and from galaxies is accordingly essential to the development of a complete theory for galaxy evolution. We observe HI in the radio regime as the 21cm emission that arises from the electron in the atom spontaneously flipping its spin from being aligned with the proton (a slightly higher energy state achieved via collisions) to anti-aligned. The return to the anti-aligned ground state configuration releases energy as a photon with a wavelength of 21cm, and occurs only roughly every 10 million years. The low density environment of the interstellar medium (ISM) means collisional excitations are rare, this together with the approximately 10 million year wait for the electron to spontaneously flip back to the anti-aligned configuration suggests a really low probability of detection. Fortunately the ISM is incredibly abundant with HI, thus at any given moment a fraction of its constituent HI is in an excited state, and detection is feasible.

The 21cm emission HI produces is, however, intrinsically faint, and our ability to detect it beyond $z \sim 0.2$ has therefore been limited until recently. That being said, single-dish (e.g. ALFALFA (Giovanelli et al. 2005), HIPASS (Barnes et al. 2001)) and inteferometric spectro-imaging (e.g. WHISP (van der Hulst et al. 2001), THINGS (Walter et al. 2008), LVHIS (Koribalski et al. 2018)) HI studies of low redshift galaxies have made significant progress in characterizing the nature of HI in the local Universe, and have established that galaxy environment plays a significant role in both depleting galaxies of their HI content, as well as replenishing their gas reservoirs. Both the cluster and group environments have been associated with various gas-removal mechanisms (see §1.2 for details), while the close-pair/merger environment appears to facilitate an influx of gas (see §1.3).

At intermediate to high redshifts (out to z$\sim$ 6), in lieu of 21cm observations, the HI content of disks have been probed using deep optical and ultra-violet observations of damped

Lyman α systems (DLAs) (Zwaan et al. 2005, Prochaska & Wolfe 2009). Such studies reveal little evolution in the integrated HI mass densities ($\rho_{\rm HI}$) of HI disks for the past $\sim$ 10 Gyr (see Figure 1.1 from Prochaska & Wolfe (2009)).

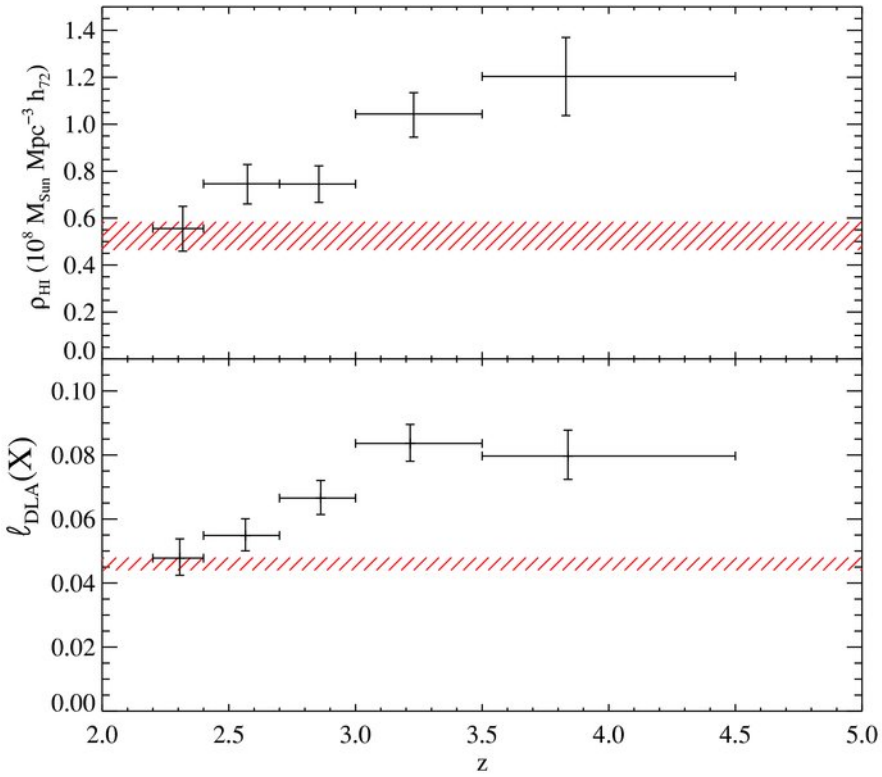

Figure 1.1: In the top panel we see the comoving HI mass density, ρHI , for galaxies with $z > 2$ assuming a ΛCDM cosmology, with the z $\sim$ 0 estimate of ρHI from 21cm surveys shown by the hatched red band. In the bottom panel we see the line density of DLAs per comoving absorption length dX. Both the covering fraction and HI mass densities decrease by a factor of 2 from redshift $\approx$ 4 to 2, where they both reach the present day value (indicated by the red band). Together these results suggest that there has been little evolution in the HI content of galaxies in the past 10 Gyr. Image credit: Prochaska & Wolfe (2009).

Similarly, SFRs within the solar neighbourhood have also been shown to be roughly constant for the past $\sim$ 10 Gyr (Twarog 1980, Binney et al. 2000). Together these observations suggest that while HI is an essential prerequisite for SF, it is insufficient in explaining the global SFR, implying the sustained SF in galaxies is driven by accretion (Sancisi et al. 2008, Prochaska & Wolfe 2009). The potential to observe accretion, however, is once again only feasible in the nearby Universe. Binney (2000) present compelling evidence for accretion in the Milky Way, and since our galaxy is extremely typical, their inference that accretion is an important phenomenon throughout our Universe is reasonable. Sancisi et al. (2008) present evidence of accretion in local galaxies, and estimate a mean 'visible' cold gas accretion rate of $0.2 M_{\odot} yr^{-1}$ by

considering observations of gas-rich dwarf companions, minor mergers and interactions (tidal tails), and extra-planar gas/cloud complexes around galaxies as direct evidence of accretion. The additional infall of large amounts of gas from the IGM is thus required to reconcile the 'visible' accretion rate with typical SFRs of $\sim 1 M_{\odot} yr^{-1}$ (Sancisi et al. 2008, Prochaska & Wolfe 2009). The galactic fountain model (Fraternali 2017), in which the continuous circulation of gas from the galactic disk into the halo is fuelled by stellar feedback (winds), predicts accretion of the order what is required to sustain star-formation (SF). Observing the diffuse HI (cloud complexes, tidal tails, swept back disks) is currently only achievable for a few nearby targets due to the costly observing requirements (high resolution, time consuming). For the same integration time and angular resolution, SKA1-MID will reach column density limits 3 times deeper than what is currently possible, probing IGM column densities for the first time in search of accretion, and resolving individual HI clouds in the Local Volume (Popping et al. 2015).

1.2 HI depletion in galaxy groups and clusters

Galaxies in clusters are well-known to be increasingly deficient in HI as they approach the cluster center (Chamaraux et al. 1980, Giovanelli & Haynes 1985, Solanes et al. 2001, Chung et al. 2009, Dénes et al. 2014), with their HI morphologies evolving from large extended disks on the cluster outskirts, to HI disks that are smaller than their optical counterparts near the center, and with tidal tails commonly observed at intermediate distances from the core (Chung et al. 2009) (see Figure 1.2), suggestive of gas removal via ram-pressure stripping (Gunn & Gott 1972). Gas removal via harassment (fast, minor gravitational encounters between galaxies) (Moore et al. 1998), galaxies tidally interacting with the intra-cluster potential (Moore et al. 1999), and starvation (the halting of gas accretion; Larson et al. (1980), Peng et al. (2015)) have also been implicated in the cluster environment. HI galaxy group studies show the group environment to have a similar depleting impact on HI content (Verdes-Montenegro et al. 2001, Kilborn et al. 2009, Cluver et al. 2011, Hess & Wilcots 2013), with their centers becoming increasingly HI deficient as group membership increases (Hess & Wilcots 2013). The group environment is now commonly pointed to as place where galaxies are transformed from gas-rich to gas poor, i.e. are "pre-processed" before entering clusters (Balogh et al. 1997, Hess & Wilcots 2013). The mechanisms pointed to as responsible for the depletion of gas in group galaxies are SF (HI reservoirs become depleted as gas is converted into stars), tidal stripping (Mihos et al. 2005, Kilborn et al. 2009, Borthakur et al. 2010), viscous stripping (in compact groups) (Nulsen 1982, Verdes-Montenegro et al. 2001, Cluver et al. 2011), harassment (Moore et al. 1998), starvation (Peng et al. 2015), ram pressure stripping (Gunn & Gott 1972, Westmeier et al. 2011), although X-ray evidence suggests that ram pressure stripping is not a dominant gas-removal mechanism in group environments (e.g. Rasmussen et al. (2008)). Cortese et al. (2021), in their review

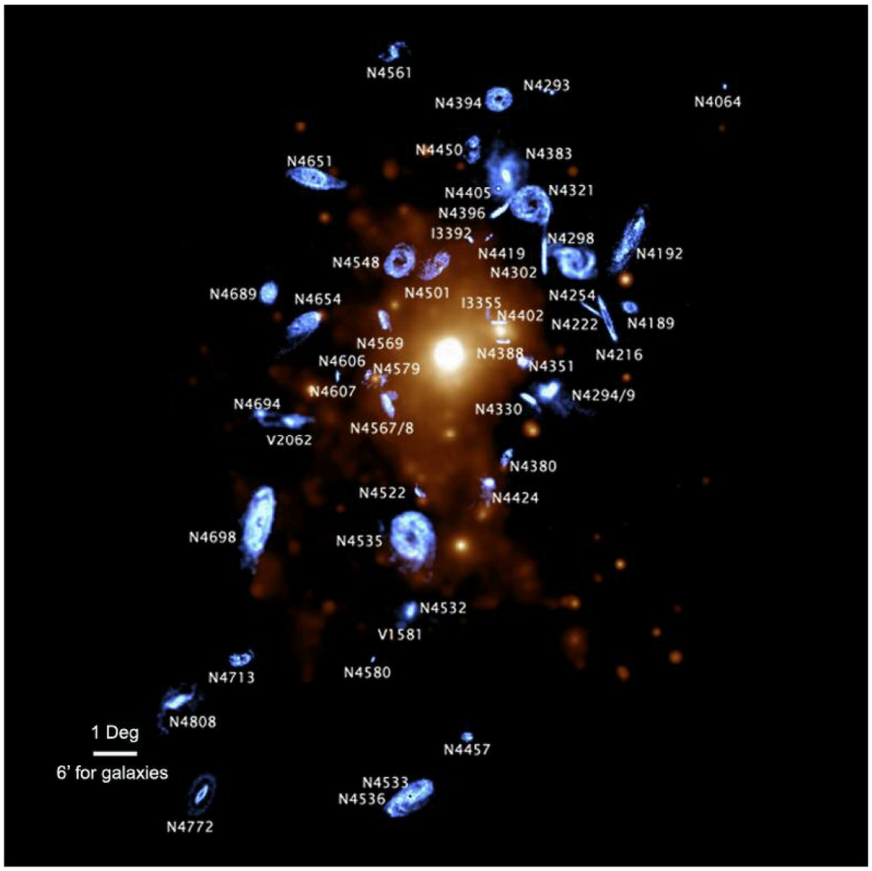

Figure 1.2: VLA HI images of 53 late-type Virgo spiral galaxies from the VIVA Survey (VLA Imaging of Virgo in Atomic gas), located at their proper positions in the Virgo cluster, however magnified by a factor of 10 to show the details of their HI distributions. This figure highlights the non-uniformity of the mass distribution in Virgo. Image credit: Chung et al. (2009).

of cold-gas stripping as a quenching mechanism in satellite galaxies, present a complex picture in which various gas removal mechanisms can be at play throughout the life cycle of galaxy, contributing to quenching on different timescales. For example, a first pericenter encounter may strip a galaxy of some of its gas content, and radically reduce SF, but won't necessarily lead to full quenching. Subsequent processes such as SF (gas consumption) and feedback have important roles to play in ultimately quenching galaxies in such scenarios (Cortese et al. 2021). The observational evidence required to disentangle the various gas-removal mechanisms is costly to acquire, and not currently feasible for large samples of groups. An example of one such deep HI study by Hess et al. (2017) combines data from the Karoo Array Telescope (KAT-7), Westerbork Synthesis Radio Telescope (WSRT), and Arecibo Legacy Fast ALFA survey (ALFALFA) to probe the HI content of the Hickson Compact Group, HCG44, with enhanced column density sensitivity. They reveal a significantly extended HI tail compared to what was previously observed with WSRT (Serra et al. 2013), and substantial additional HI beyond the tail. With their wide field of view and KAT-7 resolution they were able to postulate its origins, as well as its fate. See Figure 1.3 for the combined (KAT-7, WSRT, and ALFALFA) HI total intensity map of HCG44, with the the extended tail visible in the top right corner. This study provides valuable insight into what we are likely to observe in large samples of groups with future MeerKAT and ASKAP surveys.

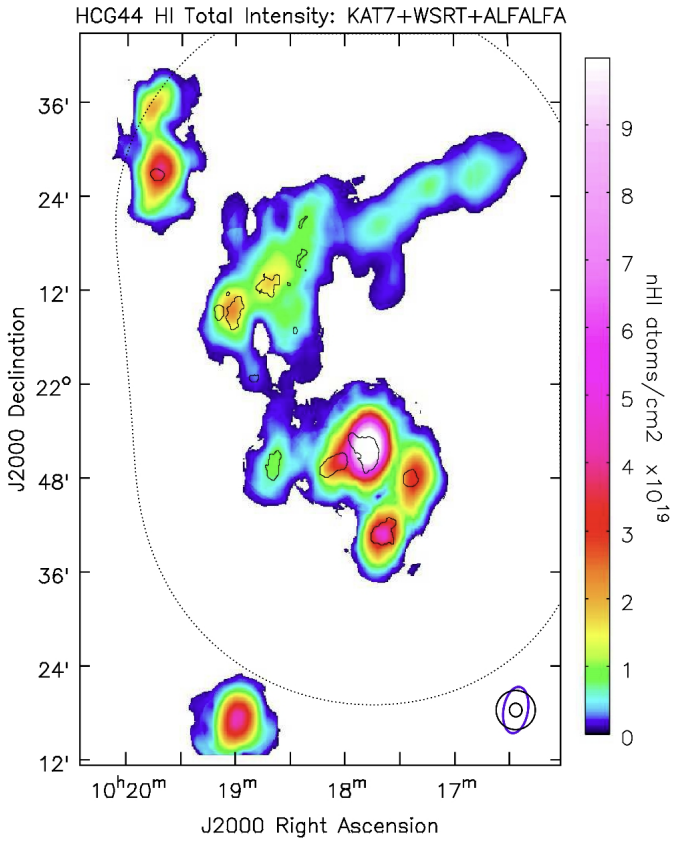

Figure 1.3: The HI total intensity map of HCG44 using combined KAT-7, ALFALFA, and WSRT observations, revealing an extended tail spanning 450 kpc (compared to the 300 kpc extent derived from HIPASS images (Serra et al. 2013)), as well as its breadth, mass, column density, and velocity dispersion, which HIPASS was unable to resolve. Image credit: Hess et al. (2017)

1.3 The galaxy pair environment: enhancing HI content, and disrupting symmetry

The galaxy pair environment, in contrast to the more densely populated group and cluster environments, has been shown to enhance HI reservoirs in galaxies. Observations of merging galaxies by Ellison et al. (2018) showed the merger components to be gas-rich on average compared to control samples, which simulations demonstrate is a direct result of the merger process. A zoom-in simulation of a major galaxy merger by Hani et al. (2018) showed that the merger process can re-distribute material into the circumgalactic medium (CGM), and increase total hydrogen covering factors by a factor of 1-1.25 for up to $\sim$ 3 Gyr. Parsec-scale galaxy major merger simulations implemented by Moreno et al. (2020) demonstrated that close galaxy encounters can elevate both HI and H_2 gas reserves, and thereby enhance SF in both pair members. A direct link between spiral-spiral merging pairs and enhanced SF activity has been shown in the work of Xu et al. (2010) and Cao et al. (2016). A re-distribution of gas as tidal tails and central molecular gas concentrations is routinely observed in merging galaxies (Hibbard & Yun 1999, Tacconi et al. 1999, Koribalski & Dickey 2004, Yamashita et al. 2017). Such observations have been attributed by simulations to the gravitational interplay of merging galaxies, which is shown to generate internal asymmetries and instabilities that funnel gas inwards (Mihos & Hernquist 1996), and re-distribute gas in the outer disk regions (Hani et al. 2018). Reichard et al. (2008) describe the merger process as capable of inducing states of non-equilibrium in both the stellar and dark matter components of galaxies, resulting in morphological departures from symmetry. Observationally the link between disturbed morphologies and asymmetries in both the stellar and gas components of galaxies and merger activity is well-known (Jog & Combes 2009), and such asymmetries are now frequently used to infer merger activity. Figure 1.4 illustrates the merger process and its impact on galaxy morphology/symmetry using 6 real examples of merging galaxies at various stages in the merger process observed in the optical regime using the Hubble telescope. We see the early signs of interaction in panel 1, a bridge of matter (dust and gas) being coaxed out by the gravitational interplay of the approaching galaxies, the emergence of tidal tails in panels 2 and 3, and increasingly disturbed/asymmetric morphologies in panels 4 to 6 representing the end stages of the merger process.

Comparing asymmetries traced in the optical with asymmetries traced by HI, as in the work of Kornreich et al. (2000), showed that asymmetry is not only quantitatively larger and more frequent in HI than in stars (Bournaud et al. 2005), but also that the amplitude of asymmetry increases with galaxy radius (Reichard et al. 2008). This, together with the fact that HI is diffuse and typically extends out to much larger radii than the stellar component of a galaxy (see Figure 1.5 from Jarrett et al. (2013) for a relative size comparison of the HI and optical

Figure 1.4: The merger sequence as represented by galaxies at various stages in the merger process, from the early (close pair) stage in panel 1, to the final merger remnant stage in panel 6. We see the emergence and growth of tidal tails of dust and gas arising from the gravitational interplay between merging galaxies as the merger process progresses in panels 2 and 3. As the cores of the merging galaxies get closer and closer (panel 4), their gas and dust clouds become greatly accelerated by the gravitational pull of matter in all directions. In the late stages of the merger sequence (panel 5), dust and gas are funnelled into the central regions, and fuel bursts of star formation. These dust clouds continue to grow, heat up, and radiate in the infrared to become some of the brightest infrared objects in the sky. The increasingly disturbed/asymmetric morphologies associated with the advanced and late stages of the merger process are presented in panels 4-6. Credit:NASA, ESA, the Hubble Heritage Team (STScI/AURA)-ESA/Hubble Collaboration and A. Evans (University of Virginia, Charlottesville/NRAO/Stony Brook University), K. Noll (STScI), and J. Westphal (Caltech)

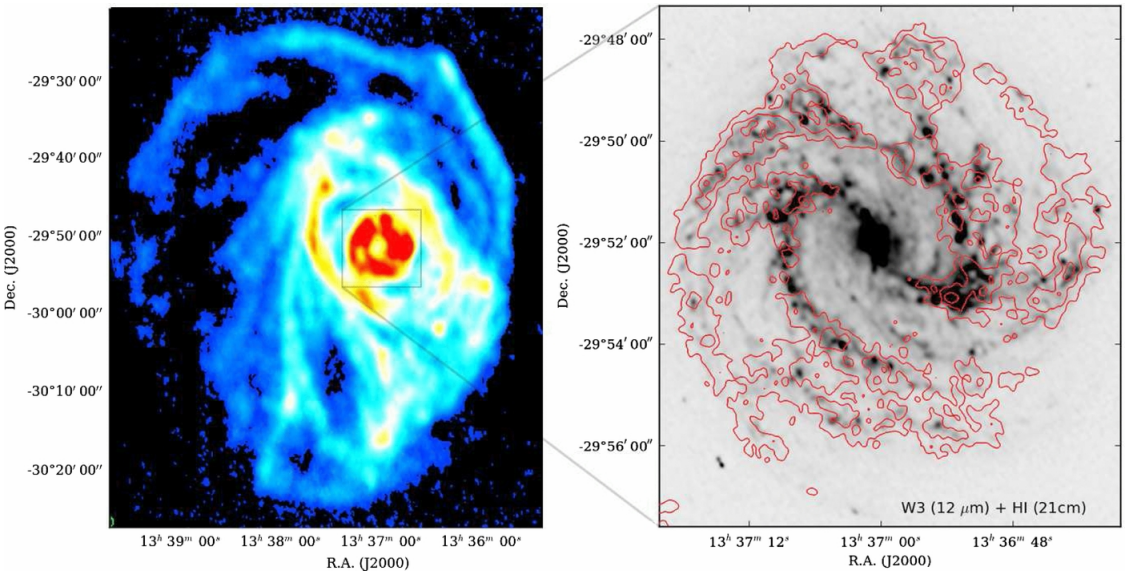

Figure 1.5: Left: Neutral hydrogen distribution (moment-0 map) of M83 constructed using Parkes and ATCA data. Right: ATCA high-resolution HI moment-0 map (red contours) overlaid onto the WISE 12 μm map (gray scale, log-stretch) of the central disk (denoted with a gray box in the left panel). Credit: Jarrett et al. (2013)

components of M83 in the left and right panels respectively) renders HI highly susceptible to external influence, often responding to and reflecting fluctuations in the galaxy environment while the stellar disk remains unperturbed. This is nicely demonstrated when we compare optical (Figure 1.6a) and HI (Figure 1.6b) images of the galaxy group M81. The HI distribution of M81 shows the group members to be clearly interacting, while almost no signs of interaction are observed when viewing the stellar light distribution alone. Asymmetries in spatial HI maps are therefore highly effective at tracing merger activity (Kornreich et al. 2002, Holwerda et al. 2011, Giese et al. 2016).

Asymmetries in HI profiles are also frequently observed (Richter & Sancisi 1994, Haynes et al. 1998, Matthews et al. 1998, Espada et al. 2011, Bok et al. 2019). The 1D global HI profile has a shape primarily dictated by galaxy kinematics, and carries with it information both about a galaxy's velocity field, as well as the distribution of HI within the galaxy. The ordered motions within a galaxy disk, where radial velocities tend to cluster, are responsible for the characteristic double-horn signature seen in HI velocity profiles. HI profiles are therefore expected to be symmetric about the systemic velocity for an unperturbed disk, with deviations from symmetry considered potential consequences of merger activity (e.g. non-circular motions, tidal tails, and distortions in the HI mass distribution), asymmetric gas accretion, or an offset of the stellar disc in a halo potential (van Eymeren et al. 2011). The frequency of these observed departures from symmetry has been the topic of investigation in a number of HI profile studies,

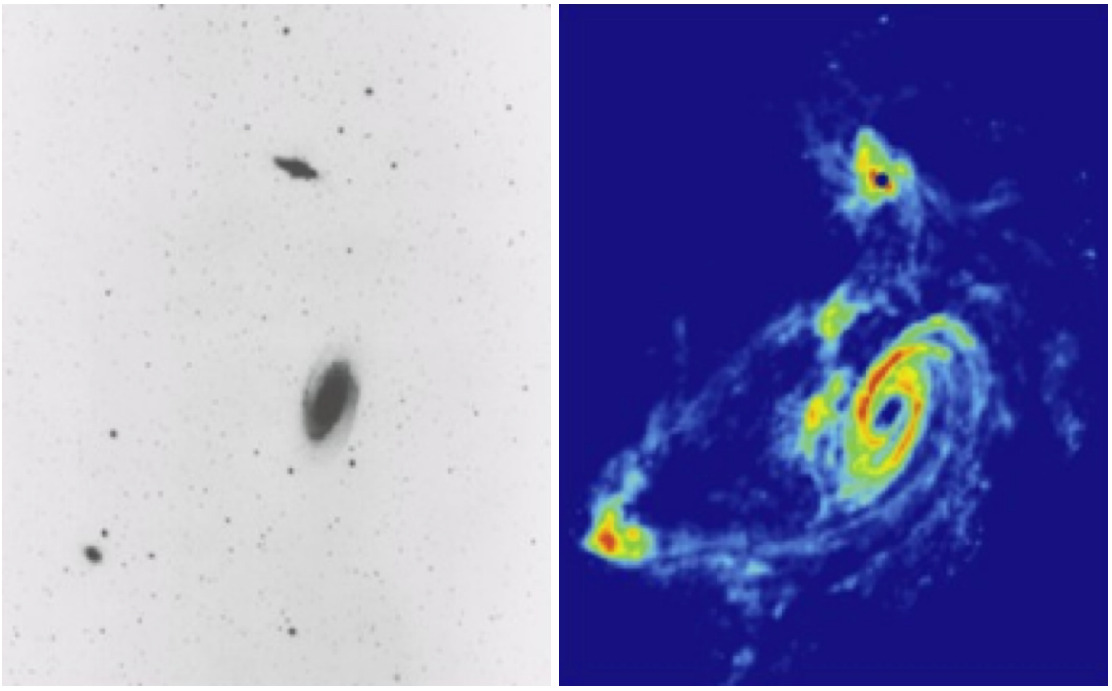

(a) Stellar light distribution of M81. (b) HI distribution of M81.

Figure 1.6: Comparison of the optical (left) and HI (right) distributions of the galaxy group, M81. Image credit: NRAO

where the degree of asymmetry has been assessed both qualitatively and quantitatively (Haynes et al. 1998, Matthews et al. 1998, Espada et al. 2011). Richter & Sancisi (1994) qualitatively measured the HI profile asymmetry on a sample of $\sim$ 1700 galaxies from various single dish HI surveys using a by eye visual classification scheme. This sample was comprised primarily of field galaxies so as to minimize the chance of the cluster environment playing a role in producing profile asymmetries. A lower limit of 50 percent of the sample was found to exhibit significant profile asymmetries, suggesting that asymmetry might well be the rule rather than the exception. Richter & Sancisi (1994) further quantified the HI profile asymmetries of their sample using Tifft & Huchtmeier (1990)'s HI flux ratio between the lower and upper velocity halves of the global HI spectrum, and found the qualitative and quantitative asymmetry measures to be highly congruent. Using a similar HI flux ratio, Haynes et al. (1998) quantified the HI profile asymmetry for an isolated sample of 104 high signal-to-noise (SNR) HI profiles obtained using the Greenbank 43m telescope. The results of the study showed $\sim$ 50 percent of the sample to have significant HI profile asymmetries (in good agreement with previous work), which the authors attribute to distortions in the HI distribution, non-circular motions, and possible confusion with unidentified companions within the telescope beam. A more recent study by Espada et al. (2011), specifically focussed on HI profile asymmetries of galaxies

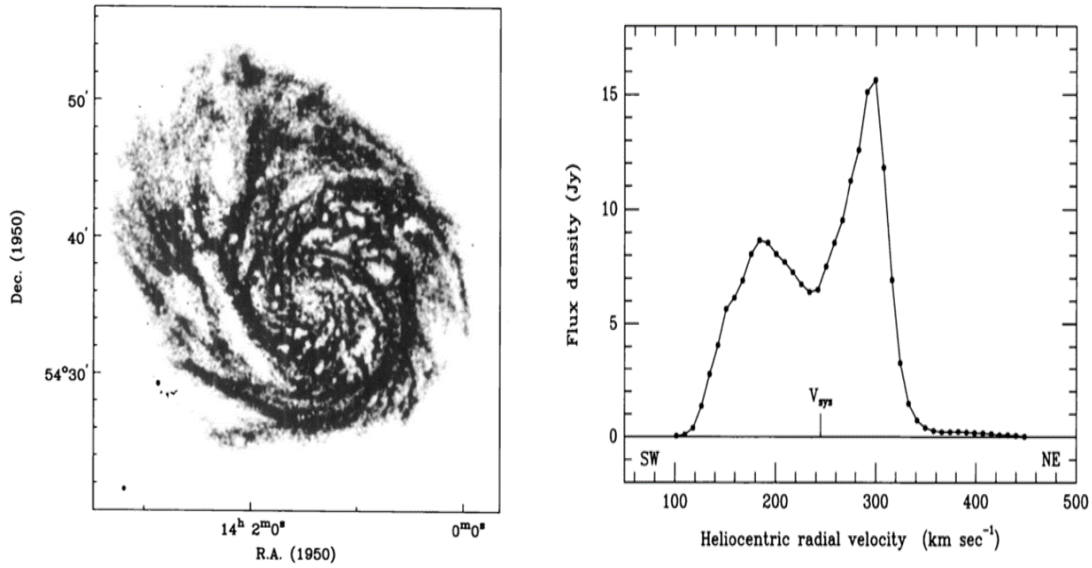

(a) HI map of M101. (b) Global HI profile of M101.

Figure 1.7: Asymmetric HI distribution of M101 (left) with its correspondingly asymmetric HI profile (right). Image credits: Richter & Sancisi (1994)

carefully selected to be isolated. Their study forms part of the AMIGA project (Analysis of the interstellar Medium in Isolated GAlaxies; Verdes-Montenegro et al. (2005)), whose aim is to disentangle those galaxy properties (morphological and structural) which are due to internal secular evolution from those which arise from interactions within the galaxy environment. HI profile asymmetries were quantified for a sample of ~166 high SNR HI profiles (the HI refined sub-sample) using the standard HI flux ratio. They describe the resulting asymmetry distribution as following a Gaussian model with width $\sigma = 0.13$ (corresponding to a flux ratio of 1.26 at the 2σ level). Furthermore, Richter & Sancisi (1994) found that HI profile asymmetries are often accompanied by an asymmetry in the corresponding HI gas distributions, supporting the idea that asymmetries in HI profiles are possibly the result of galaxy-galaxy interaction. In figure 1.7a we see the asymmetric distribution of HI in the HI map of the galaxy M101, and its correspondingly asymmetric HI profile in figure 1.7b (both graphics are from Richter & Sancisi (1994)) attributed to the dynamical interaction of several galaxies in the M101 group (e.g., NGC5204). M101 is another example where the HI disk far exceeds the size of its SF disk.

In chapter 2 of this thesis I present an investigation into the feasibility of using asymmetries in HI profiles from the ALFALFA α40 catalogue (Haynes et al. 2011) to trace merger activity. I quantify the asymmetry of close pairs of galaxies and isolated galaxies in the α40 catalogue (see sections 2.3.1 and 2.3.2 in chapter 2 for details of the pair and isolated selection criteria),

as a ratio of flux, A_c, (similar to Haynes et al. (1998) and Espada et al. (2011)) between the two velocity horns using v_{helio} from the α40 catalogue to define the centre of the profile. In defining the profile edges I use the w_{50} width given in the α40 catalogue, and I interpolate the profile to retrieve the velocity at the 50 percent level. The typical flux values at v_{20} are similar to the noise rms of the profiles, for this reason I use w_{50} over w_{20} to determine the profile edges, as it is more reliably determined. A_c is calculated as:

$$A_{\frac{l}{h}} = \frac{\int_{v_{\rm low}}^{v_{\rm helio}} I_\nu dv}{\int_{v_{\rm helio}}^{v_{\rm high}} I\nu dv} \tag{1.1}$$

and

$$A_c = A_{\frac{l}{h}} \text{ if } \mathrm{A}_{\frac{\mathrm{l}}{\mathrm{h}}} > 1 \tag{1.2}$$

$$= A_{\frac{h}{l}} \text{ if } \mathrm{A}_{\frac{\mathrm{l}}{\mathrm{h}}} < 1 \tag{1.3}$$

Here $v_{\rm helio}$ corresponds to the the galaxy's heliocentric velocity, and $v_{\rm low}$ and $v_{\rm high}$ the velocity of the galaxy at the 50 percent flux level to the left and right of $v_{\rm helio}$ respectively. Figure 2.4 provides a graphical representation of how A_c is determined. I use a Monte-Carlo approach (described in §2.4.1 in Chapter 2) to estimate the uncertainty associated with the A_c measurement.

This chapter serves as a pilot project for the SKA LADUMA survey (Holwerda et al. 2011), which will provide HI profiles for galaxies at high redshifts ($z >\sim 1$). At such distances HI maps illustrating the spatial distribution of the gas in galaxies are not feasible, sources will be largely unresolved. Here the integrated HI profile will be the only HI data product with which to probe HI. It is therefore important to maximize the utility of the HI profile in communicating information about galaxies in the early Universe, specifically their environments, such that we can test galaxy evolution models over cosmic time.

1.4 HI and its in role star formation and quenching

As the raw fuel for SF, HI is naturally crucial not only to the formation of galaxies, but also to their continued SF. Links between HI and SF potential have been established both observationally, as well as predicted by simulations. (Ellison et al. 2010, Xu et al. 2010, Cochrane & Best 2018, Pearson et al. 2019, Moon et al. 2019, Moreno et al. 2020, Bok et al. 2020). The 'galaxy main sequence' (GMS), or 'star-forming main sequence' (SFMS), illustrates the relationship

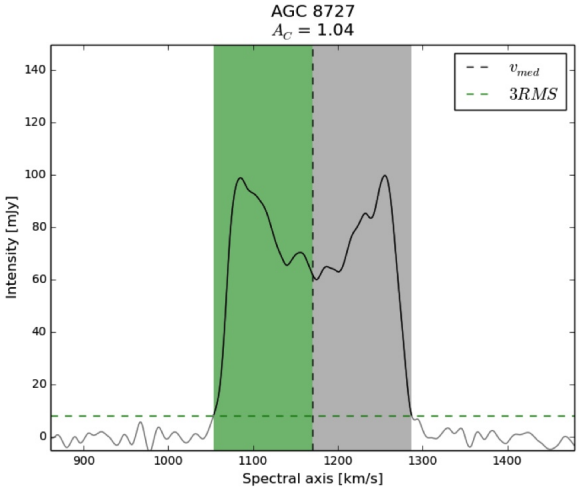

Figure 1.8: Graphical representation of how the A_c ratio is calculated by integrating a global HI profile. The black vertical dashed line marks the profile center (V_{helio}), and green and gray shading marks the extent of the left and right velocity horns (V_{low} and V_{high} respectively), as taken from the ALFALFA α_{40} catalogue. Credit: Bok et al. (2019)

between a galaxy's star formation rate (SFR) and its stellar mass (M$\star$, or $M_{stellar}$). A trend of increasing SFR with increasing M$\star$ that begins to plateau for M$\star > 10^{10.5}$ $M_\odot$ is well established (Noeske et al. 2007, Bouché et al. 2010, Lee et al. 2015), and persists at high redshifts (Lee et al. 2015, Whitaker et al. 2015, Speagle et al. 2014). The SFMS is however not without significant scatter ($\sim$ 0.2 dex on average Speagle et al. (2014)), and galaxies are observed both significantly above and below the SFMS. While the origin of scatter cannot be conclusively determined as prescriptive Kelson (2014), deviations from the main sequence *likely* indicate a break from secular (i.e. slow and steady) evolution. Quenching events can cause a galaxy to drop suddenly below the SFMS, while a starburst phase will cause a galaxy to migrate upwards off the SFMS. An example of a galaxy SFMS is shown in Figure 1.9 from Cluver et al. (2020), which nicely illustrates the scatter, as well as the use of a quenching separator (black dashed line) to identify galaxies that have moved off the SFMS. The SFMS is an incredibly useful diagnostic for investigating the processes driving SF in galaxies, and naturally calls for the inclusion of an HI content dimension. In chapter 3, I present a study of isolated and paired galaxies (see sections 3.2.1 and 3.2.2 in chapter 3) on the MIR galaxy SFMS, and examine their locations on the SFMS as a function of their HI content (gas fraction and HI deficiency). In this way I probe both galaxy environment and HI content as drivers of galaxy evolution on the SFMS.

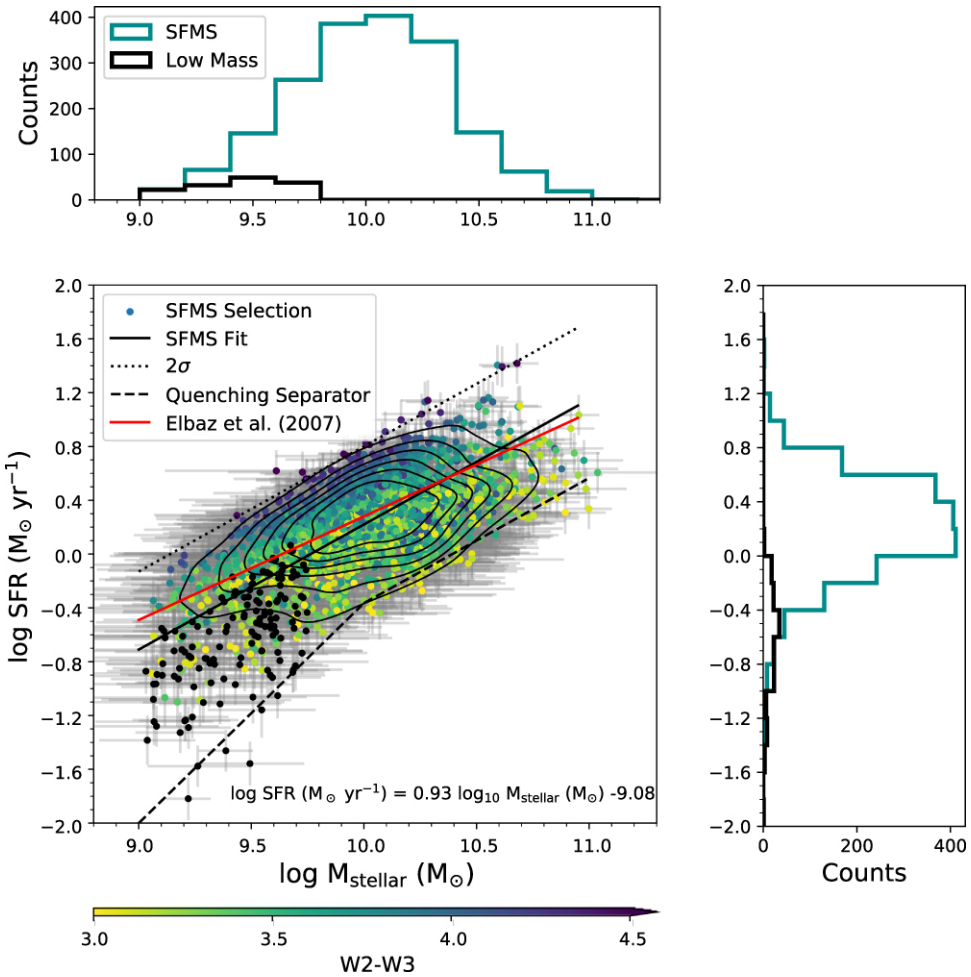

Figure 1.9: Cluver et al. (2020)'s SFMS for galaxies from the Galaxy and Mass Assembly survey (GAMA), colour-coded by the *WISE* W2-W3 colour. The solid black line represents the SFMS fit, and the dashed black line is the quenching separator developed by Cluver et al. (2020). The SFMS fit from Elbaz et al. (2011) is shown in red for reference.

1.4.1 A MIR star-forming main sequence with *WISE*

Any inference we make from a galaxy's location on the SFMS is only as valuable as the SFRs and stellar masses we use are accurate. UV observations perhaps offer the "purest" measure of SF by tracing the young stellar populations in galaxies directly, however are subject to severe extinction by dust and its 3D geometry, and hence uncertainties (Calzetti et al. 2007). Various methods have been deployed to correct for the extinction, but inevitably introduce significant scatter (Calzetti et al. 2007). In the optical we can trace the young, massive, stellar population indirectly by ionised gas. Stars with a stellar mass > 20 $M_{\odot}$ produce ionizing photons that ionize the surrounding gas, which in turn produces line emission upon recombination, notably the Hα line of the Balmer series Calzetti (2013). Hα maps have been used to trace SF (Casasola et al. 2015), and have the advantage of being less affected by extinction compared to the UV, although a correction for extinction is still necessary. The total infrared luminosity ($\sim 5 - 1000\mu m$), or L, measures the emission of dust heated by all sources, but is correlated to the UV emission of young O,B, A and F stars, and thus provides a good estimate of recent SF (1-100 Myr) (Cluver et al. 2017). Procuring sufficiently-sampled spectral energy distributions (SEDs) for dust, as in the work of Davies et al. (2017) within the DustPedia project, is an observationally intensive task, and only attainable with space-spaced telescopes (e.g. *Herschel Space Observatory* (Pilbratt et al. 2010) and *Planck* (Planck Collaboration et al. 2016)). By combining dust-obscured (UV, optical) and unobscured (infrared) measures of SF (e.g. Hα with 24μm (Kennicutt et al. 2009)), hybrid SFR indicators mitigate the effects of dust extinction and provide dependable measures of SF in general, but less so when SF levels are low (Boselli et al. 2015). Such strategies of course rely on the availability of multi-wavelength data. Investigations into the use of single-band infrared measurements (i.e. monochromatic SFR indicators), made possible with the launches of increasingly advanced space-based infrared observatories (e.g. *Infrared Space Observatory* (ISO; Kessler et al. (1996)), *Spitzer Space Telescope (Werner et al. 2004)*, and *Herschel Space Observatory* Pilbratt et al. (2010)), have demonstrated both the mid-infrared (MIR) and far-infrared (FIR) to be useful tracers of SFRs (Zhu et al. 2008). Most notably, the *Spitzer* 24μm band has been established by several studies as a particularly effective tracer of SF (Wu et al. 2005, Calzetti et al. 2007, Zhu et al. 2008, Rieke et al. 2009, Calzetti et al. 2010). The 24μm band picks up the continuum of warm dust (i.e. recent SF versus the heating from an older stellar population probed by longer wavelengths), and is relatively free of contamination (polycyclic hydrocarbons (PAHs), stellar continuum, nebular line emission; Cluver et al. (2017)).

The launch of the all-sky survey with the *Wide-Field Infrared Explorer, WISE* (Wright et al. 2010), positioned the W4 band (centered at 23μm; Brown et al. (2014)) to be the next primary SFR indicator, however a lack of sensitivity has prevented it from being used extensively (Jarrett

et al. 2013). The *WISE* W1 3.4μm and W2 4.6μm bands trace the stellar mass distribution in galaxies, and the W3 12μm and W4 23μm bands are sensitive to the ISM emission from star-forming galaxies, polycyclic aromatic hydrocarbons (PAH) and warm dust respectively (Jarrett et al. 2013, Cluver et al. 2017). Using L_{TIR} to calibrate the *WISE* W3 and W4 SFRs, Cluver et al. (2017) found W3 to be particularly good at tracing SFR, measuring a 1σ scatter in the relation of 0.15 dex over 5 orders of magnitude. Provided deep silicate absorption features (observed in ultra-luminous IR galaxies) and AGN are excluded, the W3 SFR can be considered reliable. The W4 relation has a slightly higher scatter in contrast (1σ = 0.18 dex), however both the W3 and W4 relations agree with radio continuum-derived SFRs, as well as the hybrid Hα and FUV SFR indicators. In both chapters chapter 3 and 4, stellar masses are computed using a combination of the *WISE* W1 3.4μm and W2 4.6μm bands and corresponding mass-to-light ratios from Cluver et al. (2014), and SFRs are obtained using the W3 12μm band and Cluver et al. (2017) W3 relation (Equation 3.1).

$$\mathrm{LogSFR}(\mathrm{M_{\odot}yr^{-1}}) = (0.889 \pm 0.018)\ \mathrm{LogL_{12\mu m}}(\mathrm{L_{\odot}}) - (7.76 \pm 0.15) \tag{1.4}$$

Given the relatively large beam size of *WISE*, blending of galaxies is a general problem, and is addressed accordingly in the custom *WISE* characterization pipeline we employed for this study. I note that my HI pair sample includes de-blended measurements for 6 galaxy pairs, marked on the SFMS by red squares in Figure 3.6, which shows them all to be star-forming, and relatively high mass. Adequate de-blend solutions are measured for these galaxies, which are well within the scatter of SFMS, and therefore not excluded from our analysis. Full details of the *WISE* de-blending process in general, as well as on a case-by-case basis, are discussed in Appendix A of chapter 3.

A comparison of the *WISE* stellar masses measured for our isolated sample and optical stellar masses calculated by Fernández Lorenzo et al. (2013) show them to be highly consistent, and as such we rule out uncertainty in the stellar masses as a significant source of bias.

1.5 Secular evolution

In order to truly disentangle those HI and MIR galaxy properties arising from external influence from those which simply reflect secular evolution, great care must be taken to construct a control sample of isolated galaxies. As I personally discovered in chapter 2, the task is non-trivial. The AMIGA project provides the most extensive multi-wavelength study of a well defined sample of isolated galaxies drawn from Karachentseva (1973)'s Catalogue of Isolated Galaxies (CIG), and is arguably the best possible sample with which to establish secular evolution (Verdes-Montenegro et al. 2005). The original criteria of Karachentseva (1973) classify a galaxy as

isolated only if it is separated (in projection) from any neighbouring galaxy of isophotal diameter of between 1/4 and 4 times its own diameter (in B-band) by at least 20 times the diameter of the potential neighbour, that is, it is separated from the largest of these potential neighbours by at least 80 times its own diameter.

As part of the AMIGA project the degree of isolation was first re-evaluated by Verley et al. (2007a) by analysing Digitised POSS-I E images of each CIG galaxy and constructing a catalogue of potential neighbours. Quantification of the degree of isolation was introduced by Verley et al. (2007b) by way of two complimentary isolation parameters, namely η and Q, which measure the projected surface density of neighbours out to the 5th nearest neighbour and the tidal force exerted by neighbouring galaxies, respectively. Cuts based on these two parameters were enforced to eliminate any outlying cases which may not be strictly isolated. In addition any CIG with a heliocentric redshift of less than 1500 km/s was removed as isolation is difficult to ensure for such nearby targets as a very large sky area must be considered. This left ~700 galaxies in the AMIGA sample that adhere to strict isolation criteria such that for the past ~3 Gyr they are unlikely to have interacted with any neighbour of significant mass (Verdes-Montenegro et al. 2005). Argudo-Fernández et al. (2013) reassessed the isolation of AMIGA galaxies using both photometric and spectroscopic data from the ninth data release of the Sloan Digital Sky Survey (SDSS-DR9). The η and Q metrics were recalculated based on the SDSS images, which led to an additional 16 per cent of the CIG galaxies failing the isolation criteria due to fainter neighbours being identified in the SDSS images. However, in the fields with spectroscopic data the same metrics were recalculated, but with the requirement that any neighbours must be within 500 km/s in redshift, which resulted in an equivalent fraction of the CIG galaxies being classified as isolated as in Verley et al. (2007a). The AMIGA team have further characterized the different components/phases of the interstellar medium (ISM) of these isolated galaxies, as well as their stellar components, in various different wavelengths, including a) optical (Verdes-Montenegro et al. 2005), b) FIR (Lisenfeld et al. 2007), c) radio-continuum (Leon et al. 2008), and d) Hα emission (Verley et al. 2007a), as well as e) nuclear activity (Sabater et al. 2008; 2011). (Full details of the AMIGA project and their extensive research on isolated galaxies are available at http://amiga.iaa.es)

HI data is available for a sub-sample of the full AMIGA catalogue, the AMIGA HI science sample (Jones et al. 2018). I restrict my study of isolated galaxies in chapters 3 and 4 to the HI science sample to assess the role of HI in determining the SFMS locations of our isolated galaxies. The AMIGA HI science sample (Jones et al. 2018) is an HI subset of Karachentseva (1973)'s 1050 CIG galaxy catalogue. HI spectra from the literature were compiled for 415 of these galaxies (see Table 1 in Jones et al. (2018) for observation details), and AMIGA con-

ducted their own observations of 488 galaxies using the Arecibo, Effelsberg, Greenbank, and Nançay radio telescopes. (A summary of the AMIGA HI observations is displayed in Table 2 of Jones et al. (2018).) 429 of the 488 CIG galaxies observed by AMIGA made it into the HI catalogue, and together with the 415 galaxies with spectra published in the literature, the final AMIGA HI science sample comprises 844 galaxies in total. All spectral parameters of this catalogue were extracted using the same fitting method, including the cases where existing observations from the literature were used, and as such this catalogue is considered a highly uniform HI database of isolated galaxies. Jones et al. (2018) further provide cuts to the HI sample based on completeness, isolation, and profile quality. For the purposes of my study I select only those galaxies within the complete AMIGA HI science sample that have been flagged as reliably isolated, with high quality HI profiles.

An updated HI scaling relation for secular evolution

In the seminal study of HI properties of isolated galaxies, Haynes & Giovanelli (1984) computed the HI scaling relation for 324 CIG galaxies. Using optical diameters as a proxy for stellar mass, this relation predicts the HI content of galaxies on the secular evolution track, and has been widely used since to determine the quantity 'HI deficiency' defined as:

$$\mathrm{DEF} = \log \mathrm{M}_{\mathrm{HI}}^{\mathrm{exp}} - \log \mathrm{M}_{\mathrm{HI}}^{\mathrm{obs}} \tag{1.5}$$

where $\mathrm{M}_{\mathrm{HI}}^{\mathrm{exp}}$ is the expected HI mass at a given stellar mass, and $\mathrm{M}_{\mathrm{HI}}^{\mathrm{obs}}$ is the HI mass observed.

With isolated galaxies providing a baseline for 'normal' HI content, computing this quantity for galaxies subject to various different environmental conditions allows one to gauge the impact of environment on HI content. A galaxy's environment might act to deplete it of its HI content, in which case a positive (i.e. gas-poor) value for HI deficiency is measured (as is commonly found in cluster galaxies), while negative (i.e. gas-rich) values for HI deficiency indicate an excess of HI is present (perhaps a signature of accretion). While various authors have extended upon the work of Haynes & Giovanelli (1984) and have computed HI scaling relations (and HI deficiencies) using different and larger galaxy samples (Solanes et al. 1996, Toribio et al. 2011a, Dénes et al. 2014, Bradford et al. 2015), their samples have comprised primarily of field galaxies rather than isolated galaxies, and thus do not necessarily represent evolution absent from interaction. An example of one such relation is shown in Figure 1.10, where Naluminsa et al. (2021) present the $\mathrm{M_{Hi}}$-M$\star$ relation for 228 nearby galaxies from the WHISP sample of well resolved, nearby galaxies. Naluminsa et al. (2021) use a novel method for deriving their scaling relations where the HI enclosed within the stellar disk is used rather than the total integrated HI profile mass, and they find that the enclosed mass produces a tighter fit. A

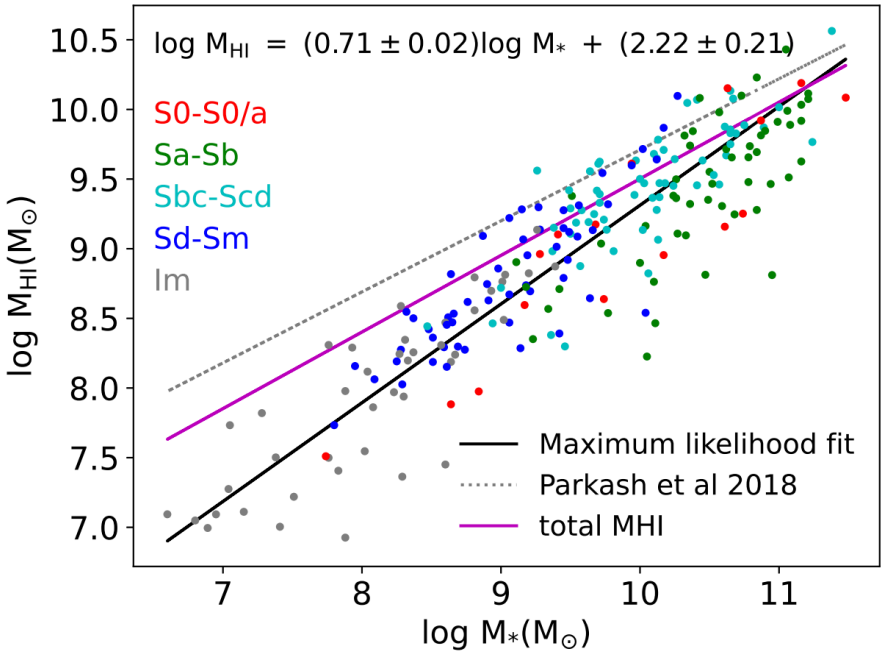

Figure 1.10: M_{HI} (enclosed) versus M⋆ for galaxies from the WHISP sample with *WISE* stellar masses, and galaxy morphology encoded as colour (red:S0,S0/a, green: Sa-Sb, Turquoise: Sbc-Scd, blue: Sd-Sm, and grey:Im). The solid black line shows the best fit for the data using the HI mass within the stellar disk, and the magenta line shows the fit using the total HI from the integrated HI profiles for comparison. Parkash et al. (2018)'s fit for the HICAT sample is shown as a gray dashed line for reference. Credit: Naluminsa et al. (2021)

revised HI scaling relation was measured by Jones et al. (2018) using the AMIGA HI science sample, a sample in which the galaxies have been without significant interaction for ∼ 3 Gyr (Verdes-Montenegro et al. 2005), and therefore well-suited to represent secular evolution. In addition to using a sample superior in both sample size (544 galaxies versus 324) and purity, Jones et al. (2018) also use a more sophisticated regression model to fit the scaling relations. They find that an isolated galaxy's HI content can be predicted by either its optical B-band luminosity or diameter with an accuracy of about 0.25 dex.

In chapter 3, I present an updated version of Jones et al. (2018) scaling relation using *WISE* W1 3.4μm stellar mass measurements as an HI predictor for the AMIGA HI science sample. The relationship between stellar and HI mass is more commonly computed in the literature for different galaxy samples. Updating the scaling relation used to compute HI deficiency to rely on stellar mass allows for a direct comparison with various relations in the literature, as well as a direct assessment of how environment impacts HI content. The resulting relation is described in Equation 3.3. I use this relation to compute the HI deficiencies of both my pair sample galaxies, and my isolated galaxies.

$$\mathrm{Log}_{10}(\mathrm{M_{HI}})[\mathrm{M}_\odot] = 0.44 \times \mathrm{Log}_{10}(\mathrm{M}_\star)[\mathrm{M}_\odot] + 5.19, \sigma = 0.33 \quad (1.6)$$

1.6 Decoding the deficiency distributions of isolated and paired galaxies: a closer look at galaxy morphology, local environment, SFE, and HI profile asymmetries

The link between SF activity and galaxy colour is well-established, with the majority of typical galaxies generally falling into two categories: the "red sequence" and the "blue cloud" (Strateva et al. 2001, Kauffmann et al. 2003, Baldry et al. 2004, Balogh et al. 2004). Hubble Type (galaxy morphology) correlates closely with these two populations. "Red sequence" galaxies are generally high mass, passive, and early-type in morphology, whereas galaxies in the "blue cloud" are typically less massive, active (star forming), and of late-type morphology. Bamford et al. (2009), however, point out that the morphology-density relation and colour-density depend on environment differently: the early type fraction varies less with environment than the fraction of red galaxies. Numerous observations have revealed star-forming galaxies to be less centrally concentrated (bulgy) than quiescent galaxies at a fixed mass (Whitaker et al. 2015). The causal relationship between a galaxy's morphology and its SF history, however, is not well understood. The process by which a blue star-forming spiral galaxy transforms into a red and dead elliptical galaxy, remains one of the biggest puzzle pieces still missing from our picture of galaxy evolution. Current theories for the morphological transformation of galaxies have been categorized as those that occur on short timescales (compared to the lifetime of galaxies), e.g. merger activity, harassment, and ram-pressure stripping (Gunn & Gott 1972, Moore et al. 1999, Fujita & Nagashima 1999), and more gradual processes such as strangulation (Larson et al. 1980, Balogh & Morris 2000) which cause a slow decline in SF. Schawinski et al. (2014) found that a rapid transition from disc to spheroid morphology only happens for a small fraction of blue early-type galaxies. A much larger fraction of blue SF galaxies with significant disks retain their morphology with a slow decline in SF. Simulations show elliptical galaxies can form through major mergers (Tinsley & Larson 1979, Barnes 1988; 1992), and thus suggest that mergers/interactions are potentially driving the galaxy bimodality distribution (Baldry et al. 2004). The findings of Baldry et al. (2004) support the scenario in which activity associated with major interactions (e.g. harassment, mergers) cause galaxies to migrate from the blue galaxy population to the red sequence. Indeed the link between galaxy environment and morphology is well established as the galaxy morphology density relation (Dressler 1980), which refers to the common observation of an increasing fraction of elliptical and S0 galaxies with increasing galaxy density (per Mpc^2), and a corresponding decrease in spirals- Figure 1.2 nicely illustrates this relation.

Links between galaxy morphology and HI content have also been observed, with late type galaxies typically observed to be more HI rich compared to earlier types (Solanes et al. 2001, Toribio et al. 2011a, Jones et al. 2018), suggesting their star-forming status is related to an availability of fuel. While a supply of fuel is of course crucial for SF, how efficiently a galaxy is able to convert its gas into stars is equally important in determining SFRs. Star formation efficiency (SFE) has been defined in the literature in many different ways, but in general refers to the star formation rate surface density per unit neutral or molecular gas surface density, i.e. SFE = ΣSFR/ΣHI (/H_2) (Leroy et al. 2008). While both quantities are frequently used, it is important to note that SFE(HI) and SFE(H_2) cannot be directly compared as the HI/H_2 ratio varies within and between galaxies. SFE comparisons should also take into consideration the SFR indicators used, in particular in the low stellar mass regime, where Audcent-Ross et al. (2018) showed that FUV-based SFR tracers produce higher SFRs, and thus a more constant SFE relation compared to an Hα derived SFE relation. SFE is the inverse of gas depletion time (how long it would take for a galaxy to consume its gas reservoir given its current SF), and thus represents a combination of the real timescale for the conversion of gas into stars, and the fraction of gas that becomes stellar (Leroy et al. 2008). Normalizing by Σgas makes SFE particularly useful (more so than SFR) at identifying where conditions are conducive to SF (Leroy et al. 2008), and relates more directly to the mechanism of turning the interstellar gas into stars (Inoue et al. 2000). While SFE does not appear to correlate with galaxy morphology (for high mass spiral types; Devereux & Young (1991)), Young (1999) found SFE(H_2) to decrease with increasing galaxy size for spirals across a broad range of environments (isolated, Virgo cluster spirals, spiral pairs, and field spirals). Young (1999) suggests that the reduced SFE in large galaxies is a result of the greater shear associated with large disks, which is expected to increase the turbulent energy in molecular clouds (the location of SF), and thus disrupt SF . On the other hand, significantly enhanced SFEs are found in merging/interacting galaxies (Young et al. 1986, Sanders et al. 1986, Solomon & Sage 1988). This result is invariant to the choice of SFR tracer (Hα or FIR emission), and galaxy size (Young 1999). One possible explanation for the enhanced SFEs observed in merging galaxies is the increased rate of molecular cloud collisions that occur during interactions (Noguchi & Ishibashi 1986), which would trigger enhanced SF in galaxies of all sizes (Young 1999).

Schiminovich et al. (2010) calculated SFE(HI) for a representative sample of massive (>$10^{10}M_{\odot}$) galaxies from the *GALEX* (*Galaxy Evolution Explorer*) Arecibo SDSS (Sloan Digital Sky Survey) survey (Catinella et al. 2010), and found very little fluctuation in SFE across the sample. With no trends in stellar mass, stellar mass surface density, NUV-r colour and concentration observed for SFE, Schiminovich et al. (2010) propose that the regulation of SF in massive

galaxies is likely driven primarily by processes that control the gas supply in galaxies (e.g. external processes or feedback mechanisms).

In chapter 4, I continue my investigation of the interplay between SF, HI content, and galaxy environment on the galaxy SFMS by further characterizing my galaxy sample in terms of morphology, local environment, SFE(HI), and HI profile asymmetries. In chapter 3, I contrasted the HI deficiency (/gas fraction) distribution of my close pair galaxies with my isolated galaxy sample and observed a broadening of the pair sample HI deficiency (/gas fraction) distribution in both direction, towards higher and lower deficiencies (/gas fractions). The pair finding method I use in chapter 3 requires only that a target galaxy have at least one close companion, triples and groups are not excluded by the criteria. Visual inspection of the pair sample suggested that there are indeed more densely populated environments present. As discussed in sections 1.2 and 1.3, galaxy environments of different densities (clusters, groups, pairs) impact the content and distribution of HI in galaxies differently. It is therefore possible that some of the observed differences in the HI deficiency distributions of the pair and isolated galaxy samples may arise from sub-populations of galaxy environments contained within the galaxy pair sample (e.g. isolated pairs, triples, compact groups, loose groups). To investigate the effect of these proposed sub-populations of galaxy environments, I quantify the local environments of my pair sample galaxies using Verley et al. (2007a)'s complimentary isolation parameters η and Q. η is a local number density of neighbours, and Q provides an estimate of tidal influence. By taking into account both the number of neighbours and their masses, η and Q work together to provide a comprehensive description of the local environment in the vicinity of each each CIG galaxy, well suited to assessing isolation. Galaxies that are truly isolated from external influence have low η and Q values, and when η and Q are both high we know that the evolution of the target galaxy can be, or already has been impacted by the environment. Verley et al. (2007a) also demonstrated η and Q to be effective at distinguishing isolated galaxies from galaxies in denser environments by comparing them with triplets from the Karachentseva's catalogue (Karachentseva 1973), compact groups from the Hickson catalogue (HCG, Hickson (1982)) and Abell clusters (ACO; Abell (1958)).

I additionally conducted a visual optical classification of the pair member optical morphologies to investigate how morphology might be driving the HI deficiency distribution, and use star-formation efficiencies to probe the mechanisms responsible for driving galaxies off the SFMS towards low SFRs despite having relatively large gas reservoirs. Finally, I compute the HI profile asymmetries of my pair sample and examine them as a function of local environment (η, Q, and number of group members for the Lim et al. (2017) group catalogue), to test the popular proposition that degree of profile asymmetry and density of environment positively

correlate.

1.7 Thesis overview

As detailed above, in this thesis I focus primarily on the galaxy pair environment and its influence on HI and MIR galaxy properties with reference to isolated galaxies. In summary:

- I investigate the impact of the merger-pair galaxy environment on HI profile asymmetries in chapter 2, and propose that high HI profile asymmetries may be used to infer potential merger activity at high redshifts in lieu of 2D HI maps (spatially resolved HI).
- I look at the galaxy pair environment as a driver of location on the MIR galaxy SFMS in chapter 3, as well as its relationship with HI content (gas fraction and HI deficiency) on the SFMS.
- In chapter 4, I invoke galaxy morphology (visual optical morphologies and MIR B/T decomposition ratios), the AMIGA isolation parameters η (local number density) and Q (tidal influence), SFE, and HI profile asymmetries to investigate trends in the HI deficiency distributions of paired and isolated galaxies, as well as their location on the MIR SFMS.
- In chapter 5, I present a summary of my findings.

By piecing together galaxy properties derived from publicly available data in the optical, radio, and MIR regimes, I present clues as to the mechanisms and scenarios potentially driving trends in HI deficiency (gas-removal and accretion), that may be used to inform our theories for galaxy evolution, and guide future scientific inquests with incoming data.

Chapter 2

Enhanced HI profile asymmetries in close galaxy pairs

This chapter is based upon the work of Bok et al. (2019), which was published in the Monthly Notices of the Royal Astronomical Society (MNRAS) journal in 2019 (J. Bok, S.-L. Blyth, D. G. Gilbank, and E. C. Elson, "Enhanced HI profile asymmetries in close galaxy pairs", 2019, MNRAS 484, 582-594.)

Abstract

Analyzing the quantified HI profile asymmetries of galaxies in different environments, we explore not only the prevalence of asymmetry in HI profiles, but also the possibility of using HI profile asymmetries to trace merger activity. We construct close pair and isolated galaxy catalogues of HI profiles from the Arecibo Legacy Fast ALFA (ALFALFA) survey, and using a simple HI flux ratio, quantify and compare the profile asymmetries between the two catalogues. In this way we investigate the popular proposition that merger activity causes HI profiles to become asymmetric, and thereby probe the role of mergers in galaxy evolution. We find small but significant differences between the asymmetry distributions of the two samples, indicating that merger activity does indeed enhance asymmetry in the global HI profile.

2.1 Introduction

Numerous observations have shown galaxies to exist in a vast variety of shapes and sizes, colours and kinematics, interaction states and environments. Astronomers have endeavored to decipher the mechanisms and physical processes by which such variety in galaxy properties arises, and significant advances in our understanding of how galaxies form and evolve have been made. According to the theoretical model for structure formation, Lambda CDM, galaxies form and evolve hierarchically through a succession of major and/or minor mergers (White &

Rees 1978). Observationally and theoretically, galaxy mergers (major and minor) have been pointed to as key processes in various aspects of galaxy formation and evolution (Mundy et al. 2017). The proposition that elliptical galaxies might be the product of a major merger between spirals, the so-called 'merger hypothesis' was first proposed forty years ago by Toomre (1977). Subsequent observations of merger remnants and faint shells/tidal features around ellipticals provide convincing support for the picture of galaxy evolution via mergers (Hopkins et al. 2010). Fernández Lorenzo et al. (2013) demonstrate the importance of environment on the growth in size of massive spirals, which they show to have larger sizes than samples of less isolated galaxies. Mergers have also been implicated in the observed growth in stellar mass of massive galaxies by a factor of 2-3 from $z \sim 2$ to the present, as well as the observed increase in size by a factor of 3-6 of massive quiescent galaxies at fixed stellar mass in the same time period (see Mundy et al. (2017) and references therein). Observing galaxies in the process of merging therefore presents a unique opportunity to test galaxy evolution models, and thereby enable the development of a more complete picture of galaxy evolution.

The general strategy for observing mergers in the optical regime is based on the fact that the gravitational interplay between merging galaxies can cause the interacting galaxies to become morphologically disturbed. Late stage mergers are thus identified as having highly disturbed morphologies, while merging galaxies are often characterized by the presence of tidal features. Close pairs of galaxies (merger candidates) on the other hand, mark the beginning stages of the merger process. The states of non-equilibrium induced by merger activity in both the stellar and dark matter components of a galaxy translate into asymmetries in the galaxy stellar light distribution (Reichard et al. 2008), and it is these asymmetries that have become useful tracers of merger activity in the optical regime. Previously asymmetries in optical images have been quantified using Fourier decomposition (Reichard et al. 2008, Jog & Combes 2009), CAS parameters (Conselice 2003), and other 2D methods (Schade et al. 1995). Such techniques have been used to show that galaxies in close pairs exhibit enhanced asymmetries in their stellar light distributions compared to galaxies that are isolated (Patton et al. 2005, De Propris et al. 2007, Ellison et al. 2010). Jog & Combes (2009), and references therein, showed that galaxies are asymmetric not only in their stellar populations, but also in their gas (molecular and neutral) distributions, kinematics (see Swaters et al. (1999), Barrera-Ballesteros et al. (2015)), and global HI velocity (spectral) profiles. It was Baldwin et al. (1980) who coined the term 'lopsided' in 1980, reserving the title for galaxies in which they detected an asymmetry in the spatial extent of their neutral gas in their pioneering paper 'Lopsided galaxies'. Comparing asymmetries traced in the optical with asymmetries traced by HI, as in the work of Kornreich et al. (2000), showed that asymmetry is not only quantitatively larger and more frequent in HI than in stars (Bournaud et al. 2005), but also that the amplitude of

asymmetry increases with galaxy radius (Reichard et al. 2008). This, together with the fact that HI typically extends out to much larger radii than the stellar component of a galaxy, suggests that HI might be a more sensitive probe of asymmetry compared to the optical light distribution.

Looking to HI imaging as a potential diagnostic for tracing asymmetries associated with merger activity, Holwerda et al. (2011) quantified the HI morphologies of a sample of 141 column density maps of galaxies from the WHISP survey, computing the CAS parameters for each galaxy as per Conselice (2003), as well as M_{20}, the Gini coefficient (Lotz et al. 2004), and G_M (the second order moment of light). The results of the study suggest that disturbed morphologies and asymmetries are indeed good indicators of merger activity. Following up on the work of Holwerda et al. (2011), Giese et al. (2016) investigated the dependence of these morphological parameters on signal-to-noise ratio, resolution, and inclination, and also found that the asymmetry parameter is the most useful parameter with which to measure galaxy lopsidedness as traced by classifications by eye. Barrera-Ballesteros et al. (2015) show kinematic asymmetries/misalignments in both the spatially resolved stellar and ionised gas components of galaxies are also good indicators of interaction status. Combining N-body/hydro-dynamics/stellar evolution code, Kornreich et al. (2002) simulated the dynamics and morphology of a galaxy in response to receiving a librational 'kick' of energy, and found that NGC 5474 (a tidally disturbed galaxy) exhibited almost all of the observed effects in the simulation. Kornreich et al. (2002) suggest that driven sloshing modes might play a role in galaxy asymmetry.

While the 2D imaging analyses are very promising, our current HI imaging datasets have limited statistics. However, large HI surveys such as HIPASS and ALFALFA consisting of thousands of spatially unresolved, but spectrally resolved detections, can be investigated. These surveys were conducted using single-dish radio telescopes, which do not spatially resolve galaxies with sizes smaller than the primary beam, however, they do provide spectrally resolved information (global HI velocity profiles) for large numbers of galaxies.

The 1D global HI profile has a shape primarily dictated by galaxy kinematics, and carries with it information both about a galaxy's velocity field, as well as the distribution of HI within the galaxy. The ordered motions within a galaxy, where radial velocities tend to cluster, are responsible for the characteristic double-horn signature seen in HI velocity profiles. HI profiles are therefore expected to be symmetric about the systemic velocity for an unperturbed disk, with deviations from symmetry considered potential consequences of merger activity (e.g. non-circular motions, tidal tails, and distortions in the HI mass distribution), asymmetric gas accretion, or an offset of the stellar disc in a halo potential (van Eymeren et al. 2011). Furthermore, Richter & Sancisi (1994) found that HI profile asymmetries are often accompanied by an

asymmetry in the corresponding HI gas distributions.

The frequency of these observed departures from symmetry has been the topic of investigation in a number of HI profile studies, where the degree of asymmetry has been assessed both qualitatively and quantitatively (Haynes et al. 1998, Matthews et al. 1998, Espada et al. 2011). Richter & Sancisi (1994) qualitatively measured the HI profile asymmetry on a sample of $\sim$ 1700 galaxies from various single dish HI surveys using a by eye visual classification scheme. This sample was comprised primarily of field galaxies so as to minimize the chance of the cluster environment playing a role in producing profile asymmetries. A lower limit of 50 percent of the sample was found to exhibit significant profile asymmetries, suggesting that asymmetry might well be the rule rather than the exception. Richter & Sancisi (1994) further quantified the HI profile asymmetries of their sample using Tifft & Huchtmeier (1990)'s HI flux ratio between the lower and upper velocity halves of the global HI spectrum, and found the qualitative and quantitative asymmetry measures to be highly congruent. Using a similar HI flux ratio, Haynes et al. (1998) quantified the HI profile asymmetry for an isolated sample of 104 high signal-to-noise (SNR) HI profiles obtained using the Greenbank 43m telescope. The results of the study showed $\sim$ 50 percent of the sample to have significant HI profile asymmetries (in good agreement with previous work), which the authors attribute to distortions in the HI distribution, non-circular motions, and possible confusion with unidentified companions within the telescope beam. A more recent study by Espada et al. (2011), specifically focussed on HI profile asymmetries of galaxies carefully selected to be isolated. Their study forms part of the AMIGA project (Analysis of the interstellar Medium in Isolated GAlaxies; Verdes-Montenegro et al. (2005)), whose aim is to disentangle those galaxy properties (morphological and structural) which are due to internal secular evolution from those which arise from interactions within the galaxy environment. HI profile asymmetries were quantified for a sample of $\sim$166 high SNR HI profiles (the HI refined sub-sample) using the standard HI flux ratio. They describe the resulting asymmetry distribution as following a Gaussian model with width σ= 0.13 (corresponding to a flux ratio of 1.26 at the 2σ level).

While previous studies show HI profile asymmetries to be a common phenomenon, their origin is still unclear. Since merger activity is known to induce asymmetries in the 2D HI distributions of galaxies, we propose that it produces asymmetries in HI profiles as well. Other potential drivers of asymmetry include harassment (Moore et al. 1995), ram-pressure stripping (Gunn & Gott 1972), viscous stripping (Nulsen 1982), outflows (Fraternali 2017), and accretion (e.g. Sancisi et al. (2008)), and while in this paper we investigate mergers in particular as an asymmetry driver, we note that it is difficult to isolate drivers without conducting a detailed environment study. Here we explore the relationship between asymmetries in HI profiles and

possible merger activity by quantifying the profile asymmetries of a sample of close galaxy pairs (merger candidates), and comparing them with the HI profile asymmetries of a reference sample of isolated galaxies. By investigating first the extreme case of close pair galaxies, where we expect the signal in HI profile asymmetry to be strongest, we explore the possibility of using HI profile asymmetries as a way to identify merger activity on different scales (loose groups, dense groups, clusters) in the future, in lieu of what is currently a very limited sample of HI maps. Upcoming surveys on SKA pathfinders will build up a more complete set of HI maps out to intermediate redshifts, ~0.2-0.3, but at higher redshifts the resolution will generally be too poor to provide an accurate measure of asymmetry (see Figure 9 from Giese et al. (2016)) and therefore the 1D HI profile will be very useful as a consistent means to measure asymmetry over a wide range of redshifts.

This paper is organized as follows: In the following section we discuss the different data sets used in this study, and in §2.3 we describe our sample selection criteria for both the pair and isolated galaxy samples. §2.4 outlines our method for quantifying HI profile asymmetry, including a description of how we estimate uncertainty. We discuss results and future work in §2.5, and summarize the conclusions in §2.6. Throughout this paper we adopt H_0=70 km $s^{-1}Mpc^{-1}$ (h= 1), Ω_M = 0.3, and Ω_Λ = 0.7.

2.2 Data

The close pair and isolated galaxy catalogues we wish to construct require both a sample of HI galaxy profiles, as well as an optical sample of galaxies from which we can draw optical neighbours for each HI galaxy. We require not only positional information, but reliable redshift information such that we can compute the 2D projected distance between nearest neighbours.

2.2.1 HI Galaxy sample

This study uses publicly available HI profiles from the first data release of the Arecibo Legacy Fast ALFA (ALFALFA) survey (Giovanelli et al. 2005), α40. The α40 catalogue (Haynes et al. 2011) covers 40% (2800 square degrees) of the total survey area. Source centroid positions, HI line flux densities, recessional velocities and line widths are provided for a total of 15855 sources in the catalogue, as well as the most probable optical counterparts (OCs) in SDSS DR7 (Sloan Digital Sky Survey Data Release 7; Abazajian et al. (2009)) for more than 98 percent of the HI sources. OCs were identified by the α40 team using distance from the HI centroid, as well as colour, morphology, and redshift information that was publicly available at the time.

We make use of a sub-sample of high signal-to-noise, good quality HI profiles (reliable detec-

tions flagged by the α40 team as code 1 profiles) with spectroscopic optical counterparts. A pool of ~6800 HI galaxies meet these selection criteria. Our HI sample has a velocity resolution of 5 km s^{-1}out to z ~ 0.06.

2.2.2 Optical neighbours

Neighbours for our HI sample, which we use to investigate the environment of each HI galaxy, are drawn from a spectroscopic sample of SDSS galaxies that are within both the ALFALFA footprint and redshift range. The SDSS galaxy sample is made up of galaxies with r-band Petrosian magnitudes r $\leq$ 17.77 and r-band Petrosian half-light surface brightnesses $\mu_{50} \leq 24.5$ mag arcsec^{-2}, above which the sample is > 99 percent complete (Strauss et al. 2002). Strauss et al. (2002) show that redshifts for the SDSS galaxy sample are reliable with a statistical error less than 30 km s^{-1}, and Toribio et al. (2011b) show that the dispersion in the difference between radial velocities of ALFALFA galaxies and their assigned optical counterparts in SDSS is ~35 km s^{-1}.

2.3 Sample selection

In order to compare the quantified HI profile asymmetries of galaxies in close pairs with those that are isolated, we first need to compile a galaxy pair catalogue of HI profiles. Here we look to previous work to inform our definition of close pair galaxies.

2.3.1 Merger pair sample

In deciding upon a useful pair definition with which to identify galaxy pairs, one must engage in a compromise between purity of the sample, and completeness. While a stringent pair definition is preferable in selecting pairs that are most likely going to merge in a relatively short timescale (~ few Gyr) (purity) , this may lead to a statistically insignificant sample size if the corresponding survey is not sufficiently large (completeness). Barnes (1988) and Patton et al. (1996) estimate that galaxies with companions at projected separations of $r_p \leq 20h^{-1}$ kpc will merge within 0.5 Gyr, and the convention of early close pair studies was to use this projected separation as an upper limit for identifying merger pairs. More recently, with spectroscopic redshift samples increasing in size, it has been possible to include a velocity separation criterion, Δv, in the galaxy pair definition (Patton et al. 2000). By determining the line-of-sight rest frame velocity difference between companion galaxies one can identify those pairs with the greatest likelihood of merging as having the lowest relative velocities.

Patton et al. (2000) use a visual interaction classification parameter based on optical morphologies to investigate the location of interacting pairs in $r_p - \Delta v$ phase space, and find

that the majority of pairs showing clear signs of interactions (tidal tails, morphological distortions/asymmetries, etc.) have projected separations of $r_p \leq 20h^{-1}$ kpc. Furthermore, 97% of the pairs with $\Delta v \geq 600$ km s^{-1}display no signs of interaction, while the strongest signs of interaction are seen for the low Δv pairs. Patton et al. (2000) thus suggest close pair criteria of $r_p^{max} \leq 20h^{-1}$ kpc and $\Delta v^{max} \leq 500$ km s^{-1}to identify interacting pairs. Robotham et al. (2014) conduct a similar analysis on a sample of optical pairs with $r_p^{max} \leq 100h^{-1}$ kpc and $\Delta v^{max} \leq 1000$ km s^{-1}, and find again that pairs with the smallest projected separations ($r_p^{max} \leq 20h^{-1}$ kpc) and lowest relative velocities ($\Delta v^{max} \leq 500$ km s^{-1}) exhibit the strongest signs of interaction. These close pair criteria are commonly used in the literature, however it is important to note that they do not recover all interacting pairs. Signs of interaction are observed at $r_p \geq 50h^{-1}$ kpc, even as far as $r_p \sim 95h^{-1}$ kpc in the case of Arp 295a/b (Patton et al. 2000). These systems, however, are not dominant. More recently, Patton et al. (2016) find that optical asymmetries are most significantly enhanced by the presence of nearby companions at projected separations less than 10 kpc, with the mean asymmetry enhanced by a factor of 2.0 ± 0.2 in this regime. Beyond 10 kpc the mean asymmetry enhancement declines, remaining statistically significant out to projected separations of 50 kpc.

It is important to note that it has been optical signs of interaction advising the close pair definitions in previous work. A close pair study in which HI is being used as an interaction diagnostic warrants careful consideration. HI typically extends further out compared to the optical component of a galaxy, and is more diffuse in nature. This suggests signs of interaction in HI might be observed at larger projected separations, indicating merger activity on a different timescale to that of optical indicators. For our work, we therefore use Robotham et al. (2014)'s loosest close pair criteria of $r_p \leq 100h^{-1}$kpc and $\Delta v \leq 500$ km s^{-1}. In this way we hope to recover as many interacting pairs as possible (and thereby obtain a more complete sample), as well as those pairs in the early stages of the merger process, the evidence of which might only be visible in HI.

The following is a summary of the steps taken to compile our catalogue of merger-pair galaxy candidates:

1. Using the optical spectroscopic counterpart R.A. and Dec. positions for each HI galaxy in the α40 sample with signal-to-noise (SNR) > 10 and inclination (i) > 30, we search in the SDSS spectroscopic catalogue for the nearest (2D projected distance) neighbour galaxy. (The SNR selection criterion is necessary for the accurate measurement of HI profile asymmetries, and is consistent with the HI asymmetry work of Tifft & Huchtmeier (1990) and Espada et al. (2011). The inclination criterion ensures we are not underestimating the HI profile asymmetry by including face-on galaxies in our sample, whose HI profiles

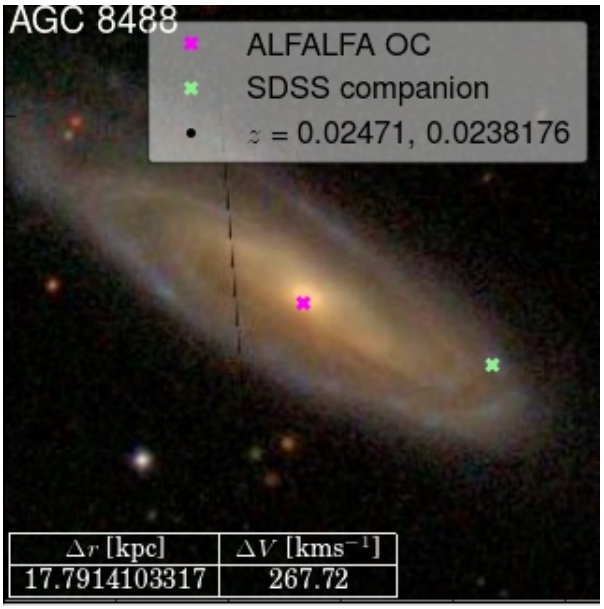

Figure 2.1: 4'x4' optical image of a galaxy pair that was classified as potentially shredded galaxies during the visual inspection process.

will be single peaked by virtue of their inclination with respect to our line of sight.)

2. $\Delta v = |v_{\rm HI} - v_{\rm optical}|$ is then determined for each pair using the $v_{\rm helio}$ from the α40 catalogue, and cz from SDSS. We identify 375 close pair galaxies as those with at least one optical neighbour within 100 kpc and 500 km s^{-1}.

3. In order to reduce the potential effects of confusion on our measurements of HI profile asymmetry, we removed all HI -HI pairs with spatial separation less than 3.5 arcminutes (size of the ALFALFA primary beam). We removed 15 close pairs using this criterion. By excluding HI -HI pairs we note the caveat that we are not considering all close pairs in our analysis, but a sub-sample of close pairs in which the HI content resides primarily in one galaxy.

4. A final visual inspection of the close pair galaxies eliminates 12 potentially 'shredded' galaxies from the sample. As a result of the DR7 deblending process, bright objects are on occasion interpreted as two or more objects (shredded). We show an example in figure 2.1. The final pair sample thus comprises 348 galaxy pairs.

2.3.2 Sample of isolated galaxies

In defining the isolated galaxy sample we prioritize purity over completeness, and conservatively select only those ALFALFA galaxies whose nearest spectroscopic optical companion is

$\geq$ 500 kpc away, with $\Delta v \geq 5000$ km s^{-1}. At such large separations one can reasonably expect the optical companions to have negligible tidal influence on their distant HI neighbours, and therefore are unlikely to produce asymmetries in the HI profiles. Outside these criteria signs of optical interaction are uncommon, and increasingly insignificant (Patton et al. 2000). We note that spectroscopic incompleteness of the SDSS optical sample could affect the purity of our isolated galaxy sample, as well as the completeness of our pair sample. If a galaxy's true nearest neighbour does not have a measured redshift in SDSS, the distance to its nearest neighbour will be overestimated, and could potentially lead to a real close pair member being classified as isolated by our isolation criteria. To this end we visually inspected 500 kpc x 500 kpc optical images of our isolated sample, and removed potential contaminants (possible pairs). In figure 2.2 we show two such examples of galaxies that were originally classified as isolated using only spectroscopic information, but which were removed after visual inspection revealed potential companions. Our final sample of isolated galaxies comprises 304 galaxies.

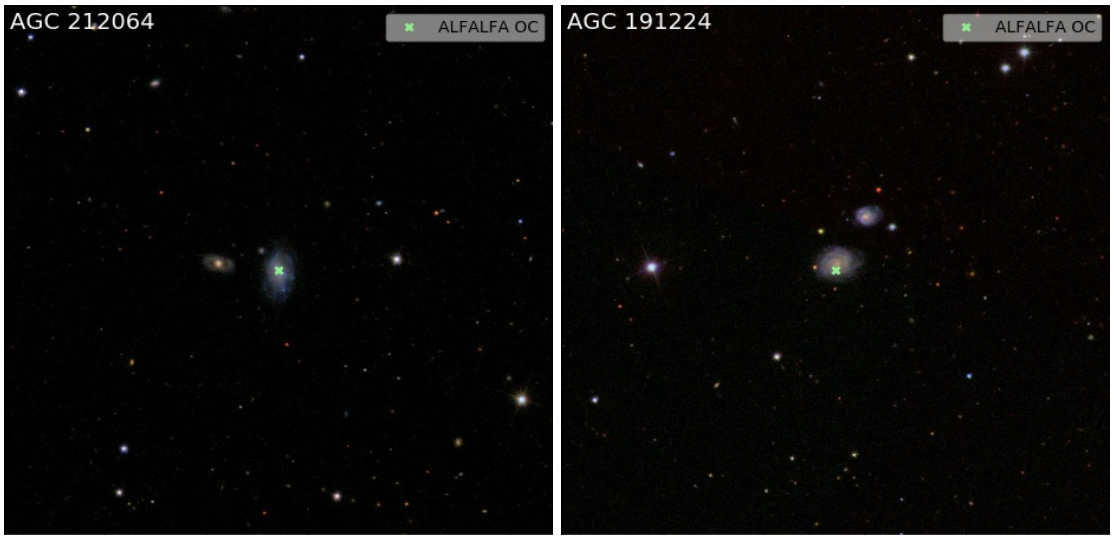

Figure 2.2: 7'x7' ($\sim$ 500 kpc) optical images of galaxies that were removed from our isolated sample due to the presence of potential neighbours. The green cross marks the location of the OC.

We note that while spectral profile asymmetries for an isolated galaxy sample have already been measured by Espada et al. (2011), we propose that a control sample of our own catalogue of isolated ALFALFA galaxies, subject to the same systematics as our pair sample, will provide the most reliable comparison for our study, however we do compare to Espada et al. (2011) in §2.5 as well.

Table 2.1: Sample selection criteria.

Catalogue	Δr [kpc]	Δv [km s^{-1}]	SNR	i	sample size	z matched sample
Pairs	< 100	< 500	> 10	>30	348	304
Isolated	> 500	> 5000	> 10	>30	304	304

2.3.3 Combined sample properties

A summary of the final selection criteria for both the pair and isolated galaxy samples can be seen in Table 2.1.

Since galaxy evolution is strongly dependent on z we match the pair and isolated samples in this quantity, and compare sample properties in figure 2.3. We note in figure 2.3 that the pair and isolated samples are well matched in SNR, and u-r colour, and thus disregard the possible impact of these quantities on the comparative measurement of HI profile asymmetry between the two samples. Since a higher fraction of the pair sample has both larger stellar and HI masses, as well as higher inclinations, compared to the isolated sample, we test the dependence of our asymmetry measure on these quantities in §2.5.

2.4 Measuring profile asymmetries

A simple and meaningful way to quantify asymmetries in HI profiles is to compute an HI flux ratio between the two profile horns, for example by using the median (/mean) velocity as the divider (e.g. Haynes et al. 1998, Espada et al. 2011). Variations of this method include using different quantities to determine profile edges (velocity width at the 50 percent level (w_{50}), velocity width at the 20 percent level (w_{20})), as well as different profile centres ($v_{\rm mean}$, $v_{\rm median}$, $v_{\rm weighted}$).

Here we quantify the asymmetry of our pair sample as a ratio of flux, A_c, between the two velocity horns using v_{helio} from the α40 catalogue to define the centre of the profile. In defining the profile edges we use the w_{50} width given in the α40 catalogue, and we interpolate the profile to retrieve the velocity at the 50 percent level. The typical flux values at v_{20} are similar to the noise rms of the profiles, for this reason we use w_{50} over w_{20} to determine the profile edges, as it is more reliably determined. A_c is calculated as:

$$A_{\frac{l}{h}} = \frac{\int_{v_{\rm low}}^{v_{\rm helio}} I_\nu dv}{\int_{v_{\rm helio}}^{v_{\rm high}} I\nu dv} \tag{2.1}$$

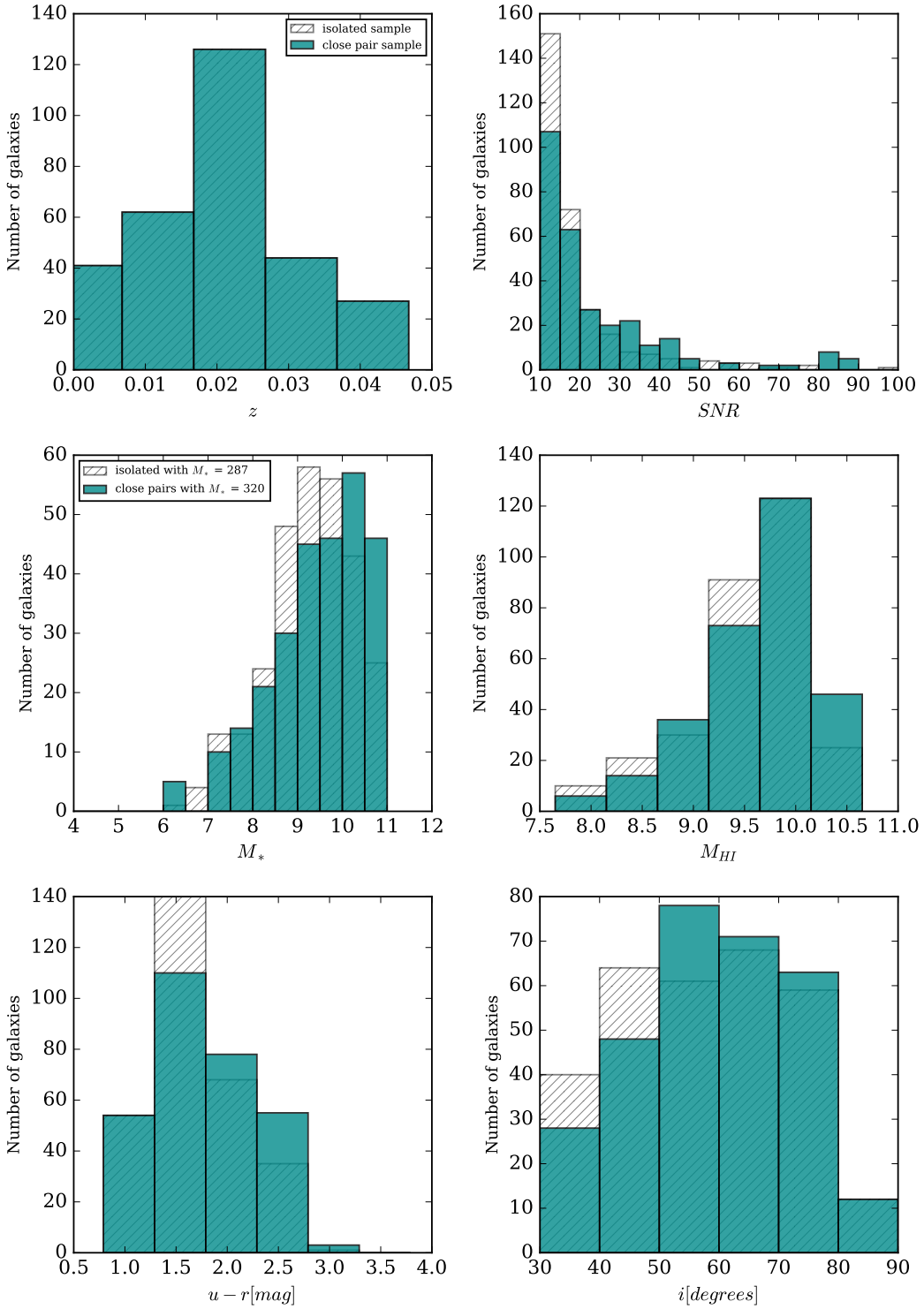

Figure 2.3: Comparison of properties between the pair (dark cyan) and isolated (hatched) samples. Top left: redshift. Top right: SNR. Middle left: $log10(M_*)$. Middle right: $log10(M_{HI})$. Bottom left: u-r colour. Bottom right: inclination.

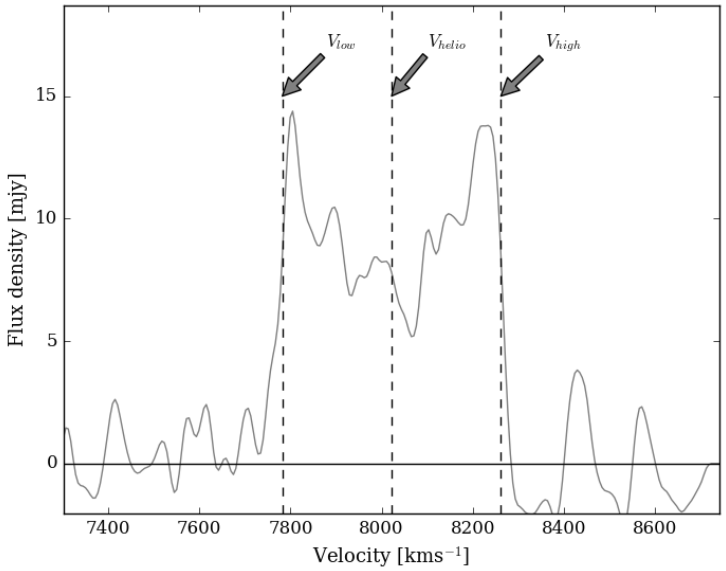

Figure 2.4: Graphical representation of how the A_c ratio is calculated on a global HI profile. Black vertical dashed lines mark the profile center (V_{helio}), as well as the extent of the left and right velocity horns (V_{low} and V_{high} respectively), as taken from the ALFALFA α_{40} catalogue.

and

$$A_c = A_{\frac{l}{h}} \text{ if } A_{\frac{l}{h}} > 1 \tag{2.2}$$

$$= A_{\frac{h}{l}} \text{ if } A_{\frac{l}{h}} < 1 \tag{2.3}$$

Here v_{helio} corresponds to the the galaxy's heliocentric velocity, and v_{low} and v_{high} the velocity of the galaxy at the 50 percent flux level to the left and right of v_{helio} respectively. Figure 2.4 provides a graphical representation of how A_c is determined.

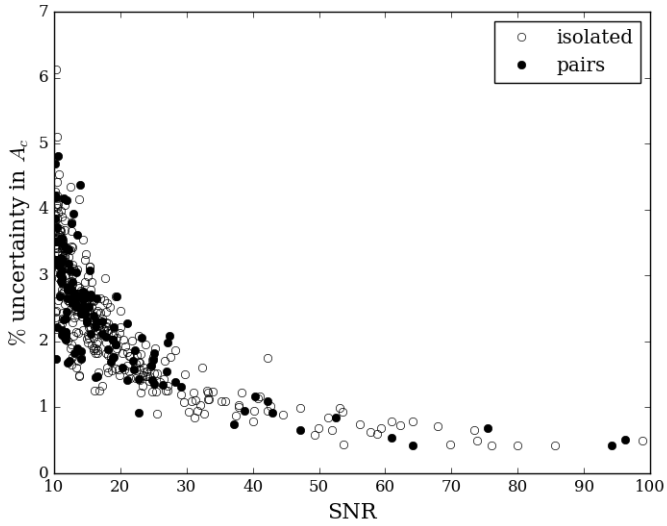

Figure 2.5: Percentage estimated uncertainty on A_c as a function of SNR. Filled circles correspond to the pair sample, while open circles mark the isolated galaxies.

2.4.1 A_c uncertainty estimation

We adopt a Monte-Carlo approach to estimate the uncertainty associated with the A_c measurement. The steps we followed were:

1. Calculate A_c on the original HI profile.
2. Replace each flux value, f_i, in the profile with a new flux value, $f_{\rm new}$, drawn randomly from the Gaussian distribution with mean f_i and width = $\rm rms_{noise}$ (as provided by the α40 catalogue for each galaxy).
3. Recalculate A_c on the adjusted profile.
4. Repeat steps (ii) and (iii) 1000 times.

We use the standard deviation of the 1000 A_c measurements calculated for each profile to serve as the estimated A_c uncertainty, and as can be seen in figure 2.5, the calculated uncertainties are for the most part less than 5 percent. Since both our pair and isolated samples are drawn from the same survey, we exclude the potential contribution of $\Delta v_{\rm mean}$ and pointing errors from our uncertainty calculation as they should impact both samples equally.

2.5 Results & Discussion

In figure 2.6 we present our results for asymmetry measurements for the close pair sample compared to our isolated sample. The most discernible feature between the two distributions is a longer tail in the pair asymmetry distribution extending towards high asymmetries. With the pair and isolated galaxies matched in redshift, and well matched in u-r colour and SNR, we tentatively attribute this enhanced frequency of high asymmetries in the pair sample to environment, and conclude that merger activity (or tidal activity) is most likely responsible for the measured difference in HI profile asymmetries between our pair and isolated sample. A statistically significant measure of this difference is provided by the k-sample Anderson-Darling (A-D) test (Scholz & Stephens (1987)). The k-sample A-D test is a modification of the more widely used Kolmogorov-Smirnov (K-S) test, however that is more sensitive to differences present in the tails of distributions compared to the K-S test, and thus more aptly suited to our data. Bootstrap re-sampling our isolated galaxy sample 10000 times, we measure a mean A-D test statistic between the pair and isolated samples of A^2 =12.18, with a mean p-value = 0.0002, we therefore reject the null hypothesis that they are drawn from the same distribution at the 1 percent level.

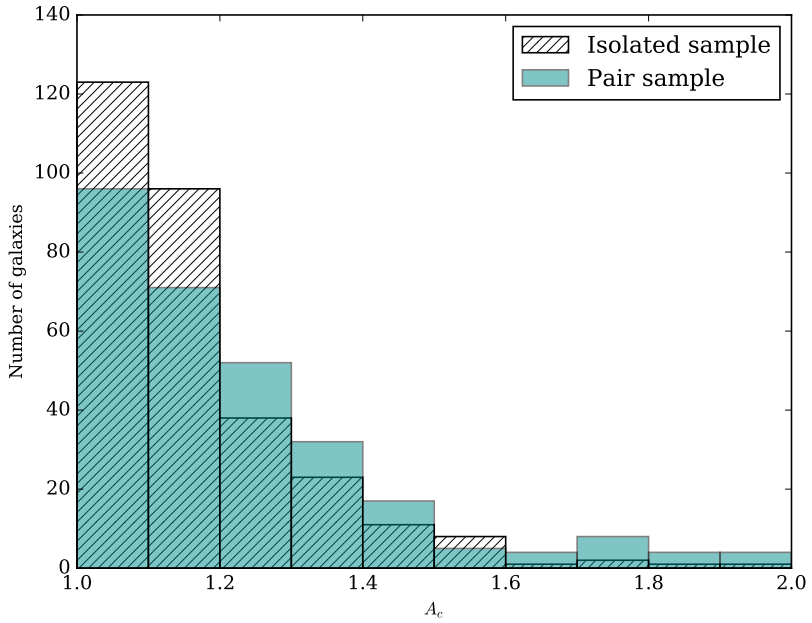

Figure 2.6: Asymmetry distributions for both the pair (dark cyan) and isolated (hatched) galaxy samples.

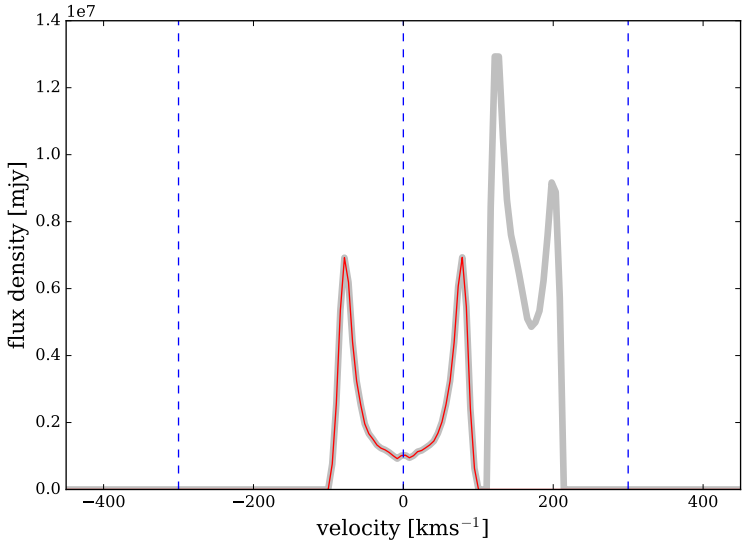

Figure 2.7: The HI spectrum of a target galaxy extracted from the synthetic HI data cube is shown in red, with the total extracted HI mass, including that of nearby neighbour, indicated by the thick grey curve.

In §2.3.3 we note that the pair and isolated galaxy samples have different M_* and M_{HI} distributions, quantities known to play a role in galaxy evolution. We find no correlation between A_c and both M_* and M_{HI} and thus conclude that these quantities are not responsible for the difference in A_c distributions we measure between the pair and isolated samples. Similarly, we find no correlation between A_c and inclination, where inclination > 30.

In order to be able to unambiguously attribute asymmetries in the HI profiles of our pair sample to merger activity, we need to first ensure that we sufficiently address confusion as the next most likely cause of asymmetry. Our ability to detect and eliminate instances of HI confusion from our pair sample (as described in §2.3.1) is limited by the ALFAFA resolution (~3.5'). We cannot account for contamination from HI sources with flux densities below the ALFALFA noise threshold. We can, however, make use of simulations to quantify the relative amount of contaminant emission contained in the HI spectrum of a galaxy. We make use of a synthetic HI data cube generated according to the methods presented in Elson et al. (2016). The cube spans a sky area of 30 square degrees and the redshift range $z < 0.06$. Each of the 3715 galaxies in the cube has an associated set of physical parameters based on the semi-analytic models of Obreschkow & Meyer (2014). Furthermore, each galaxy has the spatial and spectral distributions of its HI line emission modelling in a realistic manner. The entire cube was smoothed to a spatial resolution of 3.5'x3.5' to match the spatial resolution of the ALFALFA data. The

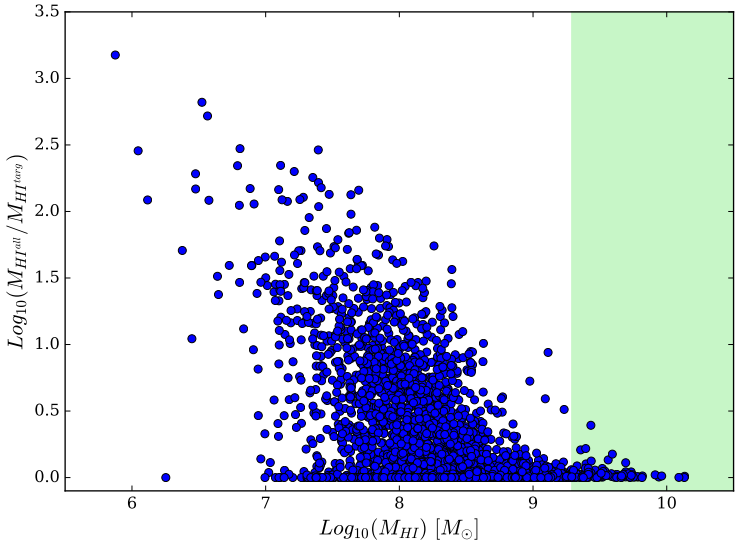

Figure 2.8: Relative amount contaminant flux ($Log_{10}(\mathrm{M_{HI^{all}}/M_{HI^{targ}}})$) of the simulated galaxy profiles as a function of HI mass, with the ALFALFA HI mass range shaded in green.

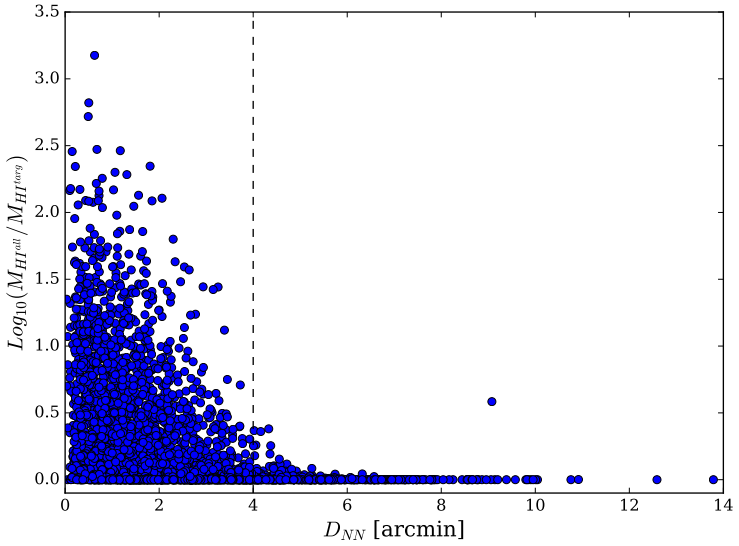

Figure 2.9: Relative amount contaminant flux ($Log_{10}(\mathrm{M_{HI^{all}}/M_{HI^{targ}}})$) of the simulated galaxy profiles as a function of angular distance to nearest neighbour ($\mathrm{D_{NN}}$).

angular size of a spatial pixel in the cube is 30"x30", whereas the median velocity width of a channel is 5.42 km s^{-1}

In order to asses the extent to which the HI spectrum of a galaxy in the cube may be contaminated by emission from neighbouring galaxies, HI spectra of all 3433 galaxies with $M* > 10^{10}M_{\odot}$were extracted using a spatial aperture of 3.5'x 3.5' and a spectral aperture of 230 channels. The true HI mass of each galaxy was compared to the total amount of HI mass spanning 300 km s^{-1}either side of its systemic velocity. This procedure is demonstrated in figure 2.7 which shows the HI spectrum of the target galaxy as the thin red curve and the HI spectrum of all the extracted mass as the thick grey curve. In this example, a significant amount of mass from a nearby galaxy falls well within the 600 km s^{-1}velocity range centered on the systemic velocity of the target galaxy. The ratio of the total amount of mass over this range (i.e., the integral of the grey curve) to the mass of the target galaxy (i.e., the integral of the red curve) is $M_{HI}{}^{all}/M_{HI}{}^{targ}$=2.54. Figure 2.8 shows the logarithm of this ratio as a function of $\log(M_{HI}{}^{targ})$ $M_{\odot}$, where $M_{HI}{}^{targ}$ is the HI mass of a target galaxy, for all 3433 of the HI spectra extracted from the synthetic cube. Clearly, galaxies with low HI masses can contain amounts of contaminant emission that are factors of hundreds to thousands greater than their true HI mass. However, over the high HI mass range probed by the ALFALFA data, contamination levels are very low. This result is further illustrated in figure 2.9 which shows the relative amount of contaminant flux as a function of nearest neighbour distance for all HI spectra extracted from the synthetic cube. These results give us great confidence that the levels of contamination in the ALFALFA spectra used in this study are negligibly small.

In §2.3.2 we discuss how spectroscopic incompleteness of the optical sample could decrease the purity of our isolated galaxy sample, as well as the completeness of our pair sample. We also note that using 2D distance information to locate merger pairs has its limitations in accurately identifying real merger pairs. Ideally we would need 3D position and velocity information to conclusively identify pairs that are going to merge. Without the 3D information we expect our pair sample to be contaminated by false 2D pairs, reducing the purity of our pair sample. Both of these effects would therefore act to increase the similarities between the isolated and pair samples. We therefore expect the measured difference in asymmetries between our pair and isolated samples must be a lower limit on this quantity.

Looking to the literature for comparison, Espada et al. (2011) describe the HI profile asymmetry distribution for their sample of isolated galaxies, the HI refined sub-sample, as a half Gaussian of width $\sigma = 0.13$. (This sample was selected as having the lowest uncertainties ($\leq$ 5 percent)

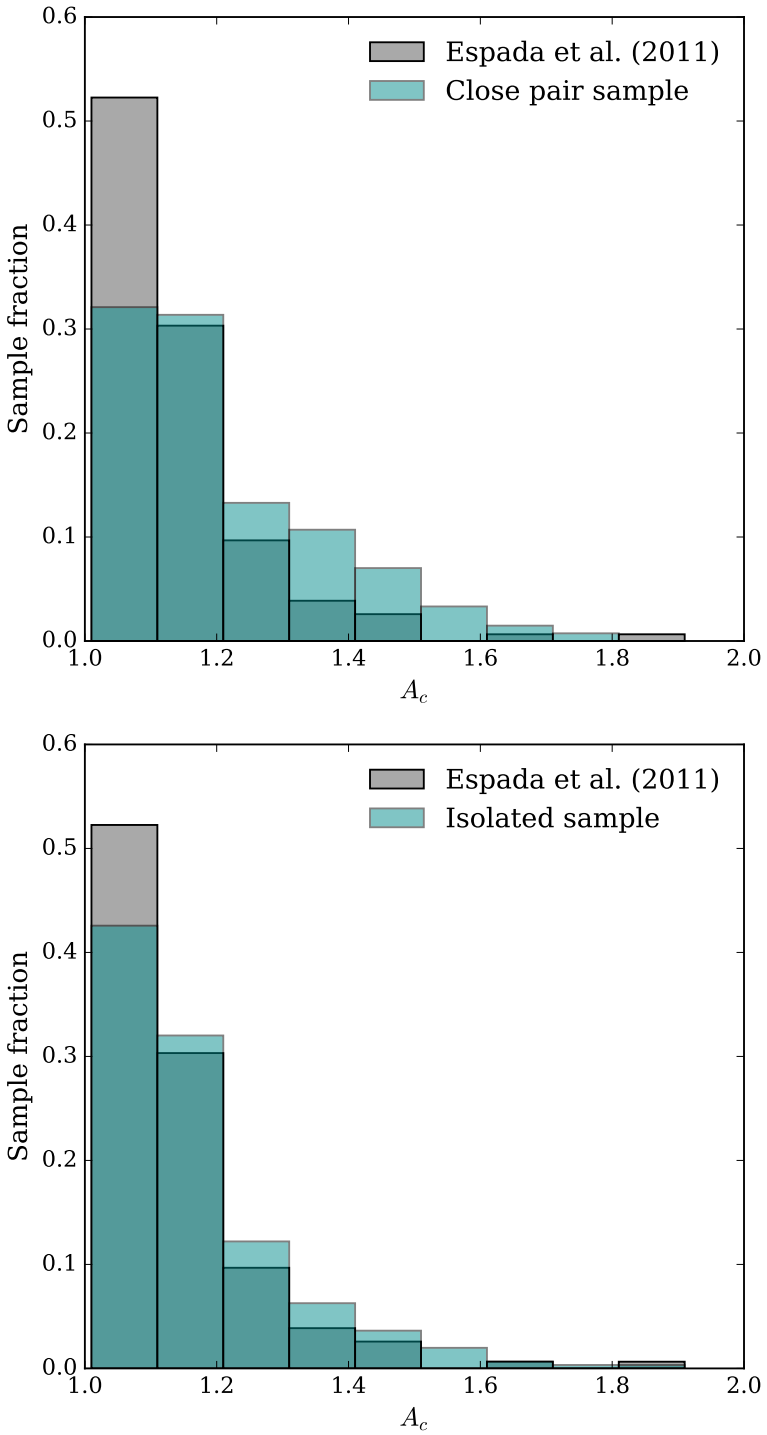

Figure 2.10: Top: Normalized A_c distributions of the HI refined sample (gray) and our pair sample (dark cyan). Bottom: Normalized A_c distributions of the HI refined sample (gray) and our isolated sample (dark cyan)

Table 2.2: Comparison between the HI asymmetry rate in our pair and isolated galaxies with isolated samples in the literature.

Galaxy sample	Sample size	A_c > 1.26	Standard error
HI refined subsample (Espada et al. 2011)	166	9%	2.2%
Haynes et al. (1988)	104	9%	2.8%
Matthews et al. (1998)	30	17%	6.8%
HI isolated sample (Bok et al. (2019))	304	18%	2.2%
HI-optical pair sample (Bok et al. (2019))	304	27%	2.6%

in their asymmetry measure.) The 2σ level is measured to be at $A_c = 1.26$, above which 9 percent of the sample lies. Espada et al. (2011) make a direct comparison with the Haynes et al. (1998) isolated sample, showing their asymmetry distribution to also follow a Gaussian of width 0.13, again with 9 percent of the sample having an A_c value > 1.26. Making the same direct comparison between our samples and the HI refined sub-sample, we find that both our isolated and pair samples exhibit higher HI profile asymmetries (see table 2.2). Approximately 18 percent of our isolated profiles have measured A_c values > 1.26, while 27 percent of pairs lie in this asymmetry regime. We note, however, that while the Gaussian fit is in good agreement with Espada et al. (2011)'s data for the lower asymmetry regime, it does not very accurately recover the high asymmetry tail (see figure 9 in the Espada et al. (2011) paper). Using the A-D test to compare our isolated sample with that of Espada et al. (2011) we do find the samples to be significantly different (A^2=5, p-value= 0.0005). We note, however, that our isolated sample is more similar to the HI refined sample than our pair sample. We also measure a particularly large difference of $A^2 = 22.18$ (p-value = 0.00002) between our pair sample and the HI refined sample. The discrepancy between our isolated sample and those isolated samples in the literature may well be attributed to systematics (different telescopes, resolution, smoothing, sample size). In this regard the HI refined sub-sample is likely more reliably isolated as the AMIGA team perform a number of follow up observations in different wavebands to more thoroughly ascertain the environment around each galaxy. The Matthews et al. (1998) sample of field galaxies, in comparison to the above-mentioned isolated samples, has 17 percent of its HI profiles measuring HI asymmetries greater than $A_c = 1.26$. While the Matthews et al. (1998) sample is indeed very small, this fraction is more similar to the fraction we measure for our own isolated sample, and suggests that perhaps our isolated sample might be better described as a sample of field galaxies rather than a strictly isolated sample (such as the AMIGA sample). This, however, does not detract from the fact that whether we compare our pair sample asymmetries with our own isolated sample, or with isolated/field samples from the

literature, we observe enhanced HI profile asymmetries for galaxies that are in close pairs. We further argue that due to the potential sensitivity of the asymmetry measurement to systematics, such a comparison is best made when comparative samples are drawn from the same data set. We note the possibility that using the ALFALFA heliocentric velocity to mark the center point of our HI profiles might lead to an underestimate of the profile asymmetry in the case of very asymmetric profiles. ALFALFA define v_{Helio} as the midpoint between the channels at which the flux density drops to 50 percent of each of the two peaks at each side of the spectral feature. If these two velocity values are not placed symmetrically about the true systemic velocity, the derived v_{Helio} is shifted closer to the v_{50} value that is most asymmetric compared to the true systemic velocity- this reduces the quantified profile asymmetry. Since this effect acts to reduce the measured asymmetry, our quantified asymmetries would in the worst cases, be underestimated. However, this should affect profiles in both the isolated and pair samples in the same way. Since our most asymmetric profiles reside in the pair sample, we pose that quantifying this effect would only enhance the difference we measure between the pair and isolated profile asymmetries, and strengthen our result.

Going forward we plan to explore what other mechanisms might be causing HI profile asymmetries. For a sample of 13 HI Magellanic type spiral galaxies, 4 of which have companions, Wilcots & Prescott (2004) found very little difference in the measured HI profile asymmetries between the apparently interacting galaxies and non-interacting galaxies. We point out, however, that the Wilcots & Prescott (2004) sample is very small (only 13 galaxies), and that the optical companions they mention were not spectroscopically confirmed. Wilcots & Prescott (2004) also find no correlation between optical and HI asymmetries for their sample. Using optical asymmetries from the Matthews et al. (1998) catalogue of 2D photometric decompositions of the SDSS-DR7 spectroscopic main galaxy sample, we also find no correlation between the optical and HI asymmetries for both our pair and isolated samples. These results suggest that perhaps asymmetries measured in HI trace merger activity on a different time scale to optical asymmetries. Espada et al. (2011) find for a sample of 166 HI galaxies that HI profile asymmetries seem to persist even in the absence of companions. A larger sample is our own isolated galaxy sample (358 galaxies), for which we also measure significant profile asymmetries. These findings suggest an alternative asymmetry driver might be at play. We check the potential dependence of our measured profile asymmetries on the major/minor status of our pair stellar mass ratios, and find a spread of asymmetries for both our major and minor pairs, with only 5 pairs having stellar mass ratios > 2. Outflows and inflows, as well as asymmetric accretion of gas from the cosmic web (van Eymeren et al. 2011) are also proposed as potential candidates for causing HI profile asymmetries, for which deeper optical imaging of the sample is required in order to investigate further. In a future paper we will explore the possibility of time scales

playing a role in the apparent lack of correlation between optical and HI asymmetries, as well as alternative HI profile asymmetry drivers. We also plan to explore the possibility that our isolated sample is contaminated by real pairs incorrectly identified as isolated galaxies due to having faint companions not detected by SDSS. With deeper optical imaging we can also investigate the prevalence of faint companions in our isolated sample, and thereby produce a purer isolated sample with which to make the pair/isolated asymmetry comparison. We propose that a purer isolated galaxy sample will only enhance the difference we see in profile asymmetries across the paired and isolated galaxy environments. Future surveys such as WALLABY, LADUMA (Holwerda et al. 2011), and the APERTIF shallow and medium-deep surveys (Verheijen et al. 2009), will enable us to study the gas in galaxies in large samples with high spatial resolution, and out to redshifts higher than ever before. At the highest redshifts, however, galaxies will be unresolved spatially, and it is only the HI profile with which we will be able to study these early Universe galaxies. The work done here endeavours to maximize the amount of information we can extract from HI profiles such that when the SKA pathfinder data becomes available, we can begin to characterize the neutral gas content of galaxies over large redshift ranges, and thereby start to put together a more complete and observationally informed picture of galaxy evolution.

2.6 Summary

In summary, a first quantitative look into HI profile asymmetries in contrasting environments for large samples of paired and isolated galaxies shows that the asymmetry distributions of close pair and isolated galaxies are statistically, and significantly different, with the paired galaxy sample exhibiting an extended asymmetry tail toward higher asymmetries compared to the isolated asymmetry distribution. We see a stronger signal in the asymmetry difference when we compare our pair sample with isolated samples in the literature. The work done in this chapter suggests that merger activity is responsible for the observed higher frequency of high profile asymmetries in our close pair galaxy sample. We thus put forward that HI profile asymmetries measured in the high asymmetry regime ($A_c > 1.26$) could be used to infer potential merger activity. While imaging techniques might provide a more robust measure of merger activity, HI profile asymmetries provide a promising alternative that can already be applied to large samples of galaxies. Furthermore, in the absence of imaging data at high redshifts, employing HI profile asymmetries as an indicator of merger activity can allow us to estimate merger activity in the early Universe (soon to be probed in HI by SKA pathfinder telescopes), and test galaxy evolution models.

Acknowledgements

We thank the anonymous referee for their very useful and valuable comments which resulted in a greatly improved paper. We also thank Lourdes Verdes-Montenegro and Michael G. Jones for their very generous expert advice, which not only improved the quality of the paper, but strengthened our results. We thank Martha Haynes for her initial input in defining the project published here, as well as Andrew Baker for his contribution of ideas and guidance throughout the project. JB, SLB, and DGG acknowledge financial support from the National Research Foundation (NRF) of South Africa, JB additionally acknowledges support from the DST-NRF Professional Development Programme (PDP), the National Astrophysics and Space Science Programme (NASSP), and the University of Cape Town. This work utilizes data from Arecibo Legacy Fast ALFA (ALFALFA) survey data set obtained with the Arecibo L-band Feed Array (ALFA) on the Arecibo 305m telescope. Arecibo Observatory is part of the National Astronomy and Ionosphere Center, which is operated by Cornell University under Cooperative Agreement with the U.S. National Science Foundation. Funding for the SDSS and SDSS-II has been provided by the Alfred P. Sloan Foundation, the Participating Institutions, the National Science Foundation, the U.S. Department of Energy, the National Aeronautics and Space Administration, the Japanese Monbukagakusho, the Max Planck Society, and the Higher Education Funding Council for England. The SDSS Web Site is http://www.sdss.org/. In addition, we make use of data from the Sloan Digital Sky Survey (SDSS DR7). The SDSS is managed by the Astrophysical Research Consortium for the Participating Institutions. The Participating Institutions are the American Museum of Natural History, Astrophysical Institute Potsdam, University of Basel, University of Cambridge, Case Western Reserve University, University of Chicago, Drexel University, Fermilab, the Institute for Advanced Study, the Japan Participation Group, Johns Hopkins University, the Joint Institute for Nuclear Astrophysics, the Kavli Institute for Particle Astrophysics and Cosmology, the Korean Scientist Group, the Chinese Academy of Sciences (LAMOST), Los Alamos National Laboratory, the Max-Planck-Institute for Astronomy (MPIA), the Max-Planck-Institute for Astrophysics (MPA), New Mexico State University, Ohio State University, University of Pittsburgh, University of Portsmouth, Princeton University, the United States Naval Observatory, and the University of Washington.

Chapter 3

HI study of isolated and pair galaxies: the MIR SFR-M★ sequence

This chapter is based upon the work of Bok et al. (2020), which was published in MNRAS in 2020 (J. Bok, R.E. Skelton, M.E. Cluver, T.H. Jarrett, M.G. Jones, and L. Verdes-Montenegro, "HI study of isolated and pair galaxies: the MIR SFR-Mstar sequence", 2020, MNRAS 499, 3193–3213.

Abstract

Using mid-infrared star formation rate and stellar mass indicators in *WISE*, we construct and contrast the relation between star formation rate and stellar mass for isolated and paired galaxies. Our samples comprise a selection of AMIGA (isolated galaxies) and pairs of ALFALFA galaxies with HI detections such that we can examine the relationship between HI content (gas fraction, HI deficiency) and galaxy location on the star-forming main sequence (SFMS) in these two contrasting environments. We derive for the first time an HI scaling relation for isolated galaxies using *WISE* stellar masses, and thereby establish a baseline predictor of HI content that can be used to assess the impact of environment on HI content when compared with samples of galaxies in different environments. We use this updated relation to determine the HI deficiency of both our paired and isolated galaxies. Across all the quantities examined as a function of environment in this work (SFMS location, gas fraction, and HI deficiency), the AMIGA sample of isolated galaxies is found to have the lower dispersion: $\sigma_{\rm AMIGA} = 0.37$ versus $\sigma_{\rm PAIRS} = 0.55$ on the SFMS, $\sigma_{\rm AMIGA} = 0.44$ versus $\sigma_{\rm PAIRS} = 0.54$ in gas fraction, and $\sigma_{\rm AMIGA} = 0.28$ versus $\sigma_{\rm PAIRS} = 0.34$ in HI deficiency. We also note fewer isolated quiescent galaxies, 3 (0.6%), compared to 12 (2.3%) quiescent pair members. Our results suggest the differences in scatter measured between our samples are environment driven. Galaxies in isolation behave relatively predictably, and galaxies in more densely populated environments adopt a more stochastic behaviour, across a broad range of quantities.

3.1 Introduction

The correlation between a galaxy's star formation rate (SFR) and its stellar mass (M$\star$) (the star-forming main sequence or SFMS) is well established, with numerous studies in the past decade demonstrating it to be both real, and able to provide keen insight into the processes driving star formation (SF) in galaxies (Noeske et al. (2007), Bouché et al. (2010), Lee et al. (2015)). The SFMS diagram shows a trend of increasing SFR with increasing M$\star$ that begins to plateau for M$\star$ > $10^{10.5}$ $M_{\odot}$ (Noeske et al. 2007). This value for stellar mass is where the break in the stellar mass-halo mass relation occurs via virial shock heating (Behroozi et al. 2013). As we look to higher redshifts, the shape of this relationship remains similar, however with the entire sequence evolving to higher SFRs (Lee et al. 2015, Whitaker et al. 2015, Speagle et al. 2014). The bulk of SF thus appears to have occurred earlier in massive galaxies compared to less massive systems (Noeske et al. 2007). For a spiral galaxy, any deviations from the main sequence likely indicate a break from secular evolution. Quenching events can cause a galaxy to drop suddenly below the SFMS, while a starburst phase will cause a galaxy to migrate upwards off the SFMS.

Galaxy structure is also correlated with SFR. Numerous observations have revealed star-forming galaxies to be less concentrated than quiescent galaxies at a fixed mass (Whitaker et al. 2015). The causal relationship between a galaxy's morphology and its SF history, however, is not well understood. The process by which a blue star-forming spiral galaxy transforms into a red and dead elliptical galaxy, the physical mechanism that quenches SF in galaxies, remains one of the biggest puzzle pieces still missing from our picture of galaxy evolution. Current theories for what shuts down SF in galaxies can be categorized into two main classes, internal processes (starburst and AGN feedback (McNamara et al. 2000, McNamara & Nulsen 2007, Cicone et al. 2014), mass quenching, and "morphological quenching" (Martig et al. 2009)) and external processes, e.g. harassment (Moore et al. 1995), ram-pressure stripping (Gunn & Gott 1972), viscous stripping (Nulsen 1982), and strangulation (Peng et al. 2015). In contrast to quenching, starburst galaxies are also observed. During starburst events galaxies undergo rapid SF causing them to jump upwards off the SFMS (Rodighiero et al. 2011, Elbaz et al. 2011, Schreiber et al. 2015). These events are short lived, and galaxies likely ultimately settle back onto the SFMS, however with substantial additional mass. The circumstances leading to such events remain unclear, as well as the prevalence of this phenomenon.

McPartland et al. (2018), in their investigation into quenching via internal processes, found the SFR-M$\star$ relation to be linear for a sample of star-forming galaxies from the DR7 SDSS catalogue with $H\alpha$-derived SFRs. Inclusion of Composite, Seyfert 2, and LINER galaxies on

the SFMS, however, produces a flattening in the relation at M$\star$ > $10^{10.5}$ M$\odot$, beyond which a negative slope is observed. Furthermore it was found that the reddest galaxies with the largest B/T ratios had SFRs > 1.5 dex below the SFMS, leading McPartland et al. (2018) to conclude that the quenching of SF in massive galaxies is strongly associated with AGN activity, with bulge growth an important pathway to this quenching. Similar results are reported by Morselli et al. (2018) who studied the spatial distribution of both stellar mass and SF activity in a sample of 712 galaxies at 0.2<z<1.2 (excluding AGN and merging systems) from the GOODS field (Giavalisco et al. 2004) with high resolution UV data from the Hubble Deep UV Survey. Galaxies above the SFMS were found to be more extended compared to their SFMS counterparts at fixed stellar masses, while galaxies below the SFMS, where SF was centrally suppressed, were mostly bulge-dominated. Quiescent galaxies, defined as those lying 1 dex below the SFMS, exhibited the highest instances of central SF suppression. With SF centrally enhanced and suppressed in galaxies above and below the SFMS respectively, the results of Morselli et al. (2018) support the scenario in which galaxies quench from the inside out.

Wang et al. (2018) also investigated the link between galaxy structure and quenching, and incorporate the role of HI in their study. Using a sample of ~1600 galaxies from the NASA-Sloan-Atlas catalogue within the ALFALFA footprint, Wang et al. (2018) investigated the two-step quenching scenario of compaction and quenching by comparing SFRs of compact star-forming galaxies (cSFGs) with extended star-forming galaxies (eSFGs). It was found that at fixed stellar mass the cSFGs exhibited similar or slightly higher SFRs compared to the eSFGs, as well as higher gas-phase metallicities. Moreover, the eSFGs were found on average to be more gas rich than the cSFGs, and had a median HI gas-depletion timescale of ~8 Gyr compared to a median gas depletion of time of ~4 Gyr for the cSFGs. With the environments of the eSFGs and cSFGs indistinguishable in their sample, Wang et al. (2018) conclude that galaxies evolve from eSFGs to cSFGs before joining the quenched population via an environment independent scenario of compaction and quenching. Bitsakis et al. (2019) looked at the SFMS for galaxies from the CALIFA survey and found the cessation of SF to be the combined result of gas deficiency and the inefficiency of the remaining gas to form new stars. The authors attribute the latter to the build-up of a bulge component (morphological evolution). In their exploration of alternative SF suppression mechanisms, Bitsakis et al. (2019) found that the action of bars, AGN activity, local galaxy environment, as well as galaxy mergers, have only temporary effects on current SF, and are not responsible for the permanent quenching of SF.

Studying SF as a function of redshift, Tacconi et al. (2013) find molecular gas content principally responsible for the cosmic evolution of the SFR. Using CO measurements provided by the PHIBSS survey and looking at the SFMS from the perspective of molecular gas content,

Tacconi et al. (2018) view gas fraction as a measure of a galaxys' gas accretion rate (regulated by mergers/fluctuations in gas transport along the cosmic web), and SF efficiency as related to internal galaxy properties. Their study shows SF efficiency to remain roughly constant as stellar mass increases, while gas fractions decrease. These results again point to the importance of considering the gas components of galaxies when seeking to understand their location above, below, or on the SFMS.

The above mentioned studies have thus far either neglected galaxy environment, or found it to be unimportant with respect to the quenching of SF. Cochrane & Best (2018), however, find strong evidence for environment-driven quenching in satellite galaxies. Probing the roles of mass and environment quenching in galaxy evolution, Cochrane & Best (2018) studied the relationship between halo mass, stellar mass, and SFR using the pioneering cosmological hydrodynamical simulation, EAGLE. Ellison et al. (2010) also look at the role of environment in enhancing/suppressing SF by studying galaxy pairs in SDSS. Instances of triggered SF were only observed in low-to-medium density environments, which the authors attribute to the higher gas fractions typical of low density environments, while mergers in high density environments are mainly without SF. The recent study of Pearson et al. (2019) compared SFRs between large samples of merging and non-merging galaxy systems from the KiDS and CANDELS imaging surveys. While large differences in SFR were occasionally observed, galaxy mergers in general were found to have little impact on SFRs, causing only minor shifts of ~ 0.1 dex above and below the SFMS. Moon et al. (2019) further investigate the influence of companions on SFR by considering different types of companions, namely SF companions versus quiescent. Their study shows quiescent neighbours acting to suppress SF in their counterparts, while SF neighbours enhance SF in their companions. Both effects are enhanced as the projected separation between companions is reduced. An earlier study by Xu et al. (2010) studied SFR enhancement in close galaxy pairs in the Local Universe, however distinguished between spiral pairs (S+S) and spiral galaxies paired with ellipticals (S+E). No enhancement in SFR was observed in the S+E pairs, and the SFR enhancement observed in the S+S pairs was shown to be highly mass dependent, with significant SFR enhancement only occurring in massive ($M_\star > 10^{10}$) S+S pairs. A follow up study by Xu et al. (2012) revealed a negative cosmic evolution of SFR enhancement in S+S pairs, and attribute this to the trend of increasing gas fraction with redshift. In high gas fraction scenarios the gas disk experiences less gravitational torque from the stellar disk, and less disk gas is funnelled to the nucleus via loss of angular momentum.

While the literature reports conflicting conclusions as to the role of environment in determining a galaxy's location on the SFMS (above or below, enhanced/suppressed SF), the location of isolated galaxies on the SFMS has yet to be determined. Constructing a sample of truly isolated

galaxies is a non-trivial endeavour, one to which the AMIGA project (Analysis of the interstellar Medium in Isolated GAlaxies; Verdes-Montenegro et al. (2005)) is dedicated. The AMIGA project is an in depth multiwavelength study of isolated galaxies in order to distinguish galaxy properties arising from secular evolution, from those which result from external influences (see §2.1 for details). It can thus be used to probe how galaxy interactions might enhance/suppress SF, which we ascertain by their location on the SFMS diagram relative to the baseline AMIGA SFMS.

A key objective of this work is to construct a SFMS for isolated galaxies that can be used as a reference for different galaxy samples to probe the role of environment in governing galaxy location on the SFMS. In this way we also seek to gain insight into the processes responsible for the shutting down of SF in a nurture-free environment, where one is unable to point the finger at an interfering companion. Since interacting systems are inherently dusty by nature, construction of our SFMS makes use of MIR indicators in *WISE* (W3 is sensitive to warm dust) to compute stellar masses and SFRs. Details of these measurements can be found in §3.

This paper is organised as follows: Our sample selection and data is described in §3.2, and the updated AMIGA HI scaling relation is presented in §3.3. We put forward and discuss our results in §3.4, namely the SFMS for our isolated and paired galaxies in §3.4.1, gas fraction in §3.4.2, and HI deficiency in §3.4.3. In §3.5 we discuss the relationship between gas (gas fraction and HI deficiency) and quenching in galaxies. Our main results and conclusions are summarised in §3.6. Throughout this paper we adopt a ΛCDM cosmology with $H_0 = 70$ km s^{-1}Mpc^{-1}, $\Omega_M = 0.3$, and $\Omega_\Lambda = 0.7$.

3.2 Sample

3.2.1 Sample of isolated galaxies

Our sample of isolated galaxies comprises galaxies selected from the AMIGA project. The AMIGA project provides the most extensive multiwavelength study of a well defined sample of isolated galaxies drawn from the Karachentseva (1973)'s Catalogue of Isolated Galaxies (CIG). The original criteria of Karachentseva (1973) classify a galaxy as isolated only if it is separated (in projection) from any neighbouring galaxy of isophotal diameter of between 1/4 and 4 times its own diameter (in B-band) by at least 20 times the diameter of the potential neighbour, that is, it is separated from the largest of these potential neighbours by at least 80 times its own diameter. As part of the AMIGA project the degree of isolation was first re-evaluated by Verley et al. (2007a) by analysing Digitised POSS-I E images of each CIG galaxy and constructing a catalogue of potential neighbours. Quantification of the degree of isolation was introduced

by Verley et al. (2007b) by way of two complimentary isolation parameters, namely η and Q, which measure the projected surface density of neighbours out to the 5th nearest neighbour and the tidal force exerted by neighbouring galaxies, respectively. Cuts based on these two parameters were enforced to eliminate any outlying cases which may not be strictly isolated. In addition any CIG with a heliocentric redshift of less than 1500 km/s was removed as isolation is difficult to ensure for such nearby targets as a very large sky area must be considered. This left ~700 galaxies in the AMIGA sample that adhere to strict isolation criteria such that for the past ~3 Gyr they are unlikely to have interacted with any neighbour of significant mass (Verdes-Montenegro et al. 2005). Argudo-Fernández et al. (2013) reassessed the isolation of AMIGA galaxies using both photometric and spectroscopic data from the ninth data release of the Sloan Digital Sky Survey (SDSS-DR9). The η and Q metrics were recalculated based on the SDSS images, which led to an additional 16 per cent of the CIG galaxies failing the isolation criteria due to fainter neighbours being identified in the SDSS images. However, in the fields with spectroscopic data the same metrics were recalculated, but with the requirement that any neighbours must be within 500 km/s in redshift, which resulted in an equivalent fraction of the CIG galaxies being classified as isolated as in Verley et al. (2007a). Furthermore, galaxies that are classified as isolated by one of these works are not necessarily classified as isolated in the other. Therefore, given that the Verley et al. (2007b) analysis covers the full sample, whereas Argudo-Fernández et al. (2013) misses a significant fraction due to the limits of the SDSS footprint, we draw our sample of isolated galaxies from the ~700 galaxies that meet the Verley et al. (2007b) criteria. The AMIGA team have further characterized the different components/phases of the interstellar medium (ISM) of these isolated galaxies, as well as their stellar components, in various different wavelengths, including a) optical (Verdes-Montenegro et al. 2005), b) FIR (Lisenfeld et al. 2007), c) radio-continuum (Leon et al. 2008), and d) Hα emission (Verley et al. 2007a), as well as e) nuclear activity (Sabater et al. 2008; 2011). (Full details of the AMIGA project and their extensive research on isolated galaxies are available at http://amiga.iaa.es)

HI data is available for a sub-sample of the full AMIGA catalogue, the AMIGA HI science sample (Jones et al. 2018). We restrict our study to the HI science sample to assess the role of HI in determining the SFMS locations of our isolated galaxies. The AMIGA HI science sample (Jones et al. 2018) is an HI subset of Karachentseva (1973)'s 1050 CIG galaxy catalogue. HI spectra from the literature were compiled for 415 of these galaxies (see Table 1 in Jones et al. (2018) for observation details), and AMIGA conducted their own observations of 488 galaxies using the Arecibo, Effelsberg, Greenbank, and Nançay radio telescopes. (A summary of the AMIGA HI observations is displayed in Table 2 of Jones et al. (2018).) 429 of the 488 CIG galaxies observed by AMIGA made it into the HI catalogue, and together with the 415

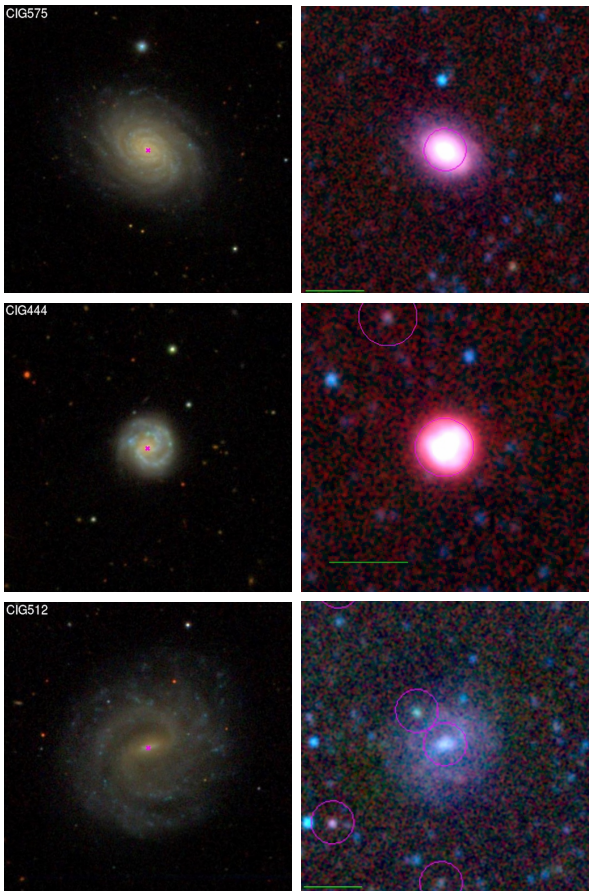

Figure 3.1: 3.5'x 3.5' SDSS cutouts (left column) of galaxies from the AMIGA-*WISE* sample with the corresponding *WISE* images shown alongside (right column). The green line in each *WISE* image marks a 1' scale, magenta ellipses mark the location of the primary galaxy in each image, as well as any potential galaxy candidates in the field.

galaxies with spectra published in the literature, the final AMIGA HI science sample comprises 844 galaxies in total. All spectral parameters of this catalogue were extracted using the same fitting method, including the cases where existing observations from the literature were used, and as such this catalogue is considered a highly uniform HI database of isolated galaxies. Jones et al. (2018) further provide cuts to the HI sample based on completeness, isolation, and profile quality. For the purposes of our study we select only those galaxies within the complete AMIGA HI science sample that have been flagged as reliably isolated, with high quality HI profiles (544 galaxies in total). Morphological classification of the AMIGA sample conducted by Sulentic et al. (2006), and later revisions by Buta et al. (2019), show the AMIGA sample to be spiral galaxy dominated, specifically intermediate to late type (Sb-Sc). A photometric analysis conducted by Durbala et al. (2008) revealed the sample to be more symmetric, less concentrated, and less clumpy when compared to galaxies selected without isolated criteria.

3.2.2 HI pair sample

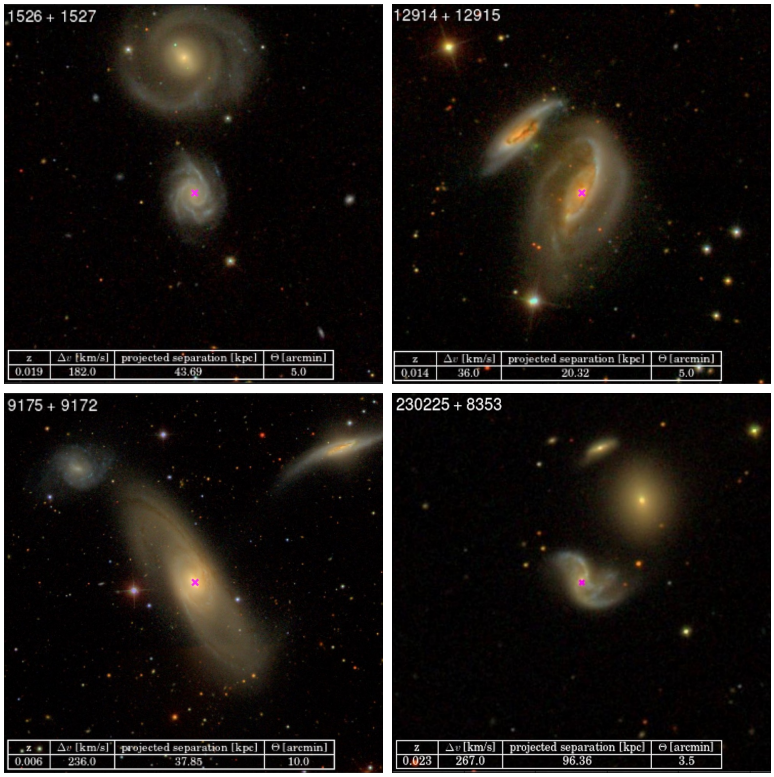

Figure 3.2: SDSS cutouts of 4 galaxy pairs from the HI pair sample. In each image the redshift, velocity [km s^{-1}] and projected [kpc] separation between the pair members, as well as the field of view of the image, are tabulated in the bottom left corner. We note that the galaxy pairs shown in the bottom panel are in fact members of groups.

For an environmental comparison to our isolated galaxy sample we construct a catalogue of close HI pair galaxies from the Arecibo Legacy Fast ALFA (ALFALFA) survey (Giovanelli et al. 2005), namely the α70 catalogue, for which integrated HI profile masses are also available. Details of the catalogue are discussed in Haynes et al. (2011) and Haynes et al. (2018). We use projected (Δr) and velocity (Δv) separations to identify a sample of potentially interacting HI galaxies to compare the impact of interactions on gas supply and SF on the SFR/M$\star$ sequence. We do not exclude triples, compact groups, and groups, but rather impose a minimum environment condition that each galaxy in our sample has at least one nearby HI neighbour. We only consider pairs in which both components have a minimum integrated HI profile mass of 10^9 $M_\odot$, marking the steep cut off in HI mass below which ALFALFA detects relatively few galaxies. A step-by-step description of our pair finding method follows here:

1. For each α70 galaxy ($M_{HI} > 10^9$ $M_\odot$) flagged as being reliably detected and with a spectroscopic counterpart in SDSS DR7 (primary galaxy), we compute the two dimensional distance (in degrees) to its nearest α70 neighbour (secondary galaxy) satisfying the same criteria. As a consequence of this selection criterion our sample is biased towards spiral+spiral pairs, with spiral+elliptical pairs making it into the sample less frequently.

2. This distance is then converted to an angular separation using kpc/" conversions calculated at the redshift of the primary galaxy.

3. The velocity separation is then computed for each pair using spectroscopic redshifts in SDSS. Photometric redshifts are highly uncertain compared to spectrocscopic redshifts, therefore insisting upon spectroscopic redshifts minimizes uncertainty in the calculation of Δv, and hence the potential for spurious pairs being introduced into our sample.

4. We construct our sample of interacting galaxies from those pairs for which the projected separation is less than 100 kpc, and Δv is less than 1000 km s^{-1}, with a minimum angular separation of 5". Our Δr and Δv cuts match the broadest selection used by Robotham et al. (2014) to denote 'close pair galaxies'. We note that a Δv of 1000 km s^{-1} is more indicative of galaxies in the same group/large scale structure, however, very few of our pairs have velocity separations exceeding 800 km s^{-1}, with the majority of the sample having $\Delta v < 400$ km s^{-1}.

We find a sample of 282 gas rich pairs in total, in which there are 7 incidents of multiplicity (galaxies paired with more than one galaxy), and therefore 557 unique pair members. As a result of the requirement that both pair candidates have $M_{HI} > 10^9$ $M_\odot$, the resulting pair sample comprises mainly systems with stellar mass ratios ~ 1. A quick qualitative visual inspection of the HI pair sample demonstrates that it is similarly spiral galaxy dominated, however with the inclusion of notably more interesting and irregular morphologies as well. We also note a range of local environments including isolated pairs, triples, and compact group candidates. While this paper focusses solely on differences in quantities measured between isolated galaxies and a control sample of galaxies that are in close arrangements (primarily pairs), we will address in detail the role of local environment in an upcoming paper where we quantitatively establish the local environments of our HI pair sample. Optical and MIR images of galaxies from the AMIGA sample are shown side by side for reference in Figure 3.1, and optical images of some example galaxies from our pair sample are shown in Figure 3.2.

HI blending in the pair sample

Of the ALFALFA pairs sample approximately 50% of the galaxies were noted as being in some form of blend with their neighbour(s) when source extraction was performed by the ALFALFA

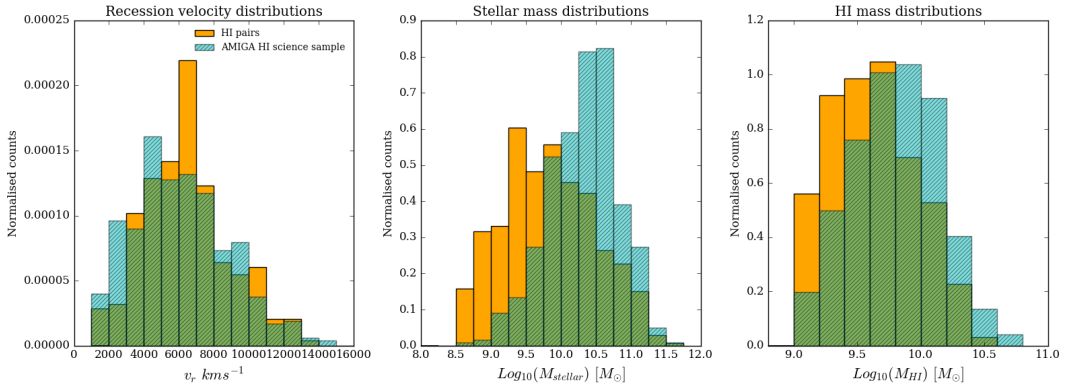

Figure 3.3: From left to right: v_r, M$\star$, and M_{HI} distributions of the AMIGA HI science sample (cyan) and HI pair (orange) samples.

team. Given the approximately 3.5' beam of the Arecibo telescope in the L-band and the close proximity of the pairs considered, this high rate of blending is not unexpected. For approximately 3/4 of the blends the human extractor from the ALFALFA team reported that the sources were separable to some degree, and thus that the sources parameters should not be heavily biased. The ALFALFA team performed this separation either by careful tailoring of the extraction box, both on the plane of the sky and in velocity space, or in more severe cases by interpolating over heavily affected regions of the source profile. The HI spectra of our pairs were all individually inspected and those with significant signs of blending were removed (49 galaxies in total). It should be noted that the removal of blended galaxies was done on an individual basis, rather than considering a pair as a single object. This is because in pairs with large mass ratios, blending can be severe for the smaller member, but almost negligible for the larger member. In these cases, although the HI properties of the smaller member may be unusable, the larger member is still in a pair and therefore belongs in the sample. We do not exclude these galaxies when only their location on the SFMS is considered as their stellar masses and SFRs, measured by *WISE* with its 6″ (W1) and 7.1″ (W3) beams (Jarrett et al. 2012), are still valid. We mark the location of these sources on the SFMS in Figure 3.6 by blue squares, and discuss a few representative cases in Appendix B.

3.2.3 Mass cuts

The recession velocities, M$\star$, and M_{HI} distributions of the AMIGA-*WISE* and HI pair samples are shown in Figure 3.3. While both samples probe a similar recession velocity range, we note fewer AMIGA-*WISE* galaxies occupying the lower M$\star$ and M_{HI} bins compared to the pair sample. We attribute the missing dwarfs in AMIGA to the particular isolation criterion used in which galaxies below 1500 km $s^{-1}$are excluded so as to avoid searching a prohibitively large area of sky for neighbours (See Verley et al. (2007a) for details on the isolation criteria). Due to

Table 3.1: Size of isolated galaxy sample after each successive cut.

	Sample size
HI Science sample	544
with WISE measurements	518
$M_{HI} > 10^9 M_\odot$	482
$M_\star > 10^{8.5} M_\odot$	481

Table 3.2: Size of HI pair sample after each successive cut.

	Sample size
Close HI pairs	282
unique pair members (with $M_{HI} > 10^9 M_\odot$)	557
$M_\star > 10^{8.5} M_\odot$	531

their low luminosity, dwarfs are only likely to be detected if they are nearby, excluding nearby galaxies therefore specifically excludes dwarfs from the AMIGA sample. To mitigate the effect of missing dwarfs in our AMIGA sample when we compare them with our pair sample we implement a stellar mass cut of $M_\star > 10^{8.5}$ $M_\odot$ across both the AMIGA and HI pair samples. Very few AMIGA galaxies exist below this stellar mass limit, and the HI pair galaxies in this low mass regime correspond to the sources with the largest uncertainties in both their stellar mass and SFR measurements. Exclusion of these low mass sources improves the quality of our study by minimizing uncertainty, and ensuring the two samples are comparable. Our final AMIGA sample comprises 481 galaxies, which we refer to as the AMIGA-*WISE* sample, while 531 galaxy pair members in our HI pair sample survive the stellar mass cut. We further refine and control our analysis by mass-matching our two samples in stellar mass. Our mass-matched samples are created by randomly selecting equal numbers of galaxies in each stellar mass bin. The number of galaxies chosen in each bin is dictated by the sample with the least amount of galaxies available in the bin. The final sample selection criteria are summarized in Tables 3.1 and 3.2 for the isolated and pair samples respectively.

3.2.4 *WISE* colours and AGN activity

In Figure 3.4 we make use of the *WISE* colour-colour diagram as a diagnostic for estimating galaxy activity in our samples, with which galaxy morphology is largely correlated. (See §5.3.3 and Figure 26 in Jarrett et al. (2011) and Jarrett et al. (2019) for a full description of the *WISE* colours and what they indicate.) Gray arrows mark the upper limits, and the galaxy sequence derived by Jarrett et al. (2019) is overlaid in red. The tightness of the AMIGA-*WISE* sample

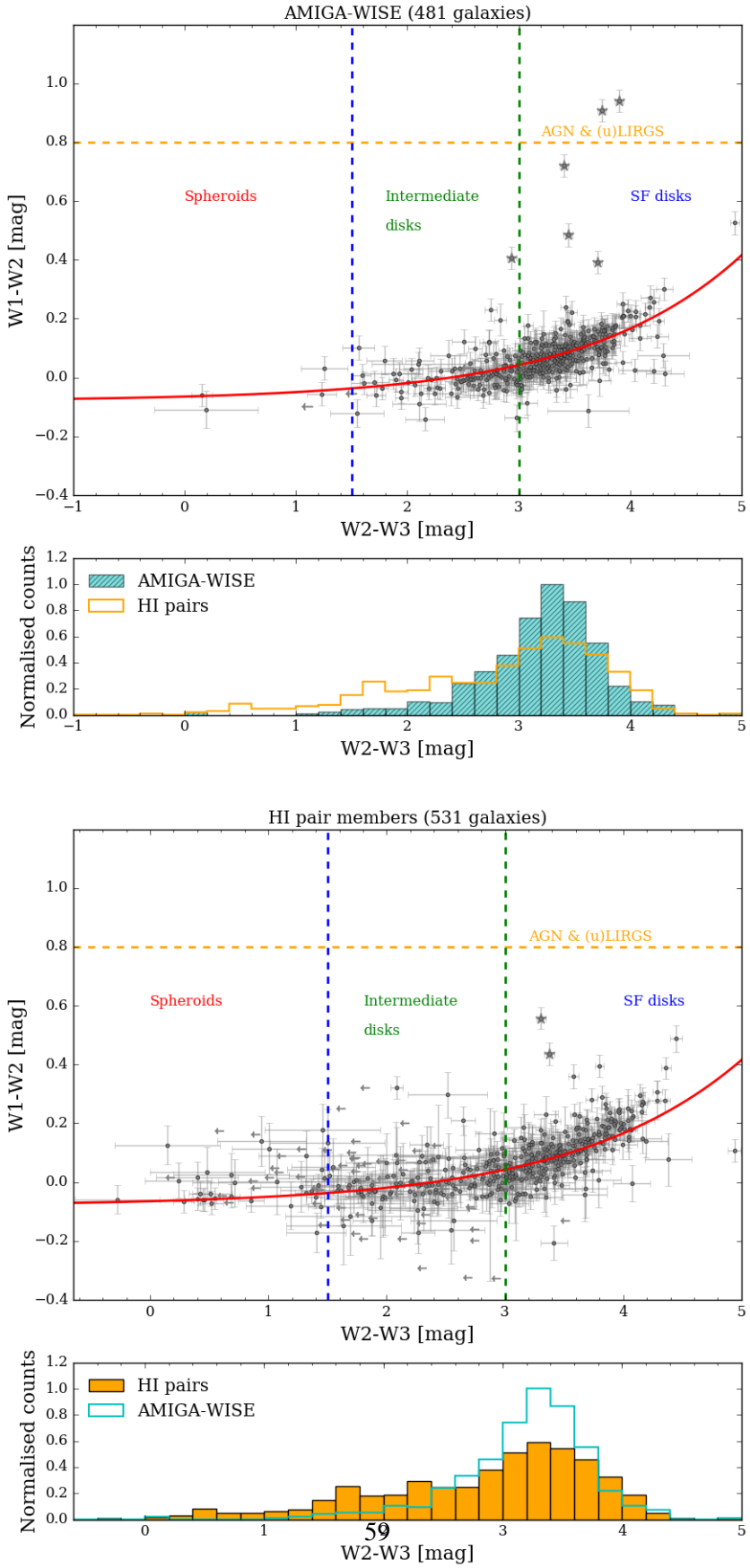

Figure 3.4: *WISE* colour−colour diagrams for both the AMIGA-*WISE* (left) and HI pair (right) samples, with the corresponding W2-W3 histogram distributions indicated below each diagram. Upper limits are depicted by gray arrows, and the red curve marks the SFMS of Jarrett et al., (2019). MIR AGN candidates are indicated by stars.

sequence is reflected in the corresponding histogram of W2-W3 color (cyan histogram), which appears to have a single peak in the star-forming disk region of the diagram. In contrast we see more colour diversity in the HI pair sample, not only in the broader distribution and larger scatter of galaxies on the colour-colour diagram, but also in the W2-W3 distribution (orange histogram). The increased scatter we observe in the pair sample relative to AMIGA appears to arise from photometric uncertainties, not to mention systematics that may arise from the fact that the pairs are in complex systems, where deblending from a companion and (if applicable) from other group members is required. The higher frequency of upper limits in the pair sample indicate lower SFRs compared to AMIGA, hinting at the presence of a larger low/no star formation population compared to the AMIGA-*WISE* sample.

In the left panel of Figure 3.4 we identify 6 galaxies in the AMIGA-*WISE* sample that are "warm" in the MIR according to their location on the MIR colour-colour diagram (i.e. well above the galaxy sequence). These galaxies are indicated by stars in Figure 3.4. Sabater et al. (2008) classified 5 of these galaxies as AGN using FIR and radio continuum (CIG248, CIG692, CIG993, CIG671, and CIG1004). Of the 2 such candidates identified in the HI pair sample (right panel), NGC 5900 is also a known Seyfert galaxy. The remaining warm MIR galaxies have emission that may be star formation dominated, arise from dust-obscured AGN, or result from a combination of SF and AGN activity. Disentangling SF from AGN activity is non-trivial, however, for the purposes of this work, we conclude that due to the small number of identified AGN candidates, these galaxies are unlikely to affect our results in any substantial way, and thus disregard them as significant contaminators. Furthermore, their locations on the SFMS in Figure 3.6 (black stars) demonstrate that these galaxies are not outliers, and therefore do not skew our results.

3.2.5 *WISE* B/T measurements

Galaxy morphology is often quantified by decomposing the disk (rotational kinematics, younger populations) and bulge or spheroidal (random motions, older components) and comparing their integrated light properties. For WISE W1 (3.4μm) imaging, Jarrett et al. (2019) estimate the bulge and disk light fractions using the axi-symmetric radial distribution, modeled with a double Sersic profile consisting of the inner bulge and the extended disk components. For normal galaxies, the resulting near-infrared B/T (bulge-to-total) ratio should provide information on the stellar populations that comprise the bulk mass of the galaxy. Jarrett et al. (2019) showed that galaxies with passive or no SF have high ratios, B/T > 0.5, indicating dominant spheroidal populations, and conversely lower-mass star-forming galaxies have low ratios, B/T < 0.3, younger disk-dominated systems, while intermediate-transition galaxies have B/T ratios that range across the spectrum. Due to the large beam of WISE (6"), small and compact galaxies

have uncertain decompositions. The AMIGA-*WISE* and HI pair sample B/T measurements are presented and discussed in §3.5.

3.2.6 *WISE* stellar mass and SFR measurements

Any inference we make from a galaxy's location on the SFMS is only as valuable as the SFRs and stellar masses we use are accurate. To this end we make use of mid-infrared M$\star$ and SF indicators in *WISE* (Wide-field Infrared Survey Explorer; Wright et al. (2010) to supply reliable stellar masses and SFRs. The *WISE* W1 3.4μm and W2 4.6μm bands trace the stellar mass distribution in galaxies, and the W3 12μm and W4 22μm bands are sensitive to the ISM emission from star-forming galaxies, polycyclic aromatic hydrocarbons (PAH) and warm dust respectively (Jarrett et al. 2013, Cluver et al. 2017). Using total infrared luminosity (L_{TIR}) to calibrate the *WISE* W3 and W4 SFRs, Cluver et al. (2017) found W3 to be particularly good at tracing SFR, measuring a 1σ scatter in the relation of 0.15 dex over 5 orders of magnitude. Provided deep silicate absorption features and AGN are excluded, the W3 SFR can be considered reliable. The W4 relation has a slightly higher scatter in contrast (1σ = 0.18 dex), however both the W3 and W4 relations agree with radio continuum-derived SFRs, as well as the 'hybrid' Hα and FUV SFR indicators. In this paper, stellar masses are computed using a combination of the *WISE* W1 3.4μm and W2 4.6μm bands and corresponding mass-to-light ratios from Cluver et al. (2014), and SFRs are obtained using the W3 12μm band and Cluver et al. (2017) W3 relation (Equation 3.1).

$$\mathrm{LogSFR}(\mathrm{M}_{\odot}\mathrm{yr}^{-1}) = (0.889 \pm 0.018)\ \mathrm{LogL}_{12\mu\mathrm{m}}(\mathrm{L}_{\odot}) - (7.76 \pm 0.15) \tag{3.1}$$

Given the relatively large beam size of *WISE*, blending of galaxies is a general problem, and is addressed accordingly in the *WISE* characterization pipeline. We note that our HI pair sample includes de-blended measurements for 6 galaxy pairs, marked on the SFMS by red squares in Figure 3.6, which shows them all to be star-forming, and relatively high mass. Adequate de-blend solutions are measured for these galaxies, which are well within the scatter of SF-MS, and therefore not excluded from our analysis. Full details of the *WISE* de-blending process in general, as well as on a case-by-case basis, are discussed in Appendix A.

A comparison of the *WISE* stellar masses measured for our isolated sample and optical stellar masses calculated by Fernández Lorenzo et al. (2013) show them to be highly consistent, and as such we rule out uncertainty in the stellar masses as a significant source of bias.

3.3 An updated AMIGA HI scaling relation

In the seminal study of HI properties of isolated galaxies, Haynes & Giovanelli (1984) computed the HI scaling relation for 324 CIG galaxies. Using optical diameters as a proxy for stellar mass, this relation predicts the HI content of galaxies on the secular evolution track, and has been widely used since to determine the quantity 'HI deficiency' defined as:

$$\mathrm{DEF} = \log \mathrm{M}_{\mathrm{HI}}^{\mathrm{exp}} - \log \mathrm{M}_{\mathrm{HI}}^{\mathrm{obs}} \tag{3.2}$$

where $\mathrm{M}_{\mathrm{HI}}^{\mathrm{exp}}$ is the expected HI mass at a given stellar mass, and $\mathrm{M}_{\mathrm{HI}}^{\mathrm{obs}}$ is the HI mass observed.

With isolated galaxies providing a baseline for 'normal' HI content, computing this quantity for galaxies subject to various different environmental conditions allows one to gauge the impact of environment on HI content. A galaxy's environment might act to deplete it of its HI content, in which case a positive value for HI deficiency is measured, while negative values for HI deficiency indicate an excess of HI is present. A revised HI scaling relation was measured by Jones et al. (2018) using the AMIGA HI science sample. In addition to using a sample superior in both sample size (544 galaxies versus 324) and purity, Jones et al. (2018) also use a more sophisticated regression model to fit the scaling relations. They find that an isolated galaxy's HI content can be predicted by either its optical B-band luminosity or diameter with an accuracy of about 0.25 dex.

In this work we update the scaling relation of Jones et al. (2018) using *WISE* W1 3.4μm stellar mass measurements as an HI predictor. The relationship between stellar and HI mass is more commonly computed in the literature for different galaxy samples. Updating the scaling relation used to compute HI deficiency to rely on stellar mass allows for a direct comparison with various relations in the literature, as well as a direct assessment of how environment impacts HI content. In Figure 3.5 we illustrate our updated HI scaling relation using *WISE* stellar masses for the AMIGA HI science sample. We fit the HI scaling relation using the maximum likelihood method (for detections) described in Jones et al. (2018). This method incorporates the measurement uncertainties in both parameters and performs a 3σ rejection to remove outliers (which removed the 3 points significantly below the main relation). The resulting relation is described in Equation 3.3 and illustrated in Figure 3.5 as a thick black line.

$$\mathrm{Log}_{10}(\mathrm{M_{HI}})[\mathrm{M}_{\odot}] = 0.44 \times \mathrm{Log}_{10}(\mathrm{M}_{\star})[\mathrm{M}_{\odot}] + 5.19, \sigma = 0.33 \tag{3.3}$$

Pink shading indicates the 1σ offset of the relation, and the dark green line marks the fit of Parkash et al. (2018) for a sample of spiral galaxies. A galaxy's location on the $M_{\star}/M_{HI}$ plane above or below the relation suggests either an excess or deficiency in HI content relative to

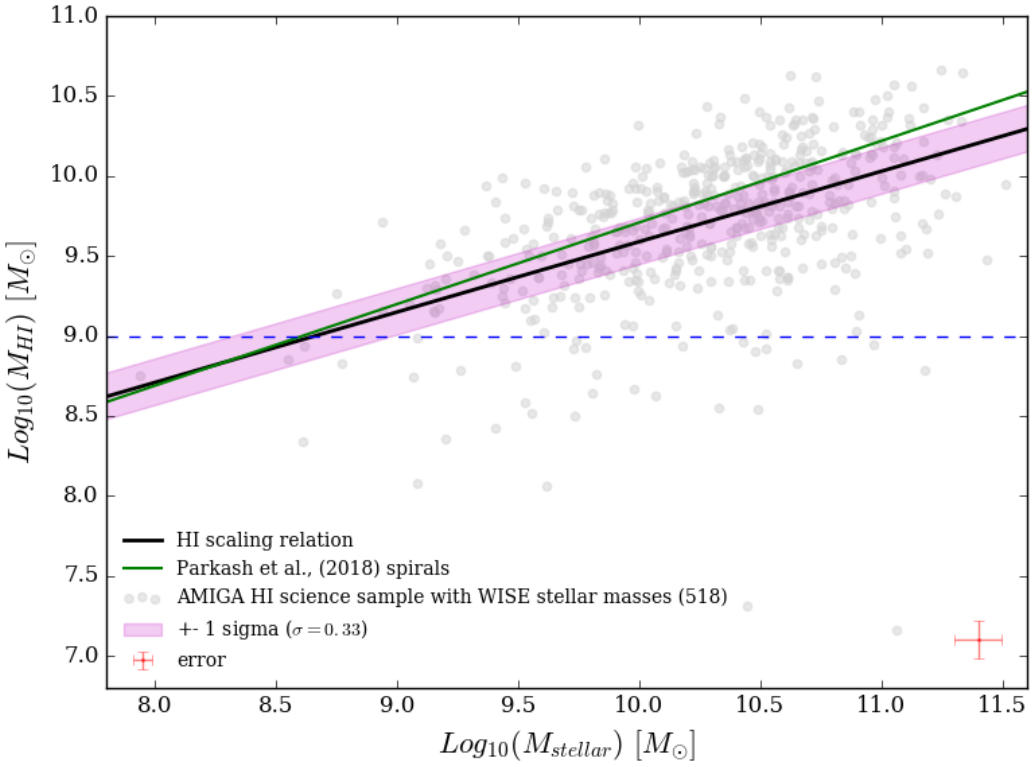

Figure 3.5: The HI scaling relation (solid black line) for the AMIGA HI science sample galaxies (gray points) with the 1σ region shaded in pink. The relation is described by the equation $Log_{10}(M_{HI})[M_\odot] = 0.44 \times Log_{10}(M_\star)[M_\odot] + 5.19$, σ= 0.33. The dark green line indicates the Parkash et al. (2018) HI scaling relation for spiral galaxies, and the dashed blue line marks the HI mass cut applied to both our isolated and pair samples ($M_{HI} > 10^9\ M_\odot$). Galaxies below this line are not included in the AMIGA-*WISE* sample.

what one would expect of a galaxy in a 'nurture free' environment. The scatter in this relation suggests there is some leeway in gas content via consumption and feedback evolution. Our isolated galaxy and pair samples lie above the horizontal dashed blue line as per the HI mass cut ($M_{HI} > 10^9 M_\odot$).

3.4 Results

3.4.1 The SFMS: Isolated galaxies vs. galaxy pairs

In Figure 3.6 we see the SFMS sequence for the full isolated galaxy (left) and pair (right) samples respectively. Upper limits on SFR are marked by gray arrows for sources that have been detected in W3, but show no signs of SF activity. These sources are bright and blue in the MIR, with continuum emission dominating the W3 band. The gray arrows most likely mark

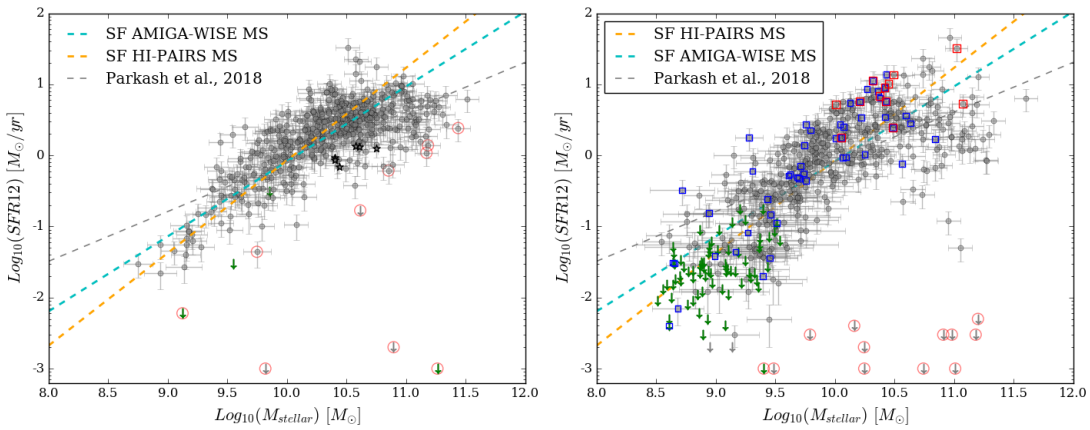

(a) AMIGA-*WISE* (b) HI pairs

Figure 3.6: The MIR SFMS. Upper limits on SFR are depicted by downward facing arrows (green indicates no W3 emission has been detected, and gray arrows indicate sources that have been detected in W3, but show no SF). Quiescent galaxies are circled in red, and black stars represent AGN candidates. The AMIGA-WISE, HI pair, and Parkash et al. (2018) SFMS lines are shown by cyan, orange, and gray dashed lines respectively. Instances of blending in WISE are marked by red squares, and blue squares identify instances of severe blending in HI that we remove from our HI analysis.

galaxies that are old and bulge-dominated in morphology. Green arrows mark the location of sources undetected in W3. No W3 emission in nearby galaxies indicates that the presence of dust re-emission from obscured SF is lacking or minimal, a condition not uncommon for dwarf galaxies. The AMIGA-*WISE* SFMS (cyan dashed line) relation is computed in HyperFit (Robotham & Obreschkow 2015) for a star-forming sub-sample of the full sample (474 galaxies) excluding upper limits and outliers. The HI pair SFMS relation (dashed orange line) is computed in the same way for a sample of 454 galaxies. The relations can be found in Equations 3.4 and 3.5 respectively.

$$\mathrm{Log_{10}(SFR_{12})[M_\odot yr^{-1}]} = 1.05 \times \mathrm{Log_{10}(M_\star)[M_\odot]} - 10.63, \sigma = 0.37 \tag{3.4}$$

$$\mathrm{Log_{10}(SFR_{12})[M_\odot yr^{-1}]} = 1.30 \times \mathrm{Log_{10}(M_\star)[M_\odot]} - 13.10, \sigma = 0.55 \tag{3.5}$$

Not only do we observe a flatter SFMS slope for the AMIGA-*WISE* sample, but also a reduced scatter. The steeper slope of the pair SFMS is indicating higher SF as a function of stellar mass, and is consistent with the findings of Ellison et al. (2010).

Focussing specifically on star-forming galaxies, however without any environmental selection, Speagle et al. (2014) report a general SFMS scatter of ~ 0.2 based on 64 SFMSs from

25 papers in the literature. We propose the significantly larger scatter we measure for our pair sample (σ= 0.55) is environment driven.

According to the Bluck et al. (2016) criterion for passive galaxies we note a significantly larger number of quenched galaxies in the pair sample compared to our sample of isolated galaxies (45 versus 12). These galaxies, which lie at least 1 dex below the SFMS relation, are circled in red in Figure 3.6. The larger population of quenched galaxies at high stellar masses in the pair sample perhaps hints at quenching via interaction. These galaxies lie primarily in the spheroid region of the MIR colour diagram with W2-W3 colours $<$ 2 mag. *WISE* colour images of these sources appear blue due to their emission being W1 3.4μm dominated.

In Figure 3.7 we plot the density contours of both samples. In the top two panels of the plot we see how the AMIGA-*WISE* sample (left) reaches higher densities compared to the HI pair sample (right), and peaks at a heavier stellar mass. We also note a more pronounced turnover and flattening out of the SFMS at M$\star$ $\approx$ $10^{10.5}$ $M_{\odot}$ in the pair sample (consistent with Noeske et al. (2007) and Behroozi et al. (2013)). In the bottom panel we overlay the AMIGA-*WISE* contours (black contours) on the pair sample filled contour plot for a more direct comparison of the samples. Here we see the AMIGA-*WISE* central density offset to higher stellar masses compared to the pair sample. A visual representation of the decreased scatter in the AMIGA-*WISE* SFMS (0.37 vs 0.55 for the pairs) is also apparent in the tightness of the AMIGA-*WISE* contours relative to the pair sample. Galaxies in isolation appear to behave in a relatively predictable manner, tightly confined to the SFMS. This is often referred to as'secular evolution' (Kormendy & Kennicutt 2004). Introducing companions into the environment appears to produce more stochastic behaviour on the SFR-$M_{\star}$ plane.

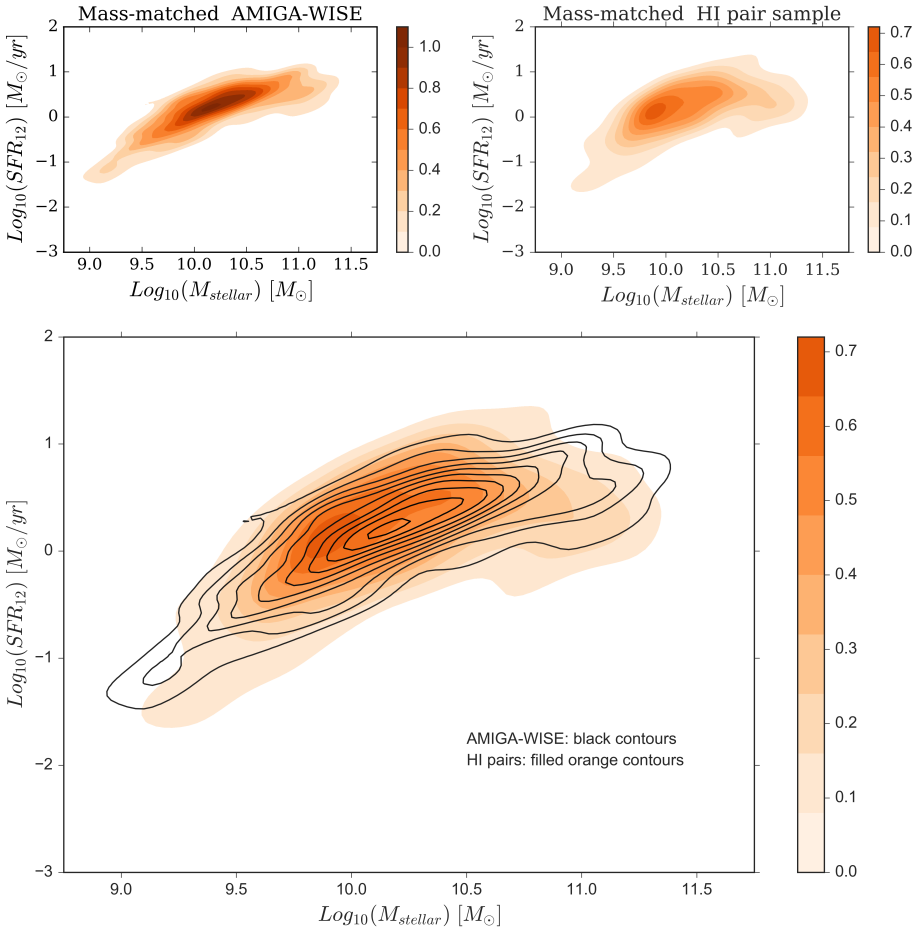

Figure 3.7: Top panel: Filled contour density plots of the AMIGA-*WISE* SFMS (left) and HI pair SFMS (right). Bottom panel: Filled contour density plot of the HI pair sample (filled orange contours) with the AMIGA-*WISE* contours overlaid in black.

3.4.2 Gas fraction on the SFMS

As per §2.2.1, 49 instances of severe blending in the HI pair sample are excluded from our HI analysis due to having unreliable HI data. In Figure 3.8 we plot the gas fraction distributions of both the original (left panels) and mass-matched (right) AMIGA-*WISE* (cyan) and HI pair (orange) samples. Here gas fraction is defined as $Log_{10}(M_{HI}/M_{star})$. In both panels the cyan histogram refers to the AMIGA-*WISE* sample and the orange histogram corresponds to the pairs, with cyan and orange dashed lines marking the corresponding distribution medians. Focusing first on the left panel, the original AMIGA-*WISE* and HI pair samples, the pair sample appears to be shifted towards higher gas fractions. We measure a median gas fraction value of -0.16 and σ = 0.58 for the pair sample, while a significantly lower median and sigma value is measured for the AMIGA-*WISE* sample, median = −0.51 and σ = 0.43. We note, however, that the

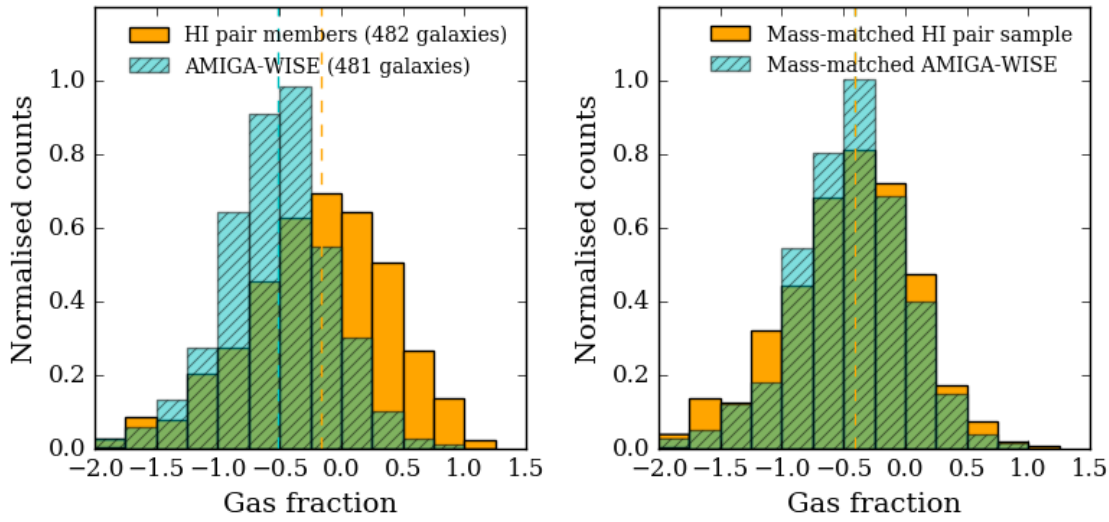

Figure 3.8: Gas fraction distributions for the full pair (orange) and AMIGA-*WISE* (cyan) samples are shown on the left, with the corresponding mass matched sample distributions on the right. Vertical dashed orange and cyan lines indicate the respective median gas fraction values for the pair and isolated galaxy samples. These lines merge to occupy the same location on the plot when the samples are matched in stellar mass.

distributions become very similar when the samples are matched in stellar mass (right panel). Here we see very similar medians for both samples, -0.42 and -0.47 for the AMIGA-*WISE* and HI pair samples, respectively. This highlights the importance of controlling for stellar mass as a driver of galaxy properties. The difference between the two mass-matched samples is however evident in the respective widths of the distributions. We can see by eye that the pair sample distribution is slightly broader than the AMIGA-*WISE* distribution, with a larger fraction of the pair sample occupying the higher and lower gas fraction bins. This is reflected by the corresponding measured sigma values: $\sigma_{\rm pairs} = 0.54$ vs $\sigma_{\rm A-W} = 0.44$. This means for a given stellar mass bin, the pairs show greater variation in gas fraction. Even though there is a scaling relation between stellar mass and HI mass, stellar mass does not appear to constrain the spread of gas fraction. The breadth in gas fraction could therefore be contributing to the increased scatter observed on the pair SFMS (see Figure 3.7).

Figure 3.9 shows how gas fraction behaves on the SFMS. We see similar trends of decreasing gas fraction with increasing stellar mass on the SFMS for both the AMIGA-*WISE* and HI pair samples. These results suggest that galaxies, regardless of environment, build up their stellar mass content while their HI reservoirs are correspondingly depleted, in agreement with the work of Saintonge et al. (2016). The sample of Saintonge et al. (2016) lacks any pre-selection against environmental features and the same trend of decreasing gas fraction along the SFMS

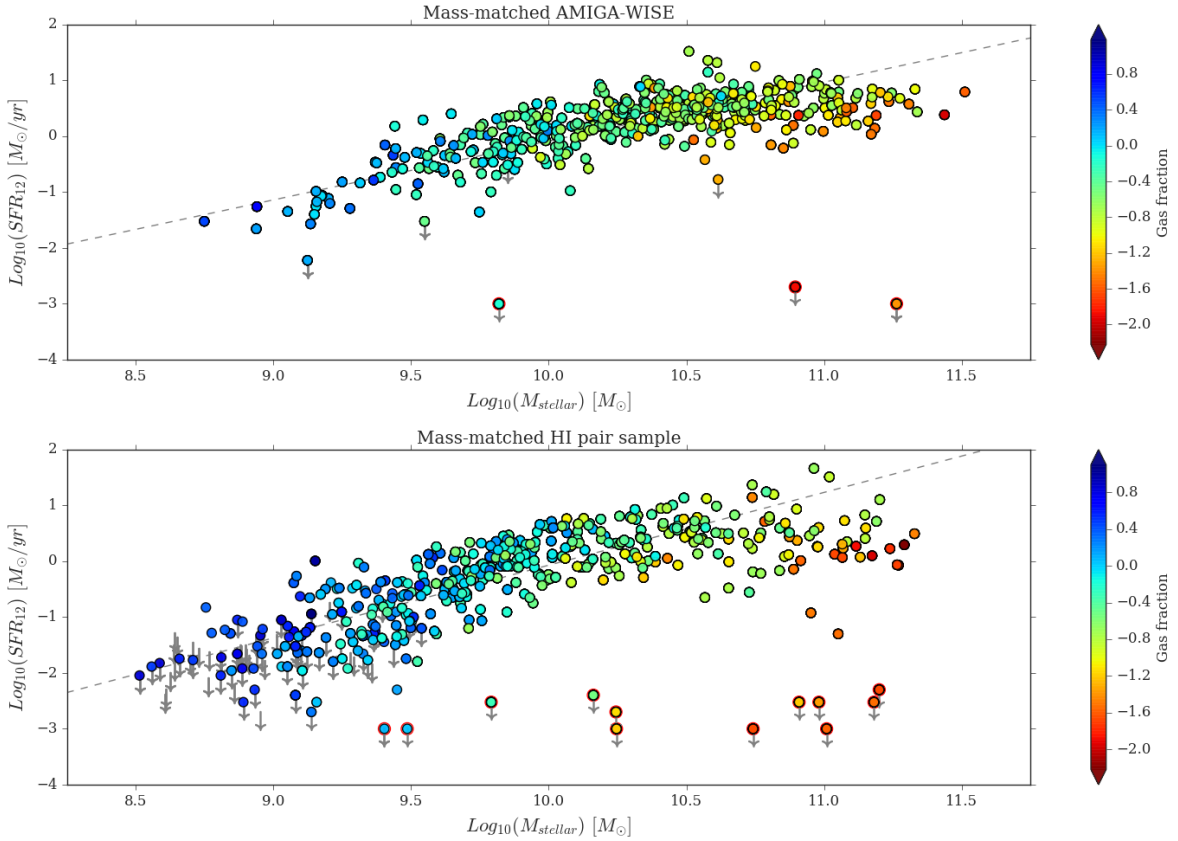

Figure 3.9: Enlarged views of the SFR/M$_\star$ sequence for both the statistical AMIGA-*WISE* (top panel) and HI pair (bottom panel) mass-matched samples colour coded by gas fraction. Gray arrows indicate upper limits on SFR, of which there are noticeably more in the HI pair sample, concentrated in the lower mass bins. Red circles mark the location of the low star-forming/quenched galaxy candidates. In both samples we see a trend of decreasing gas fraction with increasing stellar mass. We also note in the pair sample an increased availability of galaxies to choose from in the low stellar mass bins in the randomized re-sampling process of mass-matching to the AMIGA sample.

is observed. We also note a larger fraction of high gas fraction (HI dominated) sources in the low stellar mass regime of the HI pair sample compared to the AMIGA-*WISE* sample. Our pair sample selection allows for groups of galaxies, and 14 counts of multiplicity confirms the inclusion of triples/small groups (2 or more galaxies paired to the same companion). Visual inspection of the sample suggests the presence of additional potential triples, compact groups, and groups in which additional companions do not satisfy the mass selection criteria of this study. The increased fraction of high gas fraction galaxies in the pair sample may be related to the increased availability of HI in over-dense regions in the cosmic web of HI galaxies. These low mass and HI rich galaxies are missing from the AMIGA-*WISE* sample due to their isolation criterion, which not only eliminates galaxies in pair and group environments, but is biased against nearby dwarf galaxies. In the high stellar mass regime we note that gas fraction alone does not predict a galaxy's location on the SFMS. High mass galaxies with low gas fractions can be found both on and near the SFMS, as well as significantly below it in a region we conservatively define as reserved for quenched galaxies (red circles in Figure 3.9). The majority of the high stellar mass galaxies with low gas fractions found outside the 'quenched' region of the SFMS are located just below the SFMS, possibly in the process of dropping off the SFMS to join the quenched population galaxies. The colours of these galaxies, in the act of quenching, are what we call intermediate disks, sometimes referred to as:"green valley".

While gas fraction is widely used in the literature, we note that the relation is not linear, and that a significant residual remains when the $M_{HI}/M_{\star}$ ratio is taken. Gas fraction is therefore not the most appropriate quantity to use to determine 'normalcy'. We consider HI deficiency is the more robust quantity to use in this regard.

3.4.3 HI deficiency on the SFMS

Figure 3.10 shows the stellar mass/HI mass planes for both the AMIGA-*WISE* (left) and HI pair (right) samples with the updated AMIGA HI scaling relation overlaid (black dashed line; Equation 3.3). The AMIGA-*WISE* galaxies form a tight sequence on the $M_{\star}/M_{HI}$ plane as indicated by the tightness of the contours. The paired galaxies form a more irregular sequence in comparison, with fewer tightly spaced contours and a secondary central density potentially indicating two "flavours" of paired galaxies on the $M_{\star}/M_{HI}$ plane: a low mass sequence and a high mass sequence. Both samples are concentrated above the relation suggesting the presence of excess HI is more frequent than a deficiency of HI in both samples. This result is likely a consequence of the imposed lower limit on stellar and gas mass discussed in §2.5, which makes the AMIGA-*WISE* sample a gas-rich subset of the AMIGA sample.

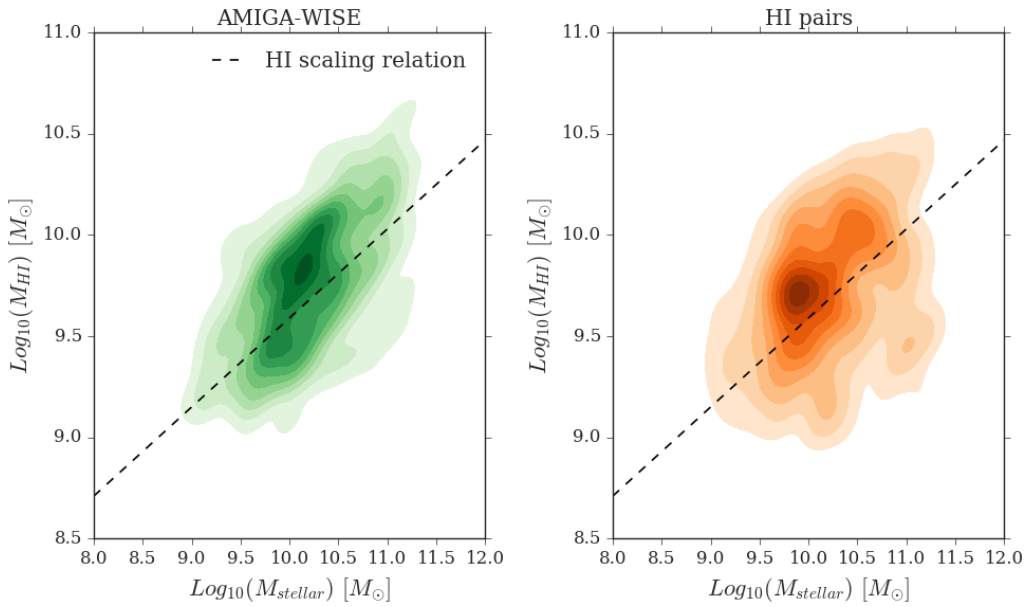

Figure 3.10: The AMIGA-*WISE* (left) and HI pair (right) samples on the stellar mass-HI mass plane. For reference, the updated AMIGA HI scaling relation (dashed black line, Equation 3.3) is overlaid. It is important to note that the slope of the HI scaling relation takes into account AMIGA galaxies with $M_{HI} < 10^9$ $M_\odot$ that are specifically excluded from the AMIGA-*WISE* sample. The AMIGA-*WISE* sample is thus a gas-rich sub-sample of the AMIGA HI sample, and as such is biased toward galaxies with an excess of HI (located above the relation).

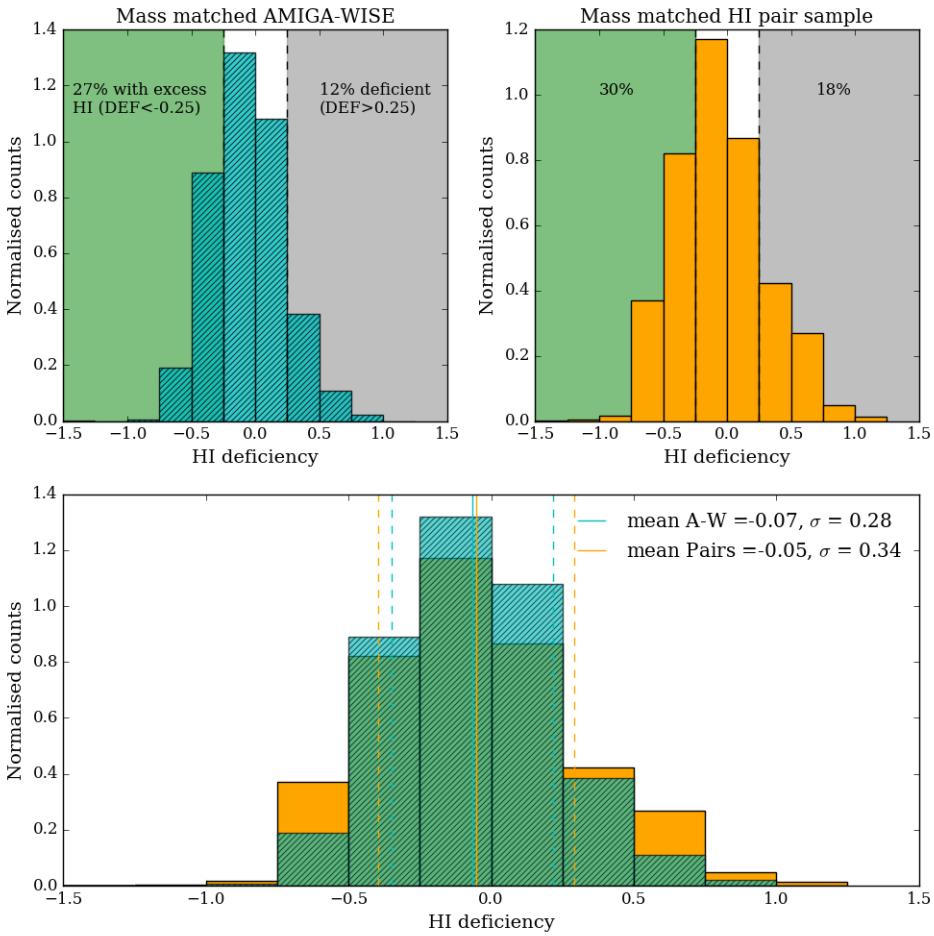

Figure 3.11: Top: distribution of HI deficiency for the AMIGA-*WISE* (left) and HI pair (right) samples. Gray shading marks the HI deficient regions in each sample, and the green shading shows the region of HI excess. Bottom: AMIGA-*WISE* HI deficiency distribution (cyan) overlaid on the HI pair deficiency distribution. Cyan and orange vertical dashed lines mark the respective distribution widths.

In the top panel of Figure 3.11 we show the distributions of HI deficiency for both the AMIGA-*WISE* (left) and HI pair (right) samples. Here we use the standard definition for deficiency, where positive values indicate a galaxy has less HI than expected given its stellar mass, and lies below the AMIGA HI scaling relation in the $M_\star/M_{HI}$ plane, and negative HI deficiency values indicate an excess of HI. These galaxies lie above the relation. Categorizing the galaxies in each sample as either deficient (DEF>0.25) or in excess of HI (DEF<-0.25), we find a slightly higher fraction of deficient galaxies in the pair sample (18% compared to 12% in the sample of isolated galaxies), while both samples have similar fractions of galaxies with an HI excess (27% and 30% in the isolated and pair samples respectively). A closer inspection of the deficiency distributions overlaid on each other (bottom panel of Figure 3.11), reveals an additional subtle difference

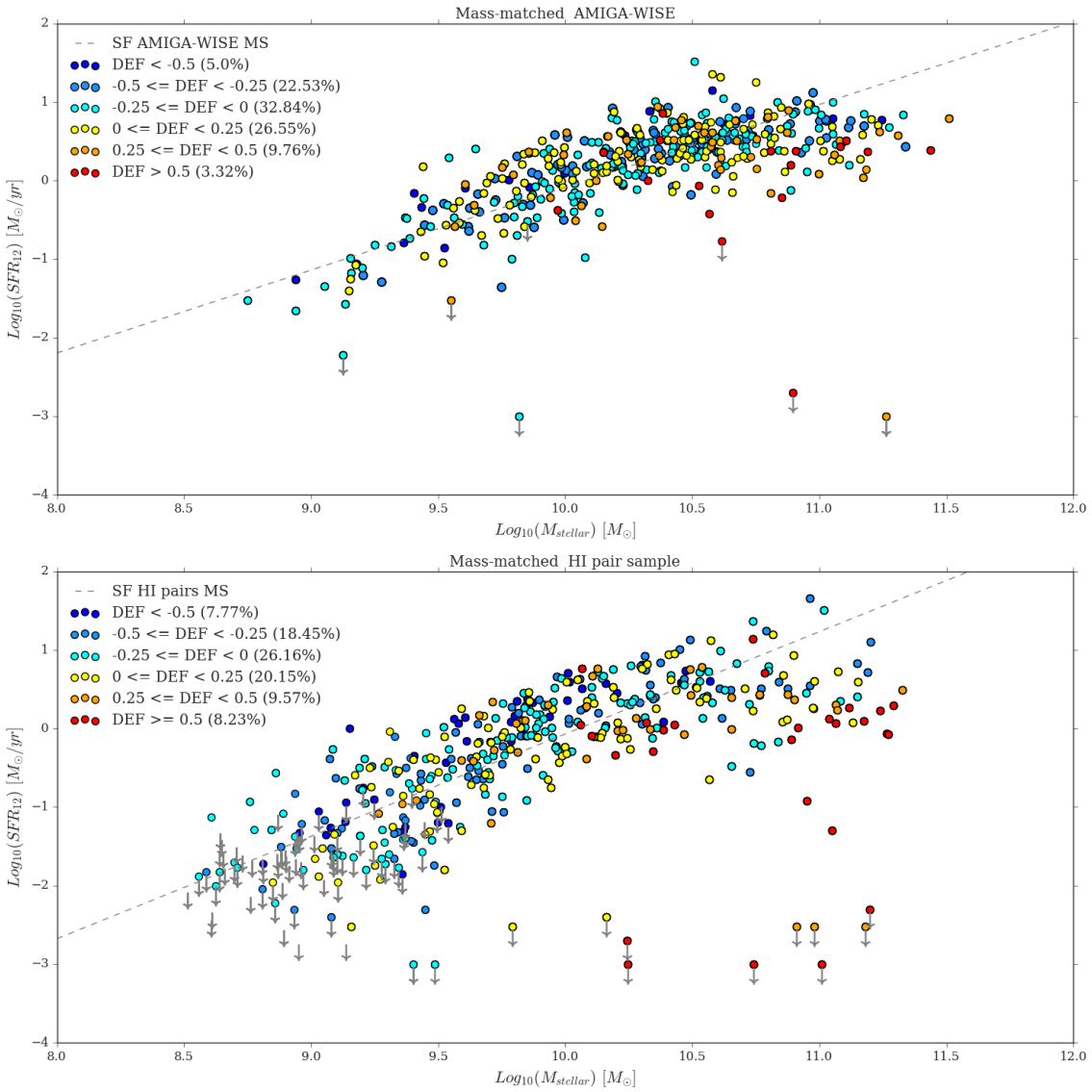

Figure 3.12: The SFR/M$_\star$ sequence for the statistical AMIGA-*WISE* (top) and HI pair (bottom) samples colour coded by HI deficiency.

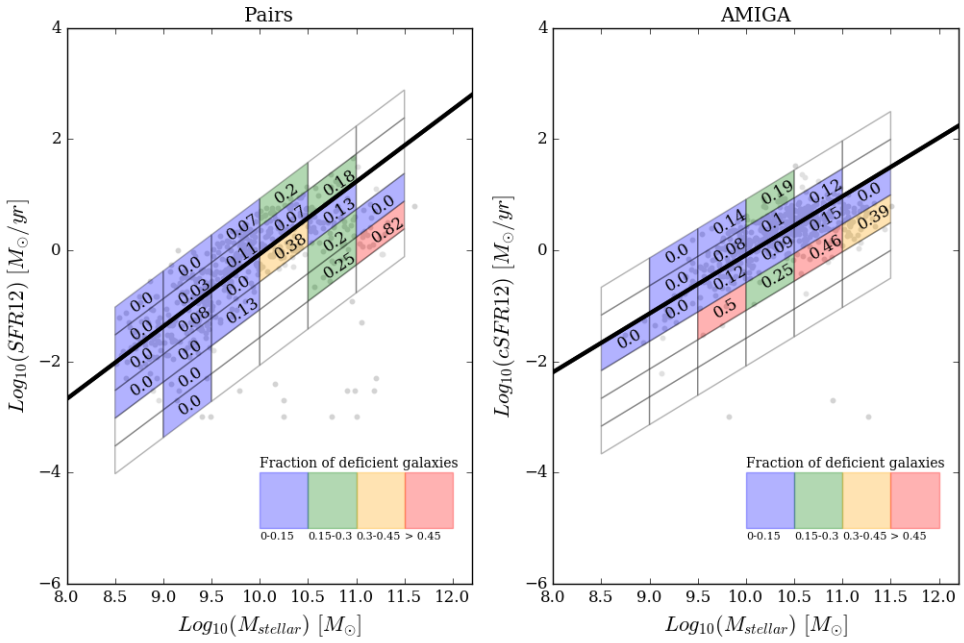

Figure 3.13: Fraction of HI deficient galaxies (DEF>0.25) on the SFMS. Here we compare the fractions of deficient galaxies below the SFMS between the pair (left) and isolated (right) galaxy samples in bins of width 0.5 dex in stellar mass, and height 0.5 dex in SFR. The number in each bin refers to the fraction of galaxies in each bin that measure DEF > 0.25, and the bins are further colour coded as blue, green, orange, or red as per the colour bar key in the bottom right corner of the plot. Bins with less than 2 galaxies are left blank.

between the two distributions. In the inner deficiency bins, from roughly DEF = -0.5 to 0.25, the AMIGA-*WISE* (cyan) distribution lies above the pair (orange) distribution. Conversely, in both the high and low deficiency bins, the pair sample dominates. This is reflected in the width of the distributions. While the samples have very similar mean values (-0.07 vs -0.05 for the AMIGA-*WISE* and pair samples respectively), the width of AMIGA-*WISE* sample (marked by vertical dashed cyan lines) is noticeably narrower than the pair sample (orange dashed lines), with a standard deviation of 0.28 compared to 0.34 for the pair sample. The Anderson-Darling (A-D) test (Scholz & Stephens (1987)) confirms a statistically significant difference between the samples, and the null hypothesis that the samples are drawn from the same sample can be rejected at the 1% level. Jones et al. (2018) present a similar comparison between their HI deficiency values for the AMIGA HI science sample and a sample of isolated pairs. They find that the isolated pair sample has more HI deficient galaxies than the AMIGA sample. A similar comparison with galaxies in the Virgo Cluster and the AMIGA sample demonstrates an even larger difference in HI deficiency values, with the Virgo Cluster galaxies exhibiting significantly higher HI deficiency values compared to the AMIGA sample. The findings of Cortese et al. (2011), Dénes et al. (2014), and Jones et al. (2018), to name a few, suggest interactions play a role in depleting a galaxy of its HI content. This work suggests environment is responsible for broadening the deficiency distribution of a galaxy sample in both directions, towards higher and lower deficiency values.

In Figure 3.12 we see the AMIGA-*WISE* (top panel) and HI pair sample (bottom panel) SFR/$M_\star$ sequences colour coded by HI deficiency. Again we see a a trend of increasing deficiency with stellar mass, but also a broad trend of increasing deficiency with increasing SFR implicating a link between the availability of HI and a galaxy's ability to form stars. This trend is cleaner in the AMIGA-*WISE* sample such that one could almost always predict the rough location of an isolated galaxy on the SFMS given its HI deficiency value. This is not the case in the pair sample where we observe highly deficient galaxies both on/near the SFMS, as well as well below it in the quenched galaxy region. Similarly, for lower masses and lower deficiencies, we see galaxies lying both on and below the SFMS. In both cases one might confuse a star-forming galaxy with a quiescent galaxy if only HI deficiency is considered. This is highly consistent with the picture in which environment drives SFMS scatter. Focusing specifically on quiescent galaxies, the low mass, high gas fraction population of galaxies discussed in §3.4.2 tend to be inefficient at forming at stars despite having an excess of HI (small HI deficiencies). The second population of high mass low gas fraction galaxies have large HI deficiencies. Looking at the fraction of deficient galaxies per stellar mass/SFR bin on the SFMS in Figure 3.13, the predictable nature of the isolated galaxy sample is demonstrated as bands of nearly uniform deficiency fractions. Each bin has a width 0.5 dex in stellar mass and height 0.5 dex in SFR (measured from the

respective SFMS lines), and is colour coded according to the fraction of galaxies with DEF > 0.25 (blue: fraction = 0-0.15, green: fraction = 0.15-0.3, orange: fraction = 0.3-0.45, and red: fraction > 0.45). The lowest band in the isolated sample is the exception with multiple bins of fractional deficiency making up the band, however the fraction is consistently above 0.25 indicating that galaxies more than 0.5 dex below the SFMS are more likely to be HI deficient. The pair sample, in contrast, shows more variance in each band. Bins with larger fractions of deficient galaxies are spread more liberally above and below the SFMS, although still more frequently below.

3.5 Discussion

In §3.4.2 we note the presence of a quenched population of galaxies in both the AMIGA-*WISE* and HI pair samples. Here we adopt a more conservative definition of quiescence to only include those galaxies that have fallen well below the SFMS, not only 1 dex below it as per Bluck et al. (2016). We circle these galaxies in red in Figure 3.9, 3 in the AMIGA-*WISE* sample and 12 in the HI pair sample. With environment selected to be the controlled variable between the two samples, we propose that the increased number of quenched galaxies found in the pair sample is environment-driven. Visual inspection of the quenched pair members reveals a potentially broader environment at play that includes triples and small groups.

In both samples we note two flavours of quenched galaxies, those with a low stellar mass and high gas fraction (LM-HG), and those with a high stellar mass and low gas fraction (HM-LG). The LM-HG galaxies also have low HI deficiencies (i.e., gas rich), and the HM-LG galaxies have high HI deficiencies (i.e., gas poor). A likely scenario for the quenching of the latter population of galaxies is simply consumption of fuel. As neutral hydrogen is converted to stars via molecular gas, the HI content of the galaxy decreases while the stellar mass content increases, thus producing high stellar mass galaxies with depleted gas fractions. The increased frequency of quenched galaxies as stellar mass increases we observe is consistent with the findings of Cluver et al. (2020), who make the same observation for samples of field and grouped galaxies from the Galaxy and Mass Assembly survey (GAMA) with *WISE* photometry, and attribute this result to mass quenching.

Considering morphology, in Figure 3.14 we look at the bulge to total (B/T) ratios of our sample galaxies. In the top panel of Figure 3.14 we plot the SFMS for both samples in bins of B/T, blue (B/T<0.2), yellow (0.2<B/T<0.5), and red (B/T >0.5). In the bottom panel we look at the stellar mass distributions of both samples in these same B/T bins. We note that the AMIGA-*WISE* sample (left) is primarily comprised of low B/T disky galaxies populating

the full stellar mass range, with only a small portion of the sample in the high mass range measuring large B/T values. These results are consistent with the work of Durbala et al. (2008) and Fernández Lorenzo et al. (2013), who demonstrated a prevalence of pseudo-bulges with low B/T values in sub-samples of AMIGA galaxies. These studies made use of optical photometry, namely the CAS parameters and GALFIT (Peng et al. 2010) to quantify bulge properties. This suggests optical and MIR B/T measurements are in good agreement.

In contrast to the isolated galaxies, a larger fraction of the pair sample has large B/T (bulgy galaxies) values, spanning a broader range of stellar mass values. The high mass quenched galaxies in particular have large bulges, supporting a possible morphological quenching scenario. In this scenario the formation of a bulge stabilizes the disk against the gravitational collapse necessary for SF to occur (Bluck et al. 2014). Cook et al. (2019), however, find little evidence to suggest that the presence of a large bulge can alter the gas disk, and cautions interpreting the link between large bulges and quenched galaxies as causal. They suggest quenching processes are more likely occur at the source of in-flowing gas.

The lower mass, low SFR galaxies are disk dominated, gas rich, with low HI deficiencies (excess HI), suggesting an alternative quenching mechanism in the low stellar mass regime. While the fuel for SF is abundant, the column density of the HI gas may be insufficient to ignite SF. The lack of SF in these galaxies might also be as a result of gravitational shock heating of their gas (Liu & Cen 2017). Alternatively, these galaxies have simply yet to reach the SFMS. While HI content is clearly important in moving galaxies along the SFMS, it does not necessarily account for the distance travelled by galaxies above and below it. Future work will therefore include an investigation into the SF efficiency of our galaxies. With gas rich galaxies found below the SFMS, and HI deficient galaxies found above it, the efficiency of converting gas into stars is an important quantity to consider next.

In the case of paired galaxies, the influence of other galaxies, in the broader/large scale environment, such as harassment, strangulation, ram pressure stripping, and merging may be disrupting the flow of gas and suppressing SF in both the low and high mass quenched galaxies. The pair sample will be more closely examined in future work, which will include a visual inspection for signs of interaction, an analysis of the impact of multiplicity, and a quantitative assessment of the range of local environments using the AMIGA tidal influence and local number density parameters (Q and η). By establishing the broader pair environment more accurately and quantitatively we will obtain a clearer picture of the role of environment not only contributing to the suppression/enhancement of SF, but in driving the observed scatter in the SFMS, potentially

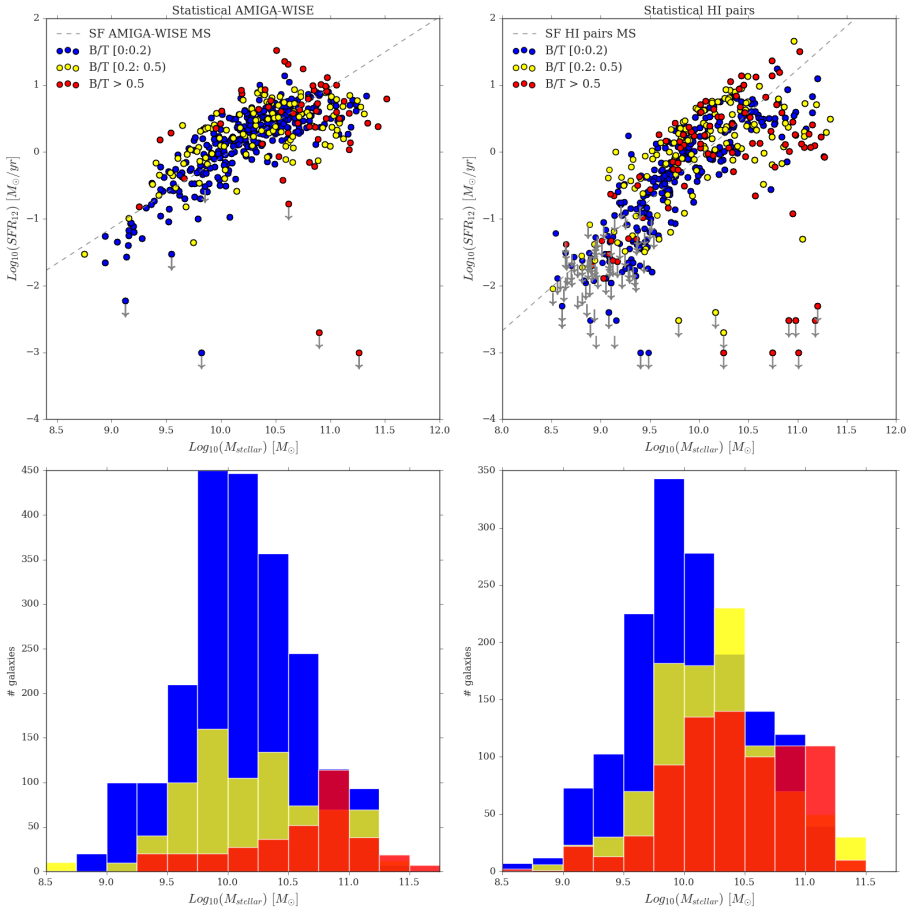

Figure 3.14: Top panel: the AMIGA-*WISE* (left) and HI pair (right) sample SFMS diagrams colour coded by B/T in bins of [0:0.2), [0.2:0.5), and B/T>0.5 (indicated by blue, yellow and red respectively). Bottom panel: stellar mass distributions in the above mentioned B/T bins for the AMIGA-*WISE* (left) and HI pair sample (right).

unlocking important pathways of galaxy evolution.

3.6 Summary

This paper probes the role of both environment and HI content (gas fraction and HI deficiency) in determining a galaxy's location on the MIR SFR-M$\star$ sequence. We summarize our main results here:

1. We update the AMIGA HI scaling relation for isolated galaxies of Jones et al. (2018) using *WISE* stellar masses on the x-axis as opposed to the previously used optical B-band diameters and luminosities. This relation, Equation 3.3, can be used as a baseline predictor of HI content in the absence of environmental influence, and we encourage its use in establishing the impact of environment on HI content by comparing it with galaxy samples in different environments.

2. We compare the SFR-M$\star$ sequence of the AMIGA-*WISE* HI sample with a sample of gas rich HI pairs and compute the SFMS fit for both samples using HyperFit (Robotham & Obreschkow 2015) (Equations 3.4 and 3.5). We observe a flatter slope for the AMIGA-*WISE* sample, as well as a reduced scatter compared to the HI pair sample (σ = 0.37 versus σ = 0.55). We attribute the tightness of the AMIGA-*WISE* SFMS to the isolated neighbourhood in which these galaxies are located, whereas the more stochastic behaviour of the HI pairs is likely the result of the more densely populated environments in which they live.

3. We compare the mass matched AMIGA-*WISE* gas fraction distribution to that of the HI pair sample and find that while the distribution medians are essentially identical, the significant difference between the two distributions lies in the width. The pair sample gas fraction distribution is notably broader by eye, and quantitatively measures a larger scatter (σ = 0.54 versus σ = 0.44 for the AMIGA-*WISE* sample). We also track the behaviour of gas fraction on both the AMIGA-*WISE* and HI pair sample SFMS. In both samples we observe a trend of decreasing gas fraction with increasing stellar mass. This suggests galaxies build up their stellar mass content via the consumption of HI fuel regardless of the environment in which they reside. The relationship between gas fraction and SFR, however, is non-linear, and does not reliably predict the location of a galaxy on the SFMS plane. High stellar mass galaxies with similarly low gas fractions are found both on the SF sequence and well below it.

4. The width of the AMIGA-*WISE* HI deficiency distribution is noticeably narrower than that of the pair sample, with a smaller standard deviation of σ = 0.28 compared to

σ = 0.34 in the pairs. We also note that the pair sample dominates in both the high and low HI deficiency bins, suggesting the potential role of environment simultaneously increasing and depleting HI content. The Anderson-Darling test confirms a statistically significant difference between the samples.

5. MIR B/T values measured in *WISE* show the AMIGA-*WISE* sample to be dominated by low B/T disky galaxies, in agreement with optical B/T measurements conducted by Durbala et al. (2008) and Fernández Lorenzo et al. (2013). In comparison, a higher frequency of large B/T values is observed in the pair sample, with some of the largest B/T values belonging to the high mass quiescent population galaxies.

The AMIGA sample has previously been shown to have the lowest measured dispersion in various quantities (HI profile asymmetry (Espada et al. 2011), FIR emission (Lisenfeld et al. 2007), and g-r colour (Fernández Lorenzo et al. 2013)) when compared to galaxies selected without isolation criteria considerations. Similarly, this work shows isolated galaxies to have a lower dispersion in both gas fraction and HI deficiency in comparison to a sample of galaxies in denser environments, as well as a reduced scatter on the SFR-M$\star$ sequence.

Acknowledgements

We thank the anonymous referee for their very useful comments which resulted in a greatly improved paper. This work is based on the research supported in part by the National Research Foundation of South Africa (Grant Numbers UID: 101099 and 111745). JB additionally acknowledges support from the DST-NRF Professional Development Programme (PDP), and the University of Cape Town. MC is a recipient of an Australian Research Council Future Fellowship (project number FT170100273) funded by the Australian Government. THJ acknowledges funding from the National Research Foundation under the Research Career Advancement and South African Research Chair Initiative programs, respectively. We acknowledge the work of the entire ALFALFA team for observing, flagging and performing signal extraction. MGJ is supported by a Juan de la Cierva formación fellowship (FJCI-2016-29685) from the Spanish Ministerio de Ciencia, Innovacion y Universidades (MCIU). MGJ also acknowledges support from the grants AYA2015-65973-C3-1- R (MINECO/FEDER, UE) and RTI2018-096228-B-C31 (MCIU). This work has been supported by the State Agency for Research of the Spanish MCIU through the 'Centro de Excelencia Severo Ochoa' award to the Instituto de Astrofísica de Andalucía (SEV-2017-0709). This publication makes use of data products from the Wide-field Infrared Survey Explorer, which is a joint project of the University of California, Los Angeles, and the Jet Propulsion Laboratory/California Institute of Technology, funded by the National Aeronautics and Space Administration. This work also utilizes data from Arecibo Legacy Fast ALFA (ALFALFA) survey data set obtained with the Arecibo L-band Feed Array (ALFA)

on the Arecibo 305m telescope. Arecibo Observatory is part of the National Astronomy and Ionosphere Center, which is operated by Cornell University under Cooperative Agreement with the U.S. National Science Foundation. Funding for the SDSS and SDSS-II has been provided by the Alfred P. Sloan Foundation, the Participating Institutions, the National Science Foundation, the U.S. Department of Energy, the National Aeronautics and Space Administration, the Japanese Monbukagakusho, the Max Planck Society, and the Higher Education Funding Council for England. The SDSS Web Site is http://www.sdss.org/. In addition, we make use of data from the Sloan Digital Sky Survey (SDSS DR7). The SDSS is managed by the Astrophysical Research Consortium for the Participating Institutions. The Participating Institutions are the American Museum of Natural History, Astrophysical Institute Potsdam, University of Basel, University of Cambridge, Case Western Reserve University, University of Chicago, Drexel University, Fermilab, the Institute for Advanced Study, the Japan Participation Group, Johns Hopkins University, the Joint Institute for Nuclear Astrophysics, the Kavli Institute for Particle Astrophysics and Cosmology, the Korean Scientist Group, the Chinese Academy of Sciences (LAMOST), Los Alamos National Laboratory, the Max-Planck-Institute for Astronomy (MPIA), the Max-Planck-Institute for Astrophysics (MPA), New Mexico State University, Ohio State University, University of Pittsburgh, University of Portsmouth, Princeton University, the United States Naval Observatory, and the University of Washington.

3.7 Appendix A: *WISE* De-Blending of Resolved Galaxies

Blending of resolved galaxies with other nearby (in projection) galaxies is a general problem for *WISE* because of its relatively large beam size, but is notably a feature of dense structures, such as galaxy clusters, compact groups and pairs. Accordingly, de-blending is a necessary component of *WISE* galaxy characterization pipelines. Jarrett et al. (2013; 2019) created a general processing pipeline that also includes expert interaction to carry out de-blending operations. The success of the de-blend for pair-galaxies depends on a few factors, including how close the pair members are located to each other, the relative brightness, the relative orientation (e.g., disk orientation for spirals), and the asymmetry of one or both of the pair galaxies. Sources that are too close (within or comparable to the beam of *WISE*) may not have acceptable de-blended fluxes. Sources that are faint compared to their companion and located close to the companion core, may also not de-blend well. Asymmetric sources (e.g., significant tidal distortion) are not easily modeled.

The principle assumption with these algorithms is that the galaxy light can be modeled using axi-symmetric averaging to produce a smoothed, underlying surface brightness distribution. Each galaxy is modeled accordingly, masking the nearby galaxy, measuring the light shape

at the 3-sigma isophotal level, fitting an ellipsoid to the 2D image, and then the approximate ellipsoid shape is then used to to subtract from the image instead of masking. Each iteration of the process, moving from one galaxy component to the next, creates a model that is closer to the actual light distribution for each galaxy of the pair. Several iterations are executed until convergence of the fitting metric is achieved. At this point, the expert user inspects the result, and makes adjustments to the original fitting parameters, including the disk orientation and axis ratio (for each galaxy in the pair), as well any other emission that may not be relevant to the galaxy pair (stars, background galaxies, artifacts). The user then runs the pipeline with these new parameters, and repeats the cycle as needed. Additional masking may be required for residual subtractions near the nuclei and other high surface brightness regions. The de-blend tends to work best for those pairs that have more than half their light unaffected by the blend (i.e., they are well separated). It becomes a significant challenge when most of the light is over-lapping (e.g., with physical merging systems) or when the disk orientations are parallel (disks overlap in the same direction). A relatively simple case is for a blue-red pair, where one galaxy is star-forming, and the other is passive or quenched (appearing blue in *WISE* colors), because only two bands – W1 [3.4 μm] and W2 [4.6 μm] – have any blending. Whereas, for two SF galaxies all four *WISE* bands require de-blend procedures.

An example of a galaxy pair in this current study that is clearly blended is the AGC 200466 – AGC 200463 system, both of which are star-forming galaxies. The nuclei are separated by 20″ (12.92 kpc projection) and approximately half of their light is overlapping with each other. Fig. 3.15 shows the four bands of *WISE* for this galaxy pair. It is clearly seen that AGC 200466 is the brighter of the two, and hence we can expect its final de-blend to be higher quality than its fainter companion (200463). The de-blend pipeline, after iterating the masking and subtraction procedure, constructs the axi-symmetric models, shown in the second-row panel of Fig. 3.15. Visually the models appear highly satisfactory, notably for the short-wavelength bands where the surface brightness is higher and angular resolution is better. Jarrett et al. (2012) note that the *WISE* angular resolution for drizzle-mosaiced images is about 6.0, 6.5, 7.1 and 12.4″ for W1 [3.4 μm], W2 [4.6 μm], W3 [12 μm] and W4 [22 μm], respectively. The de-blend pipeline assumes the same axi-symmetric shape (based on W1 measurements) for all four bands, which is simplistic for the longer wavelengths, but generally adequate for de-blend purposes. Some additional circular, small-radius masking was carried out to suppress large subtraction residuals. The resulting de-blended image for each galaxy of the pair is seen in the bottom panels of Fig. 3.15. The brighter companion (200466) has an excellent solution in all four bands: the de-blend was successful. The fainter companion (200463) appears to be acceptable, although it clearly has some residual emission from the brighter companion to the south-east. This extra emission is estimated to be less than 10% of the total, for this case.

In addition to the AGC 20466/3 system, we identify another five pairs in this study that have de-blended measurements. We provide the 3-color (W1 + W2 + W3) images of these systems, along with their solutions (again in 3-color), shown in Fig 3.16. All of these pairs are star-forming, and are relatively high stellar mass systems (see Figure 3.17). The de-blend solutions are adequate, with 10-20% additional uncertainty, but well within the scatter of the SFMS.

The first example, AGC100166/7 shows a bright primary and a relatively faint secondary, while also contaminated by a nearby star. The star is 'blue', meaning it is only bright in W1 and W2, so it has potential to alter the stellar mass estimation, but not the star formation. The de-blend solution is satisfactory for the primary (100167), but may have some excess W3 emission for the secondary (100166). The second example is AGC 011984/5, two inclined disks blending at a sharp angle, with the brighter companion (11984) having its outer disk cross the nucleus of the fainter companion (11985). This represents a challenging de-blend case because of the crossing orientation. It is clear that the brighter companion has its outer disk reduced by the de-blend and recovery of the secondary (whose resulting de-blend looks good). The third example, AGC09618-1/2, is an insidious case in which the two disks are blending in parallel, making it difficult to distinguish between the two. The de-blend solutions look adequate to the eye, but clearly there is some uncertainty in this case. The final two cases have pair angular separations such that the de-blend solution was clean, and clearly extracted sources successfully. It is interesting to note, the last example, AGC12914/5, is the famous "Taffy" interaction system, in which both galaxies are greatly disturbed – and hence highly asymmetric – and likely active by tidal-triggering (Jarrett et al. 1999). Nevertheless, the separations are large enough for the de-blend pipeline to clearly separate the pair components.

3.8 Appendix B: Example cases of blending in HI

We exclude a total of 49 pair members from our HI analysis on the basis of being in a blend too severe to render reliable HI data, as reported by the ALFALFA extraction team. A representative example of such a case is demonstrated by the pair AGC 1766/1768, where it is impossible to allocate which flux belongs to each galaxy due to their spectra completely overlapping in velocity space (see first plot in Figure 3.18). In this instance both galaxies were removed from our analysis. The second plot is an example of a dwarf companion (AGC 180048) sitting on the HI flux pedestal of its parent (AGC 4231). We exclude AGC 180048 from our sample since it is impossible to accurately measure its flux, however keep AGC 4231. The remaining plots in Figure 3.18 are examples of pair members that were not excluded from our analysis despite being flagged as in some sort of blend by the ALFALFA team. In these instances the blend

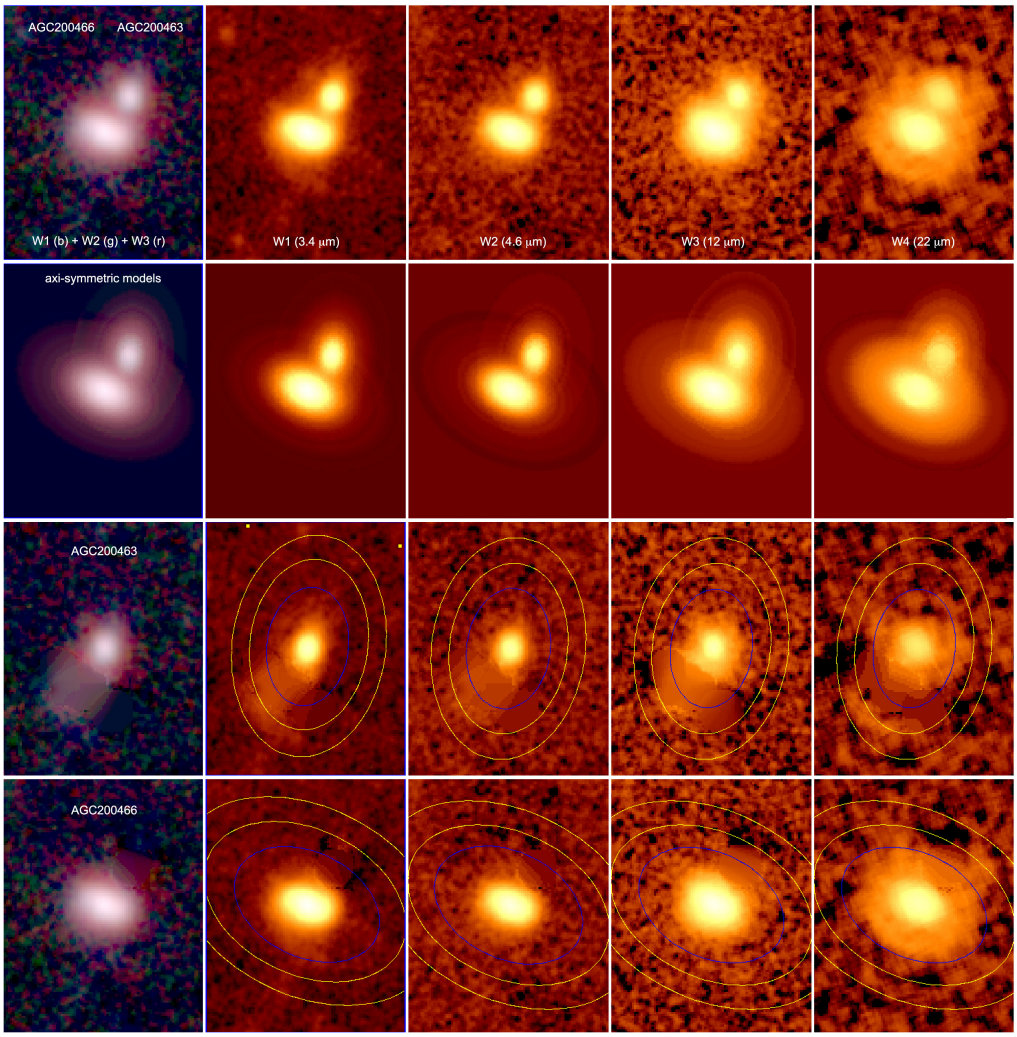

Figure 3.15: *WISE* view of the galaxy pair AGC200466 and AGC200463, de-blended using the *WISE* user-interaction pipeline. The top panel shows the four bands of *WISE*, and a 3-color combination. Note both galaxies are gas-rich and star-forming; hence all four bands require de-blend. The middle panel shows the resulting axi-symmetric models that represent the smoothed and symmetric emission from each galaxy. The bottom two panels show the resulting de-blend for each galaxy pair, with their respective 1-σ isophotal apertures (blue ellipse) and background sky annuli (yellow). The field-of-view is 46".

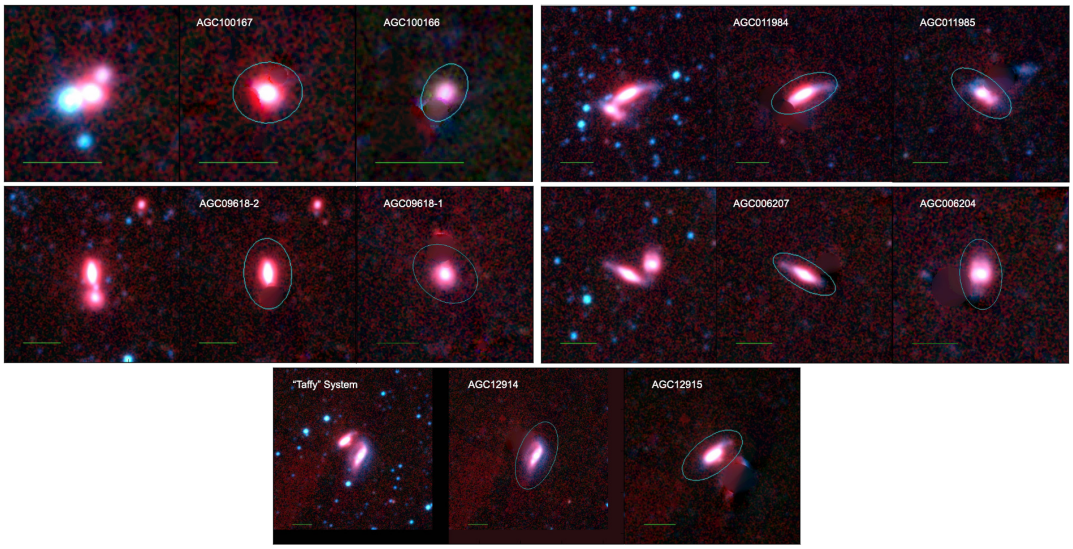

Figure 3.16: De-blended pair systems in this study. These five systems have been identified has having significant blending, notably the first three in the sequence shown here. The images are visualized using three bands of *WISE*: W1 [3.4 μm] in blue, W2 [4.6 μm] in green, and W3 [12 μm] in red. The green dash indicates 1 arcmin scale.

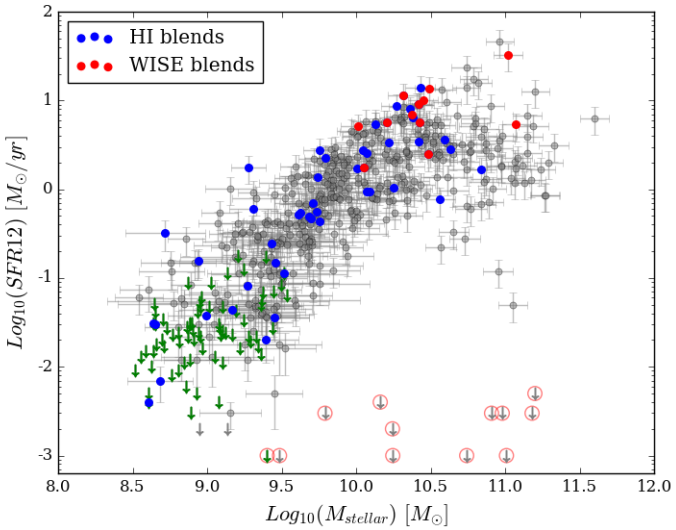

Figure 3.17: The pair SFMS of Figure 3.6b with the location of all noted HI blends highlighted in blue, and *WISE* blends highlighted in red. Based on the locations of these blends (i.e. not outliers) we pose that blending in general does not appear to be driving the scatter in the pair SFMS, nor the consequent observed difference in scatter between the pair and isolated galaxy samples.

is noted as not severe, and the HI properties are regarded as reliable by the ALFALFA team. The pair members AGC 448/449, for example, are very close together on the sky and therefore noted as in a blend, but separated enough in velocity to prevent significant blending of their profiles. No significant blending was reported for the pair AGC 246/102918 since the sources are separated just enough on the plane of the sky. The pair AGC 240208/9120 is an example where there is definite blending between the sources, but it is does not appear to be severe. The blending here was noted, but both sources were kept. In the pair AGC 241188/9073, one side of the profile was extrapolated by the ALFALFA team to prevent significant blending. This was noted, but both sources were kept. These cases are extremely rare.

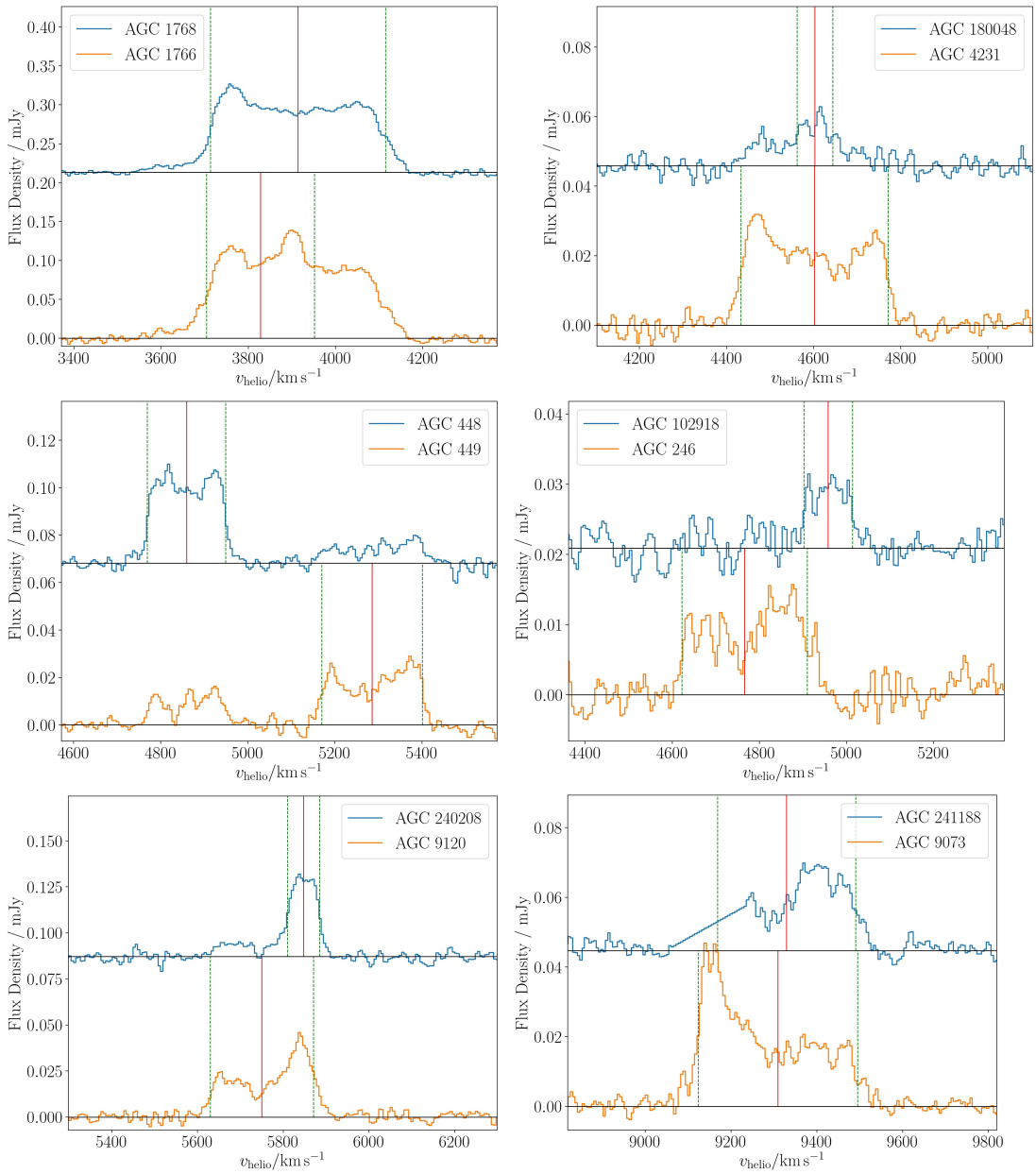

Figure 3.18: Representative cases of HI blending in the pair sample.

Chapter 4

Decoding the HI deficiency distribution of isolated and paired galaxies

This chapter is based upon the work of J. Bok, M.E. Cluver, T.H. Jarrett, R.E. Skelton, M.G. Jones, and L. Verdes-Montenegro, and will be submitted to MNRAS for publication in June 2021

Abstract

This third paper extends the analysis of Bok et al. (2020) in which the HI content of isolated and paired galaxies was examined as a potential driver of galaxy location on the *WISE* mid-infrared SFR-M$\star$ sequence. By further characterizing the isolated and pair galaxy samples, here in terms of optical galaxy morphology, a more detailed and quantitative description of local galaxy environment by way of the AMIGA local number density (η) and tidal strength (Q) parameters, star formation efficiency (SFE_{HI}), and HI profile asymmetries, we present plausible pathways for the broadening of the pair sample HI deficiency distribution towards both high and low deficiencies compared to the narrower isolated galaxy sample distribution. We associate the gas-rich tail of the pair deficiency distribution with the highest Q values, large profile asymmetries, and low SFEs. From this we infer that merger activity is enhancing gas supplies, as well as disrupting the efficiency of star formation, via strong gravitational torques. The gas-poor wing of the deficiency distribution appears to be populated with galaxies in denser environments (with larger η values on average), more akin to groups. The small population of early type galaxies in the pair sample (mostly excluded by our gas-rich selection criterion) live exclusively in the deficient tail of the distribution, suggesting a combination of a denser galaxy environment, early type morphology, and higher stellar mass, is contributing to the broadening of the deficiency distribution to the right.

4.1 Introduction

With SKA pathfinders fast becoming operational and HI (atomic hydrogen) science set to dominate the next decade of astronomy in terms of new discovery space, studies of the HI properties of galaxies have become increasingly popular, and our understanding of the important role HI content plays in galaxy evolution greatly advanced. As the fuel for star formation, HI is now understood to be a key piece of the galaxy bimodality puzzle; the transition from a star-forming spiral to a passive elliptical, i.e. the ultimate cessation of star formation, is naturally linked not only to the availability of star fuel, but also to how efficiently a galaxy can convert its fuel to stars. A useful diagnostic for examining the processes driving star formation (SF) in galaxies is the SFR-M_{star} sequence, otherwise referred to as the galaxy main sequence (GMS), or star-forming main sequence (SFMS). The relation shows a general trend of star-formation rate (SFR) increasing with stellar mass (Noeske et al. 2007, Bouché et al. 2010, Lee et al. 2015), but not without significant scatter. Galaxies are observed to jump up off the SFMS as they undergo triggered bursts of rapid SF (starburst events), and drop off the SFMS to due quenching events. Recent studies have shown HI to be an important driver of galaxy location on the SFMS (Saintonge et al. 2016, Bok et al. 2020), with bursts of enhanced SF associated with an increased availability of HI (Ellison et al. 2010, Moreno et al. 2020), and low SF galaxies deficient in HI (Bok et al. 2020). Galaxy environment is also implicated in many studies as linked causally to both the elevation and suppression of SF (Ellison et al. 2010, Xu et al. 2010, Cochrane & Best 2018, Pearson et al. 2019, Moon et al. 2019, Moreno et al. 2020). Our current understanding is that environment drives SF via its impact on the HI content of galaxies. The fragile nature of the diffuse, extended, and high angular momentum HI disk component of a galaxy makes it particularly sensitive to the local environment in which it resides, and the significant impact galaxy environment has on both HI content and distribution is well documented (Cortese et al. 2021).

Numerous studies have revealed galaxies in the centers of clusters to be gas-poor compared to less densely populated environments (Chamaraux et al. 1980, Giovanelli & Haynes 1985, Solanes et al. 2001, Chung et al. 2009, Dénes et al. 2014), with ram-pressure stripping generally attributed as the dominant gas removal mechanism in such environments (Gunn & Gott 1972). Chung et al. (2009) conducted an HI morphology census of galaxies in the Virgo cluster at different radii from the center and found that close to the core (within 0.5 Mpc), the HI disks of the galaxies were generally smaller than their optical counterparts, and in many cases these galaxies were also shown to have displaced gas— potentially evidence of current stripping, or the in-fall of previously stripped gas. Conversely, gas rich galaxies with gas disks extending well beyond their stellar components were found to dominate in the cluster outskirts. At in-

termediate distances from the cluster core a significant number of galaxies had long one-sided HI tails pointing away from the center, and the authors proposed that these galaxies were in the process of falling into the cluster core for the first time.

Galaxies in groups have also been reported as being HI deficient compared to field galaxies (Verdes-Montenegro et al. 2001, Kilborn et al. 2009, Hess & Wilcots 2013), with the cores of groups becoming increasingly HI deficient as group membership increases (Hess & Wilcots 2013). Hess & Wilcots (2013) present compelling evidence that galaxies transition from gas-rich to gas-poor in the group environment, via either star formation, tidal interactions, starvation, viscous stripping, or ram pressure stripping. Interestingly, X-ray studies of the IGM (intragroup medium) in Hickson compact groups suggest that ram-pressure stripping is not the dominant gas removal mechanism in groups (Rasmussen et al. 2008). High quality single-dish Green Bank Telescope (GBT) observations of the groups revealed a diffuse HI component suggestive of tidal stripping (Borthakur et al. 2010), and it is generally suggested that HI deficiency in groups is primarily a consequence of tidal stripping via galaxy-galaxy or galaxy-group interactions (Kilborn et al. 2009), although a recent review by Cortese et al. (2021) suggests full quenching is the combined result of various gas-removal mechanisms, acting simultaneously, or at different stages throughout the galaxy life cycle. Observing the diffuse HI (intra-group clouds, tidal tails, swept back disks), that would allow us to concretely differentiate between the various gas-removal mechanisms, is currently only feasible for a few nearby groups due to the costly observing requirements (high resolution, time consuming). SKA1-MID (the first stage of SKA) will significantly outperform current facilities. For the same integration time and angular resolution, SKA1-MID will reach column density limits 3 times deeper than what is currently possible, probing IGM column densities for the first time, and resolving individual HI clouds in the Local Volume (Popping et al. 2015).

Simulations of merging galaxy pairs also demonstrate the pair environment to have a significant impact on the HI content of galaxies, but different from the cluster and group environment. Numerical simulations show the gravitational interplay of merging galaxy pair members to generate internal asymmetries and instabilities that funnel gas inwards, producing the well known central concentration (Mihos & Hernquist 1996), and more recently, Hani et al. (2018) used a zoom-in simulation to show that a major merger can also re-distribute material into the circumgalactic medium (CGM), and increase total hydrogen covering factors by a factor of 1-1.25 for up to $\sim$ 3 Gyr. Parsec-scale galaxy major-merger simulations implemented by Moreno et al. (2020) demonstrated that close galaxy encounters can elevate both HI and H_2 gas reserves, and thereby enhance SF in both pair members. Alongside simulations, a re-distribution of gas as tidal tails and central molecular gas concentrations is routinely observed in merging galaxies

(Hibbard & Yun 1999, Tacconi et al. 1999, Koribalski & Dickey 2004, Yamashita et al. 2017), and Ellison et al. (2018) find merging galaxies to be on average gas-rich compared to control samples.

In order to truly disentangle the impact of external influence from secular evolution, we need a non-interacting control sample. To this end we defer to the AMIGA project (Analysis of the interstellar Medium in Isolated GAlaxies; Verdes-Montenegro et al. (2005)), who provide the most comprehensive multi-wavelength study of a well-defined sample of isolated galaxies, and therefore the best possible estimate of secular evolution to date. In our previous paper (Bok et al. 2020) we contrasted the HI deficiency (and gas fraction) distribution of ALFALFA galaxies in close pairs with isolated galaxies from the AMIGA project, and observed a broadening of the pair sample HI deficiency (/gas fraction) distribution in both directions, towards higher and lower deficiencies (/gas fractions), relative to the isolated galaxy sample. The pair finding method used in Bok et al. (2020) requires only that a target galaxy have at least one close companion, triples and groups are not excluded by the criteria. Visual inspection of the pair sample suggested that there are indeed more densely populated environments present. Since we know that different environments impact the HI content and distribution in galaxies differently, we propose that the broadening of the pair HI deficiency distribution towards both higher and lower HI deficiencies can potentially be explained by the presence of a broader local environment.

The subject of this work is therefore to further characterise the local environment of the pair sample by invoking the use of Verley et al. (2007a)'s local number density parameter, η, and tidal influence estimator, Q, which provide complementary information about the local environment in the vicinity of target galaxies. η, or η_k, probes the local vicinity of a target galaxy by taking into account the distance to its kth nearest neighbour, and is defined as:

$$\eta_k \propto log \frac{k-1}{V(r_k)}$$

where r_k is the distance to the kth nearest neighbour measured in arcminutes. To probe the local vicinity of the target galaxy, that is, the vicinity in which principal perturbers can be expected to lie, k is set to equal 5, or less should there be too few neighbours in the field. To mitigate contamination by background galaxies, only neighbours of similar size are considered in the calculation (i.e. neighbours with diameters between 0.25 and 4 times the target galaxy)(Verley et al. 2007a). Using formalism developed by Dahari (1984), the tidal strength parameter, Q, then estimates the strength of the tidal forces exerted on the target galaxy by its k neighbours, and is proportional $M_i R_{ip}^{-3}$, where M_i is the mass of the ith neighbour and R_{ip} is its distance

from the primary. Q is ultimately defined as the logarithm of the ratio of the external tidal force to internal gravitation binding energy, i.e.:

$$Q = log(\sum_i Q_{ip})$$

where

$$Q_{ip} \equiv \frac{F_{tidal}}{F_{bind}} \propto (\frac{M_i}{M_p})(\frac{D_p}{S_ip})^3$$

where $M_{i,p}$ is the mass of the ith neighbour and the primary respectively, D_p is the diameter of the primary, and S_{ip} is the projected separation (Verley et al. 2007a). For both the calculation of η and Q we draw neighbours from the SDSS photometric catalogue, and make use of photometric r-band magnitudes to serve as a proxy for stellar mass. We also use the SDSS galaxy group catalogue of Lim et al. (2017) to search for existing groups associated with the pair sample. We additionally conduct a visual classification of the pair member optical morphologies to investigate how morphology might be driving the observed differences in HI content we measured between our paired and isolated galaxy samples on the SFMS, and we use star-formation efficiencies to probe the mechanisms responsible for driving galaxies off the SFMS towards low SFRs, despite having relatively large gas reservoirs. Finally, we compute the HI profile asymmetries of our pair sample and examine them as a function of local environment (η, Q, and number of group members for the Lim et al. (2017) groups), to test the popular proposition that degree of profile asymmetry and density of environment positively correlate.

4.2 Sample: isolated and paired galaxies

This paper uses the pair and isolated galaxy samples defined in chapter 3, where full details of the selection criteria can be found in §3.2. The close pair galaxy sample admits HI-rich ($M_{HI}>10^9$ $M_\odot$) galaxies from the α70 ALFALFA catalogue with at least one similarly gas-rich companion within 100 kpc and 1000km s^{-1}(as per the Robotham et al. (2014) close pair criteria). Our isolated galaxy sample comprises a selection of gas-rich galaxies from the complete AMIGA HI science sample that have been flagged as reliably isolated, and with high quality HI profiles (544 galaxies in total). By admitting only gas-rich galaxies into our isolated and pair samples we preferentially select star-forming late type galaxies. To mitigate the effect of missing low-mass galaxies in the AMIGA sample we implement a (low) stellar mass cut of $M_\star > 10^{8.5}$ $M_\odot$ across both the isolated and HI pair samples, which allows for a more fair comparison between the two samples. Our final isolated galaxy sample comprises 481 galaxies, while 531 galaxy pair members in our HI pair sample survive the stellar mass cut. A summary of the sample criteria are listed in tables 3.2 and 3.1.

4.2.1 Quantification of the broader 'pair' environment: η & Q

In their 2007 paper Verley et al. (2007a) quantified the degree of isolation of Karachentseva (1973)'s CIG galaxies using a local number density of neighbouring galaxies (η), and the tidal strength exerted by these neighbouring galaxies on the candidate CIG galaxy (Q). By taking into account both the number of neighbours and their masses, η and Q work together to provide a useful description of the local environment in the vicinity of each CIG galaxy, well suited to assessing isolation. Galaxies that are truly isolated from external influence have low η and Q values, and when η and Q are both high we know that the evolution of the target galaxy can be, or already has been, impacted by the environment. The latter is therefore not representative of evolution in isolation. η and Q can also be used to differentiate between environments in which a single close neighbour (low η) has a considerable tidal influence (high Q) on a target galaxy, and environments densely populated (high η) with relatively small (low mass) galaxies (low Q). Verley et al. (2007a) also demonstrated η and Q to be effective at distinguishing isolated galaxies from galaxies in denser environments by comparing them with triplets from the Karachentseva's catalogue (Karachentseva 1973), compact groups from the Hickson catalogue (HCG; Hickson (1982)) and Abell clusters (ACO; Abell (1958)).

[H]

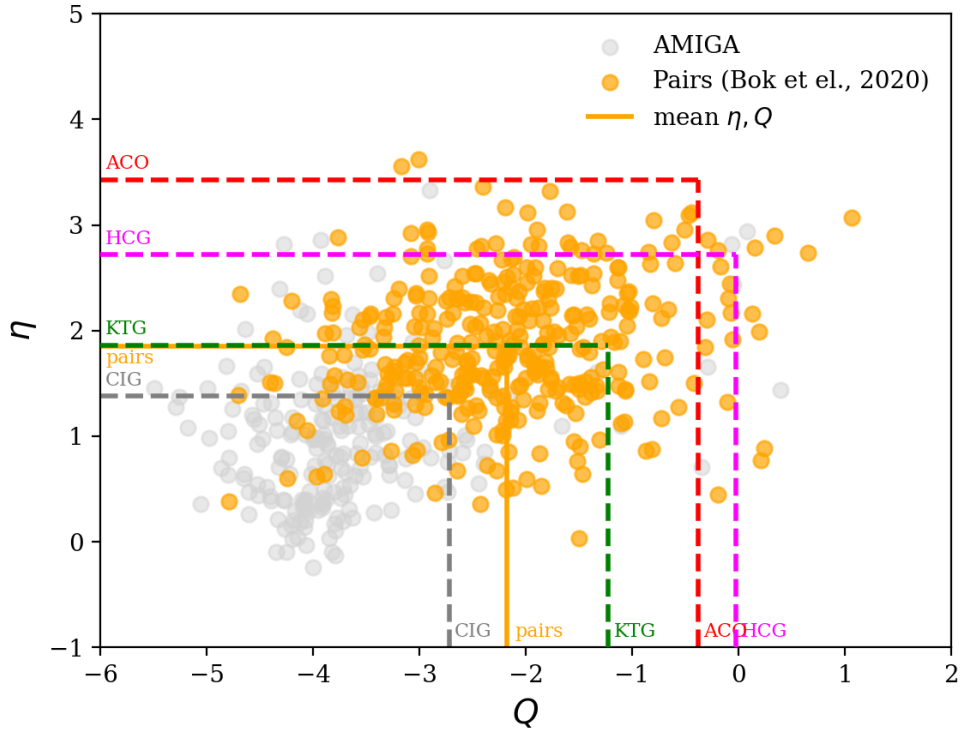

Figure 4.1: HI pair sample on the $\eta - Q$ plane (orange) with the control sample of isolated galaxies in AMIGA shown in gray. The solid orange line marks the location of the mean pair sample η and Q values, while dashed lines show the mean η and Q values found by (Verley et al. 2007a) for isolated galaxies (gray), (Karachentseva 1973) triples (KTG; green), Hickson Compact Groups (HCG; magenta), and Abel Cluster galaxies (AC; red) for reference.

In Figure 4.1 we present the η and Q measurements for our pair sample (orange points) and contrast them with our isolated sub-sample of AMIGA galaxies (gray points) on the $\eta - Q$ plane. Mean values for each parameter are shown as orange and gray dashed lines for the respective samples. We note that while the HI pair sample is distinctly separate from isolated galaxies on the diagram (demonstrating the efficacy of the parameters to distinguish between the two environments), it does appear to probe a broad range of more densely populated environments according to the mean η and Q values of Karachentseva (1973) triples, Hickson Compact Groups, and Abel Cluster galaxies shown as green, magenta, and red dashed lines, respectively.

Groups in the pair sample

The presence of potential groups in the pair sample was noted by Bok et al. (2020) in the previous paper, and is also suggested by the broad range of environments spanned by the pair sample on the $\eta - Q$ plane (Figure 4.1). Lim et al. (2017) produced a galaxy group catalogue of the low-redshift Universe using a compilation of large redshift surveys, and cross-matching with their SDSS group catalogue confirms the inclusion of 85 galaxy groups in our pair sample, with at least N>2 members. The halo-based group finding methods employed by Lim et al. (2017) are based on those of Yang et al. (2007), however with an improved halo mass assignment, which extends the group catalogue to include more low-mass systems (see Lim et al. (2017) for full details). It is important to note that the Lim et al. (2017) groups do not necessarily represent all the pairs in our sample that are in groups.

4.2.2 Pair member morphologies

The link between SF activity and galaxy colour is well-established, with the majority of 'normal' galaxies generally falling into two categories: the "red sequence" and the "blue cloud" (Strateva et al. 2001, Kauffmann et al. 2003, Baldry et al. 2004, Balogh et al. 2004). Hubble Type (galaxy morphology) roughly correlates with these two populations. "Red sequence" galaxies are generally high mass, passive, and early-type (bulge-dominated) in morphology, whereas galaxies in the "blue cloud" are typically less massive, active (star forming), and of late-type (disk dominated) morphology. To assess the role of morphology as a driver of our results, we conducted a visual classification of each galaxy using optical SDSS images. Each galaxy was classified by more than two people, and in most cases ($\sim$ 85% of the time) the classifications were in agreement. Disagreements were appropriately reclassified by vote. In Figure 4.2 we plot the pair SFMS colour-coded by morphology and see the familiar trend of spiral (late-type) galaxies dominating the SF regions of the plot, namely on and around the SFMS (blue points), whereas as the small population of elliptical/S0 (early-type) galaxies are mostly high mass with very low SFRs (pink points). Our visual morphology classifications, which show the pair population to be spiral galaxy dominated, are in good agreement with the MIR morphology diagnostics presented in Bok et al. (2020), namely the *WISE* infrared colour-colour diagram (Figure 4), which delineates 4 general galaxy types, and *WISE* B/T measurements (Figure 14), which is sensitive to the bulge and disk-dominated systems. Using the Cluver et al. (2020) quenching separator (dashed black line in Figure 4.2) to define the fraction of quenched galaxies in each population, we find a strong correlation between our visual morphology classification scheme and SF activity. Our elliptical/S0 (early type) sample is largely passive (70% quenched), and our spiral sample is predominantly SF (14% quenched). Our visual inspection yielded a total of 377 spiral (68 %), 95 irregular (17%), and 27 elliptical/S0 (5%) galaxies. Kelvin et al. (2014)

find the local Universe to be approximately 70% disk dominated, and 30% spheroid dominated based on 3727 galaxies from the Galaxy and Mass Assembly (GAMA) survey. The relative absence of spheroids in our pair sample compared to the GAMA sample is a consequence of our gas-rich requirement, which strongly selects active disk galaxies, and excludes passive/early type galaxies.

4.2.3 AMIGA morphologies for the isolated sample

Morphologies for the full AMIGA sample are available in Table 1 of Fernández Lorenzo et al. (2012), who revised the classifications performed by Sulentic et al. (2006) using CCD images from either SDSS or their own. Of the AMIGA galaxies that form our isolated galaxy sample in Bok et al. (2020), 466 (97 %) are classified as spirals, 8 as irregular (2 %), and 4 (1 %) as elliptical/S0. Early type galaxies are typically found in the centers of galaxy clusters (the galaxy-morphology density relation) and are therefore specifically excluded by the AMIGA isolation criteria.

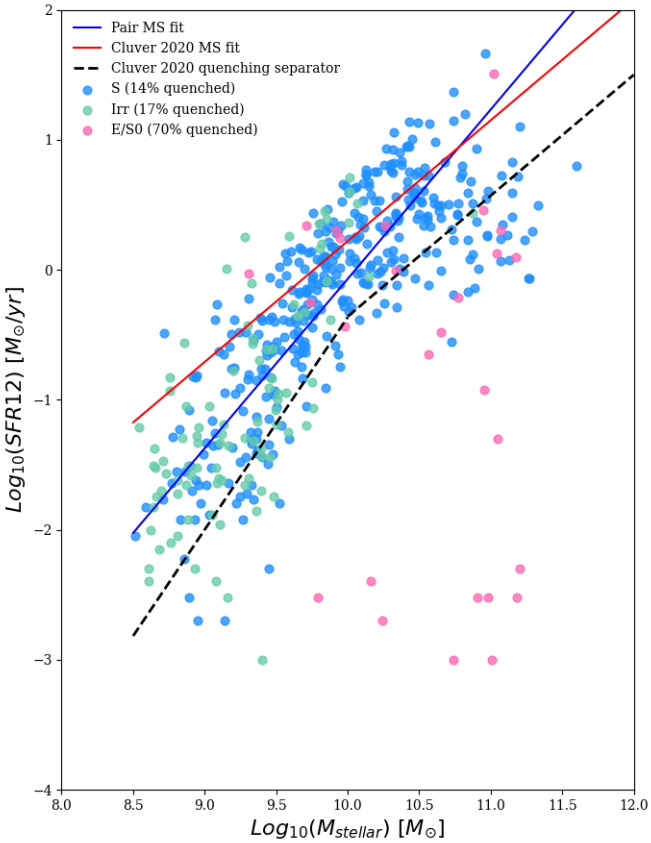

Figure 4.2: Galaxy morphology on the pair SFMS. Here blue represents the spiral population, green the irregulars, and pink the elliptical/S0 population. The fraction of quenched galaxies in each morphology group, determined as per the quenching separator from Cluver et al. (2020) (black dashed line), is indicated as a percentage next to each category in the legend. The SFMS fit from Cluver et al. (2020) for the non-grouped GAMA sample is shown for reference in red.

4.3 Decoding the HI deficiency distribution of paired galaxies: a closer look at environment & morphology

4.3.1 HI deficiency on the $\eta - Q$ plane

In Figure 4.3 we show deficiency as a function of tidal strength, Q, (top) and number density, η, (bottom) separately. The mean values of Q and η per deficiency bin are shown as orange horizontal lines. This plot indicates a trend of decreasing Q with increasing deficiency, and a tentative trend of η increasing with deficiency. These results suggest that tidal influence is better suited to predicting HI content than density of environment, and demonstrate that a galaxy living in a densely populated environment is not necessarily subject to a larger tidal pressure than a galaxy living in a less densely populated environment- the mass of neighbours

is important. Since Q and HI deficiency are inversely correlated, we rule out tidal forces as a dominant mechanism for gas-depletion in our pair sample.

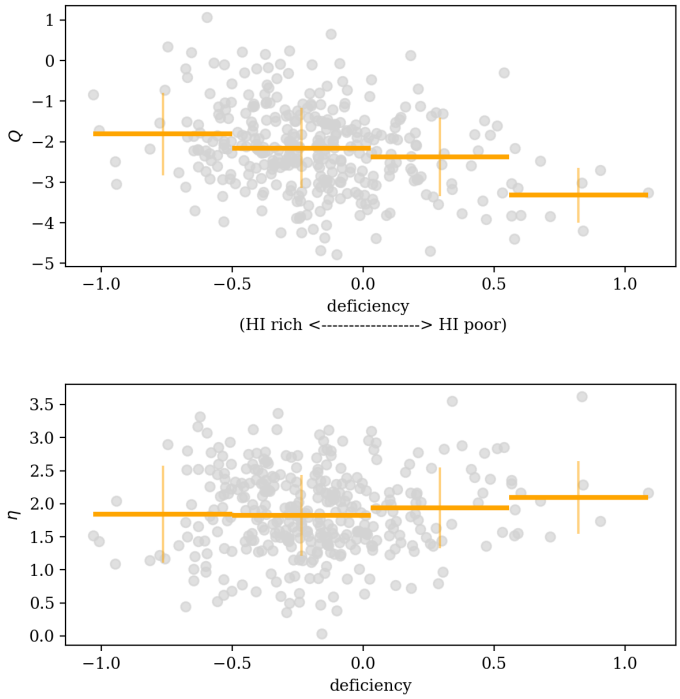

Figure 4.3: Deficiency as a function of tidal strength (Q) (top) and η (bottom). Orange horizontal lines show the mean Q and η per deficiency bin.

Figure 4.4 highlights the location of both the most HI deficient (here defined as DEF>0.4) galaxies in our pair sample (red points), as well as the most gas rich (DEF < -0.4, blue points), on the $\eta - Q$ plane. Visually we note a subtle separation between the two populations, with the most gas rich galaxies appearing to occupy a larger region of the $\eta - Q$ plane, spanning a broad range η and Q values, and in particular, extending out towards high Q values. The most deficient galaxies, in contrast, rarely reach high Q values. Quantitatively we note that the gas-rich population is subject to larger tidal forces on average compared to the gas-poor population.

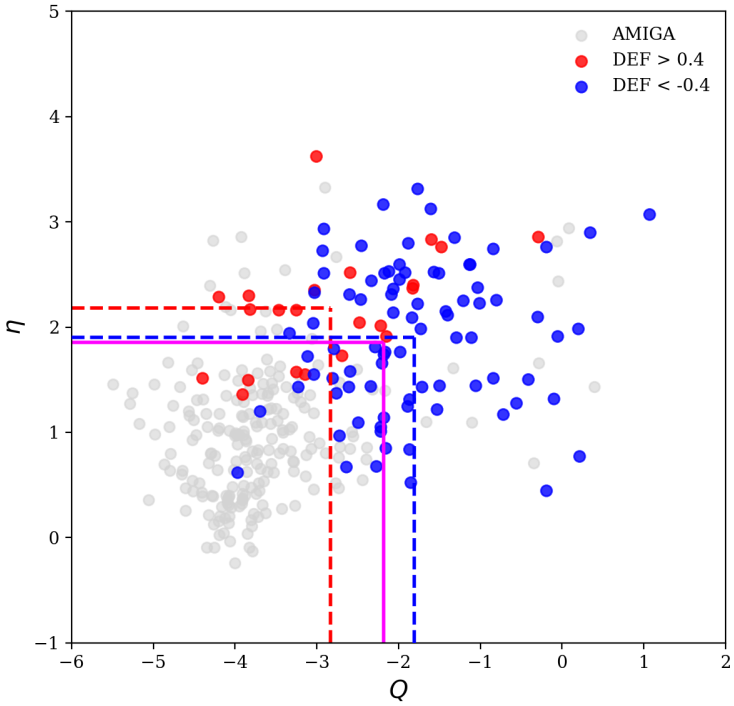

Figure 4.4: HI deficiency on the $\eta - Q$ plane. Highly deficient (DEF>0.4) galaxies are shown in red, and galaxies with low deficiencies/excess HI (DEF <-0.4) are shown in blue. AMIGA galaxies are shown in gray for reference. Red and blue dashed lines mark the mean η and Q values for the respective sub populations of high and low deficiency galaxies. Mean values for the full pair sample are marked by magenta lines.

In the top panel of Figure 4.5 we show separate deficiency distributions for the group galaxies from Lim et al. (2017) in blue and the remainder of the pair sample in green, and find no evidence to suggest that the group environment is specifically responsible for broadening the HI deficiency distribution of the pair sample in either direction. In the middle panel of Figure 4.5 we compare the normalized HI deficiency distributions of the pair (green), group (blue), and isolated (pink line) galaxy samples, and note that the group distribution appears shifted towards lower deficiency values (i.e. are more gas-rich) compared to both the pair and isolated samples. The bottom panel of Figure 4.5 displays the HI deficiency for the group galaxies as a function of number of members in a group (N). Small groups (N<=4), which make up the majority of the group sample, exhibit a broad range in HI deficiencies, while larger groups (N>4) appear to become increasingly deficient as optical membership increases. However, we note the limitations of small sample statistics in the large N regime.

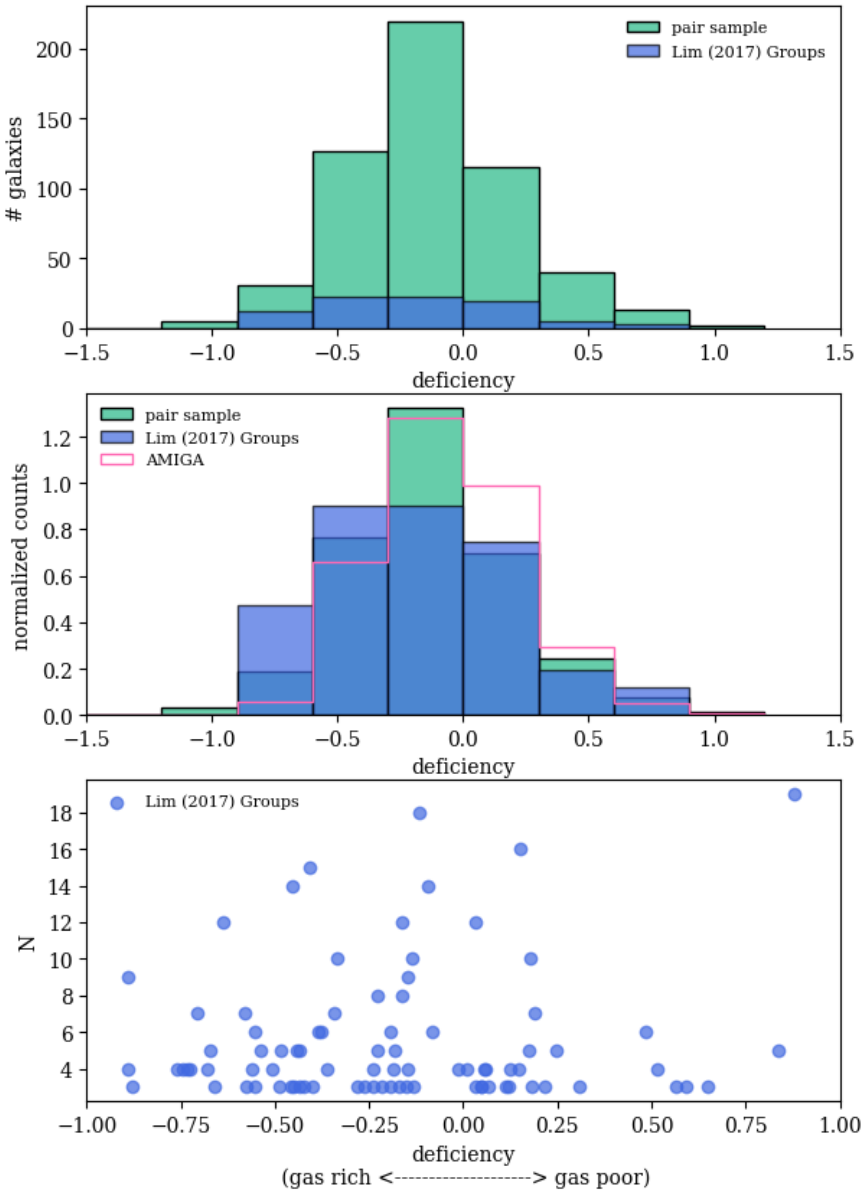

Figure 4.5: HI deficiency in galaxy groups. Top panel: Distribution of HI deficiency values for the pair sample with the Lim et al. (2017) groups shown in blue. Middle: Normalized HI deficiency distributions for the pair, group, and isolated galaxy samples shown in green, blue, and pink respectively. Bottom panel: HI deficiency of galaxies in groups as a function of the number group members, N. We see a broad range of deficiencies for small groups (N<=4), while larger groups (N>4) become increasingly deficient as N increases.

4.3.2 Galaxy morphology and HI deficiency

In Figure 4.6 we show the pair member deficiency distributions of the spiral, irregular, and elliptical/S0 galaxy populations in blue, green, and pink respectively. The sample is spiral dominated as a consequence of our selection criteria, so the comparisons we make between the spiral and the elliptical/SO galaxy sub-samples are not statistically significant, however we note that the elliptical/S0 deficiency distribution is shifted towards higher deficiencies, while the irregular galaxy sample galaxies are on average more gas-rich compared to both the spiral and elliptical/S0 populations. This result is not unexpected as later type galaxies are generally found to be more HI-rich compared to earlier types (Solanes et al. 2001, Jones et al. 2018). Our isolated galaxy sample in comparison is essentially devoid of elliptical/S0 galaxies (only 1% are classified as E/S0), indicating that the broadening of the pair sample deficiency towards higher deficiencies is morphology-driven. Such galaxies (early types) typically live in dense environments and are thus specifically excluded by the strict AMIGA isolation criteria.

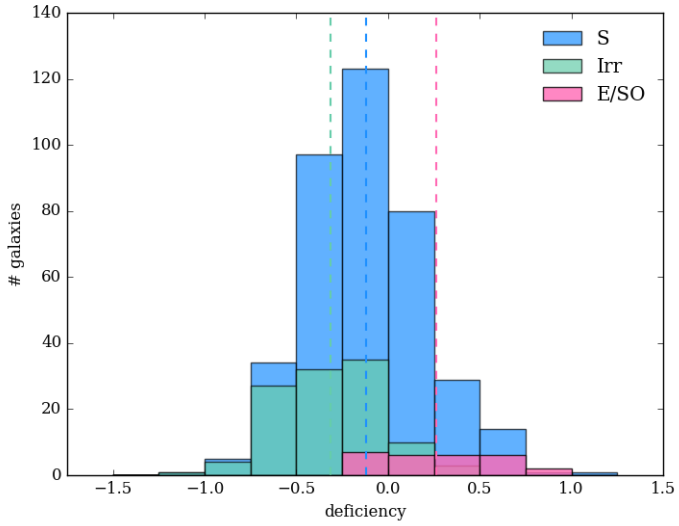

Figure 4.6: Deficiency distributions of the spiral (blue), irregular (green), and elliptical/S0 (pink) pair sub-samples. The corresponding mean deficiency values are shown as dashed vertical lines in blue, green, and pink respectively, highlighting the relative gas-richness of the spiral and irregular samples compared to the elliptical/S0 population.

4.3.3 Star formation efficiency

While a supply of fuel is of course crucial for SF, how efficiently a galaxy is able to convert its gas into stars is equally important in driving galaxy location on the SFMS. As we saw in our previous paper (Bok et al. 2020), galaxies can have large gas reservoirs (high gas fractions) and very low SFRs. To investigate potential scenarios that could lead to these results we calculate

the efficiency of SF for both our paired and isolated galaxy samples using the Schiminovich et al. (2010) definition of star formation efficiency: SFE = SFR/M_{HI}. In Figure 4.7 we present the SFEs for both the paired (left) and isolated (right) galaxy samples as colour on the SFMS. We show the full galaxy samples here (not mass-matched). The relative fraction of paired and isolated galaxies in each stellar mass bin can be found in Table 4.1, which highlights the relative absence of low mass galaxies in the AMIGA sample. In both samples we observe a general trend of SFE increasing along the SFMS with increasing stellar mass and SFR. Migration off the SFMS and low SFEs appear in both samples, suggesting SFE is an important factor in quenching regardless of environment. The increased frequency of galaxies migrating off the SFMS in the pair sample, however, suggests a link between environment and SFE. In Figure 4.8 we plot the mean SFE per stellar mass bin for our pair (left) and isolated (right) samples, and observe a noticeable turnover at around SFMS $10^{10.25}$ $M_{\odot}$ in both. This is consistent with the break in the stellar mass-halo mass relation (Behroozi et al. 2013) corresponding to the mass scale where virial shock-heating of accreting gas begins to dominate. The significantly enhanced scatter we found for the pair SFMS (particularly in the low mass regime) compared to the isolated SFMS in chapter 3 appears to have translated into a similarly enhanced scatter in the pair SFE-M$\star$ sequence, which we observe here as smaller errors for the isolated sample (cyan vertical lines) compared to the pair sample errors (blue vertical lines). We compare the means directly in the right hand panel with the pair sample shown in blue and the isolated sample in cyan, that the pair sample SFE turns over more quickly. In Figure 4.9 we plot HI deficiency as a function of SFE and colour code the data by gas fraction. Here we see a subtle trend in both samples of increasing SFE with increasing deficiency, and decreasing gas fraction, suggesting *efficient star formation depletes galaxies of their gas reservoirs.* A small population of low SFE, HI deficient galaxies with depleted gas fractions perhaps marks a later stage in the cycle in which previous high SFE has depleted gas content, and in turn caused SFE to plummet. We also note that the AMIGA sample is missing high gas fraction galaxies relative to the pair sample. This is a selection effect arising from their strict isolation criteria, which specifically excludes dwarfs (assessing the isolation of nearby dwarfs requires a prohibitively large search area for neighbours; Verley et al. (2007a)). Dwarfs are naturally gas rich as they have only recently begun converting their gas to stars. Besides gas richness being associated with the early stages of galaxy formation/evolution, gas richness could also be the result of potential accretion, except for a galaxy to be accreting gas it is most likely not isolated. At the very least we do not expect to see the extreme case of accretion of gas from mergers in an isolated galaxy sample.

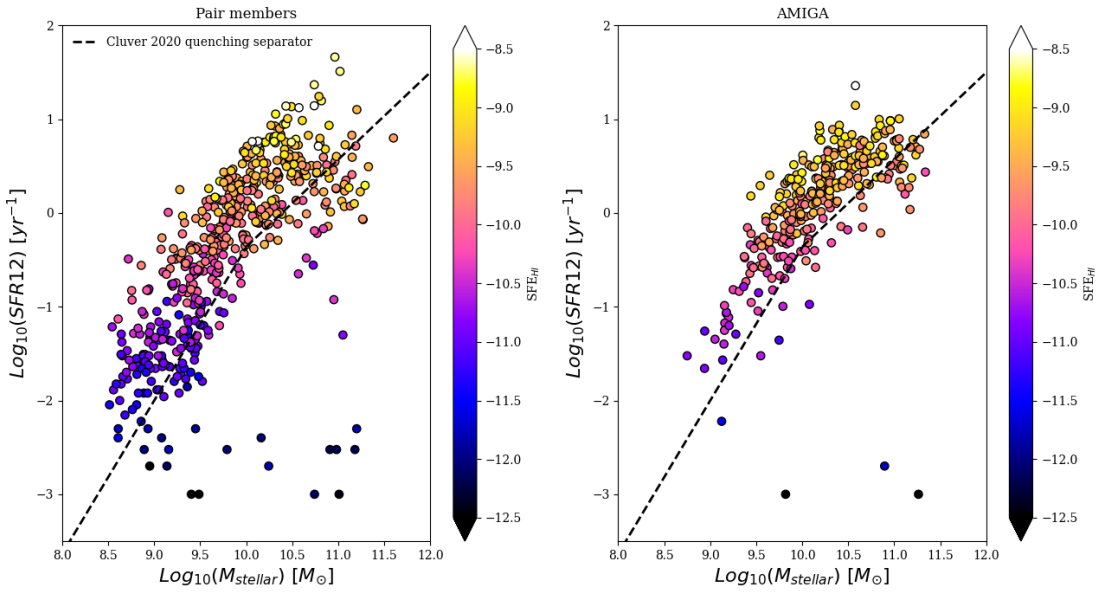

Figure 4.7: Pair (left) and isolated (right) SFMS colour coded by star formation efficiency (SFE(HI)). We see a general trend of SFE increasing along the SFMS. Galaxies with low SFRs appear to be similarly inefficient at forming stars regardless of their stellar mass.

Table 4.1: Fraction of paired and isolated galaxies per stellar mass bin.

Log(M⋆) bins [$M_\odot$]	**8.5-9**	**9-9.5**	**9.5-10**	**10-10.5**	**10.5-11**	**>11**
Pair sample (%)	11.78	23.9	26.23	21.67	12.35	4.75
Isolated sample (%)	0.62	5.61	19.95	35.13	30.35	8.31

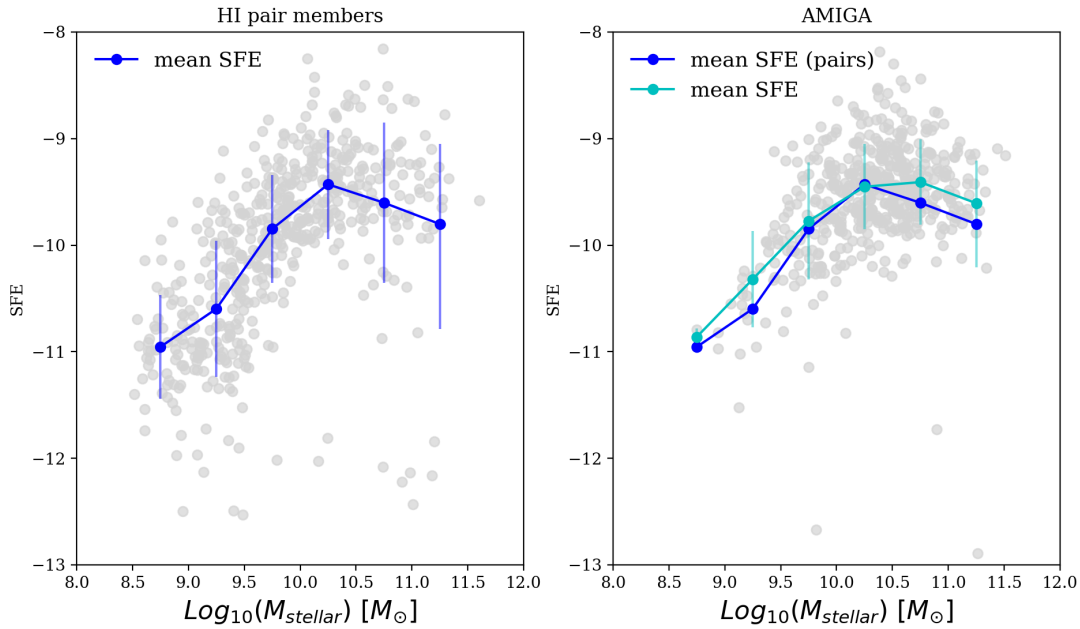

Figure 4.8: Mean SFE(HI) per stellar mass bin (with standard errors depicted as vertical lines) for the pair (left panel) and isolated (right panel) galaxy samples illustrating a pronounced turnover at $\sim 10^{10.25} M_\odot$ in both samples, after which the pair sample mean SFE declines more quickly.

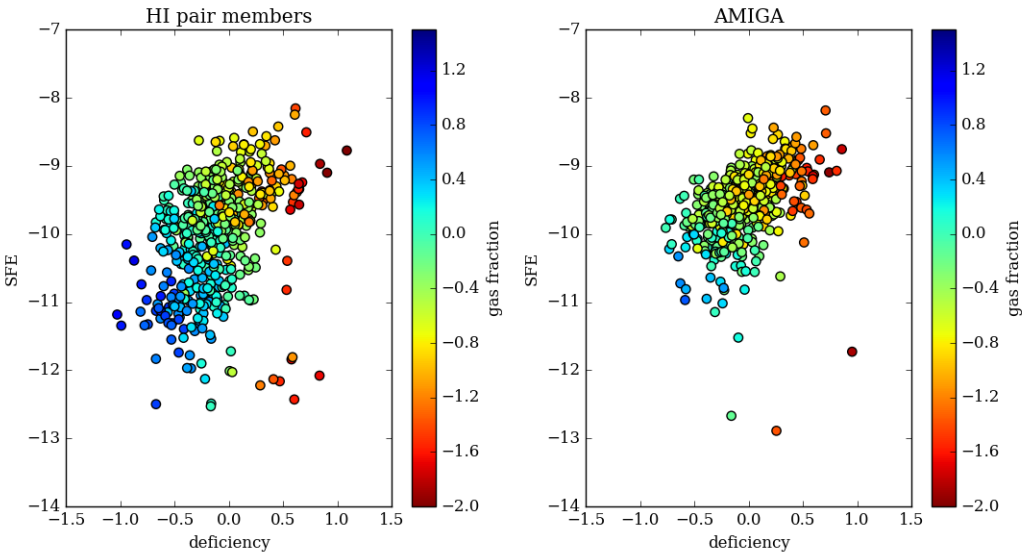

Figure 4.9: HI deficiency as a function of SFE for the pair (left) and isolated (right) galaxy samples. Both plots are colour-coded by gas fraction. Efficient star formation appears to deplete galaxies of their gas reservoirs in both environments, with galaxies becoming increasingly deficient in HI as SFE increases. In the pair sample we see SFE ultimately plummet for a small number of galaxies (bottom right corner of the plot), perhaps marking a later stage in the cycle, where previous high SF has depleted fuel supplies, and halted SF as a result.

4.3.4 HI profile asymmetry

With the integrated HI profiles readily available for our ALFALFA pair members, we maximise their utility by including a study of the profile asymmetries as a function of local environment, as well as HI deficiency. In a previous paper (Bok et al. 2019) we explored the possibility of tracing merger activity via asymmetries measured in the HI profiles of galaxies in close pairs using a simple flux ratio to quantify asymmetry. Our results demonstrated that environment does indeed enhance profile asymmetry, and we proposed that asymmetries measured in the high asymmetry regime (A_c>1.26) could, in turn, be used to infer potential merger activity. We focused exclusively on ALFALFA galaxies with a single close optical (not HI) companion (isolated HI-optical pairs) in our 2019 paper; here in this updated work, we use the pair sample of Bok et al. (2020) in which a single close HI companion is a minimum requirement. Systems with additional companions (HI and otherwise) are not excluded. Consequently, the pair sample of Bok et al. (2020) spans a broad range of local environments, allowing us to study HI profile asymmetry in this more inclusive local environment bracket, and explore the plausible proposition that density of local environment and the degree of measured HI profile asymmetry positively correlate.

Table 4.2: HI profile asymmetry measurements from the literature

Galaxy sample	size	A_c>1.26	error
HI refined subsample (Espada et al., 2011)	166	9%	2.2%
Haynes et al., 1988	104	9%	2.8%
Matthews et al., 1998	30	17%	6.8%
HI isolated sample (Bok et al. ,2019)	304	18%	2.2%
HI optical pair sample (Bok et al., 2019)	304	27%	2.6%
HI pair members (Bok et al., 2020)	**347**	**35%**	**2.6%**

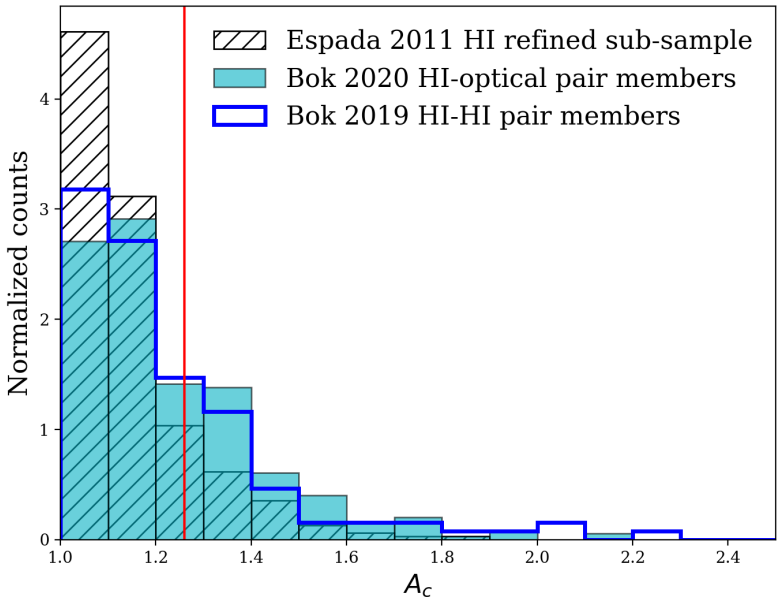

Figure 4.10: Distribution of the Bok 2020 HI pair sample asymmetry measurements (cyan), the Bok 2019 HI-optical pair sample asymmetry measurements (blue line), and the Espada 2011 asymmetry measurements for the HI refined sub-sample of AMIGA galaxies (hatched histogram). The red line marks the threshold for profile symmetry at A_c = 1.26, above which profiles are considered asymmetric.

In Figure 4.10 we contrast the pair sample asymmetry distributions of Bok et al. (2020) (cyan) and Bok et al. (2019) (blue line) with asymmetry measurements from Espada et al. (2011) for the HI refined sub-sample of AMIGA galaxies (hatched histogram). Espada et al. (2011) described the asymmetry distribution of their isolated galaxy sample as a half Gaussian centred on 1 (representing perfect symmetry) with a width σ = 0.13. In recent studies by Scott et al. (2018) and Bok et al. (2019), galaxies with A_c> 1.26 (corresponding to the 2σ width of the isolated distribution) are considered significantly asymmetric. Qualitatively we note that the Bok et al. (2019; 2020) samples follow similar distributions, and are similarly different from

the Espada et al. (2011) sample of isolated galaxy asymmetries in that both exhibit extended tails towards high asymmetries. In Table 4.2 we compare directly with the literature, and note a significantly larger fraction of the Bok et al. (2020) pair sample lie in the $A_c > 1.26$ bins (35%) compared to all previous samples in less densely populated environments: 9% for the isolated galaxies (Espada et al. (2011), Riccardo Giovanelli and Martha P. Haynes (1988)), 17% for field galaxies (Matthews et al. (1998)), and 27% for isolated pairs (Bok et al. (2019)).

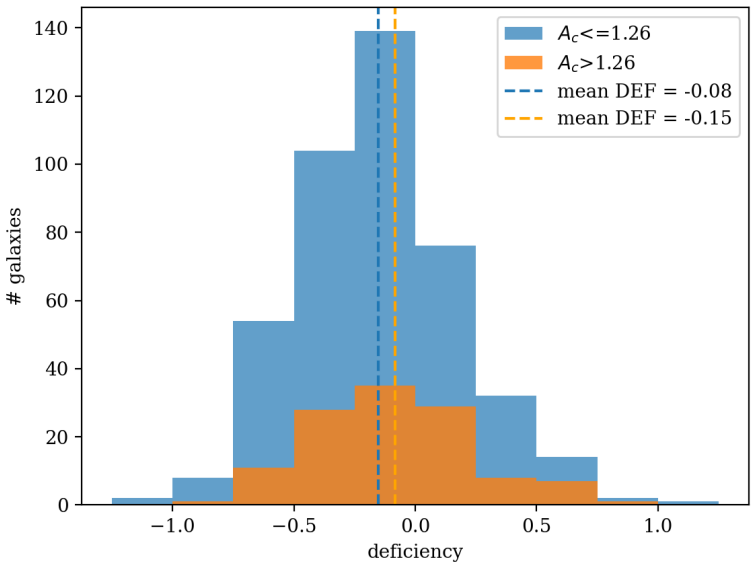

Figure 4.11: Here we contrast the asymmetric (A_c>1.26) deficiency distribution (orange) with the symmetric (A_c<=1.26) deficiency distribution (blue).

Figure 4.11 displays the HI deficiency distributions of the asymmetric (A_c>1.26) and symmetric (A_c<=1.26) populations separately as orange and blue histograms respectively. This plot highlights the relatively small size of the asymmetric population compared to the symmetric population (37% asymmetric versus 63% symmetric), as well as how similarly shaped the asymmetric and symmetric deficiency distributions are. Quantitatively we note that the mean deficiency of the asymmetric population (orange dashed line) is slightly larger than the symmetric deficiency mean (blue dashed line), although both means (-0.08 and -0.15 for the respective asymmetric and symmetric samples) lie in the 'normal' gas content range (-0.25<DEF<0.25). A statistical significance test for the equality of the two distributions is provided by the two-sample Kolmogorov-Smirnov test, which confirms that the asymmetric and symmetric deficiency distributions are not significantly different (D = 0.013, p-value = 0.091).

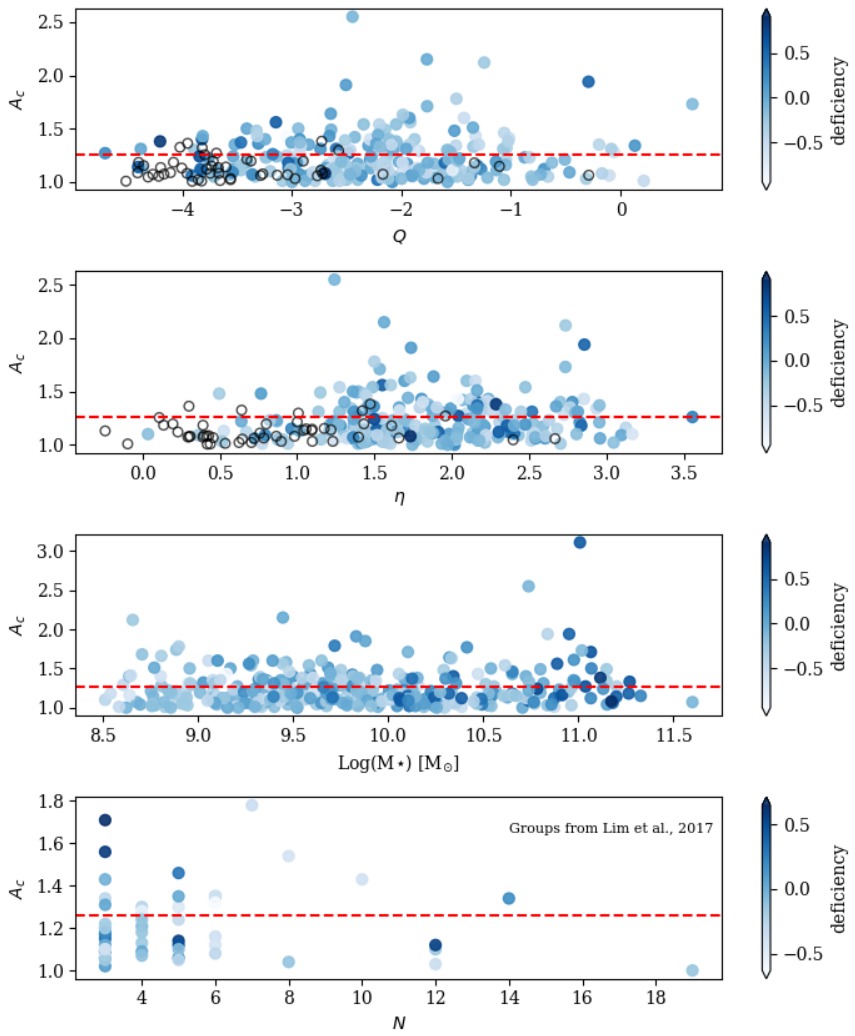

Figure 4.12: From top to bottom: Asymmetry (A_c) as a function of tidal strength (Q), local number density (η), number of group members (N) for the Lim et al. (2017) groups in the pair sample, and stellar mass, colour-coded by HI deficiency. The red horizontal dashed line in each plot corresponds to A_c= 1.26, marking the baseline for asymmetry (profiles with A_c> 1.26 are considered significantly asymmetric). Empty circles (outlined in black) show the location of the AMIGA galaxies for reference in panels 1 and 2. While there are no apparent trends with asymmetry and Q, η, or stellar mass, we note that the largest asymmetries (those with A_c> 1.75) have Q values strictly greater than -2.5. The majority of the group galaxies (shown in the fourth panel) do not measure significant profile asymmetries, and of those that do, the degree of asymmetry does not appear to depend on N.

Table 4.3: Fraction of asymmetric galaxies in bins of Q, η, HI deficiency, Log(M$\star$)

Q bins	**[-5,-4)**	**[-4,-3)**	**[-3,-2)**	**[-2,-1)**	**[-1,0)**	**>0**
A_c**>1.26 (%)**	27.27	20.00	28.46	24.32	13.33	100
(# galaxies)	(3)	(13)	(37)	(27)	(4)	(2)
η **bins**	**[0,0.5)**	**[0.5,1)**	**[1,1.5)**	**[1.5,2)**	**[2,2.5)**	**>2.5**
A_c**>1.26 (%)**	17.24	3.86	28.00	21.78	29.88	25.00
(# galaxies)	(35)	(1)	(21)	(22)	(26)	(15)
Deficiency bins	**<-0.5**	**[-0.5,-0.25)**	**[-0.25,0)**	**[0,0.25)**	**[0.25,0.5)**	**>0.5**
A_c**>1.26 (%)**	15.78	21.21	20.11	27.62	20.00	32.00
(# galaxies)	(12)	(28)	(35)	(29)	(8)	(8)
Log(M$\star$) bins [M$_\odot$]	**[8.5,9)**	**[9,9.5)**	**[9.5,10)**	**[10,10.5)**	**[10.5,11)**	**>11**
A_c**>1.26 (%)**	25.81	24.59	23.19	12.28	29.69	40.00
(# galaxies)	(16)	(30)	(32)	(14)	(18)	(10)

In the top two panels of Figure 4.12 we look at Q and η individually as a function of asymmetry, with HI deficiency additionally encoded as colour. The dashed red horizontal line in each panel corresponds to A_c= 1.26, signifying the baseline value for asymmetry. We find no clear trends between asymmetry and either environment parameter (η or Q). In Table 4.3 we show the frequency of asymmetry (% of galaxies with A_c> 1.26) in bins of both Q, η, and HI deficiency, and again find no indication of a correlation between A_c and the AMIGA environment parameters, or HI content. If we look exclusively at the highest asymmetries in the pair sample (those with A_c> 1.75), we note that their Q values are strictly larger than -2.5, and that they correspond in general to galaxies that are either gas-rich (DEF < -0.25) or have normal HI content (-0.25<DEF<0.25) according to their HI deficiency values, with only 1/6 measuring a positive deficiency (DEF = 0.53).

In the fourth panel of Figure 4.12 we show profile asymmetries measured for the Lim et al. (2017) group galaxies as a function of their group size (N), as well as HI deficiency. We note first that the majority of HI gas (in pairs) lives in small (low N) groups, and that only a relatively small fraction of these group galaxies measure significant HI profile asymmetries (13% with A_c> 1.26). Of the galaxies that are asymmetric in their profiles, group size (N) does not appear to influence the degree of asymmetry, although we acknowledge small numbers in the high N regime. For small groups in particular (N<=4), we observe a broad range of asymmetries, suggestive of active transformation. We additionally look at A_c as a function of stellar mass in panel 3, which demonstrates these quantities to be uncorrelated. We quote the fraction of asymmetric galaxies per stellar mass bin in the last row of Table 4.3, and confirm that stellar mass cannot be used to estimate the frequency of asymmetry in our pair sample.

Table 4.4 lists the most asymmetric (A_c>1.75) galaxies in our pair sample, together with

their Q values, deficiency values, and their local environments as per visual inspection of their optical images. This table demonstrates how similarly high profile asymmetries can arise from a range of different configurations. For example, the gas-poor merger, AGC6965, and the gas rich merger, AGC201011, have equally asymmetric profiles (both with A_c = 1.94). Similar can be said for both pairs and groups. We show the optical images and HI profiles of a subset of these galaxies in Figure 4.13 for reference.

Table 4.4: Q and DEF values for the high asymmetry (A_c >1.75) population, with notes on the local environment as per visual inspection of the optical SDSS cutouts indicated in the last column. Red indicates a galaxy is gas-poor (i.e. DEF>0.25), and blue indicates gas-richness (DEF<-0.25).

AGC #	A_c	**Q**	**DEF**	**Environment note**
6965	1.94	-0.29	0.53	merger
102774	1.79	–	0.38	pair
201011	1.94	–	-0.40	merger
215143	2.12	-1.24	-0.25	pair
230069	1.91	-2.51	0.13	pair
233692	2.15	-1.76	0.007	pair
240367	2.55	-2.44	-0.08	potential group
715991	1.85	–	0.05	potential group
732066	1.78	-1.49	-0.33	pair
1286	3.11	–	0.6	potential group
330779	1.77	–	0.2	potential group

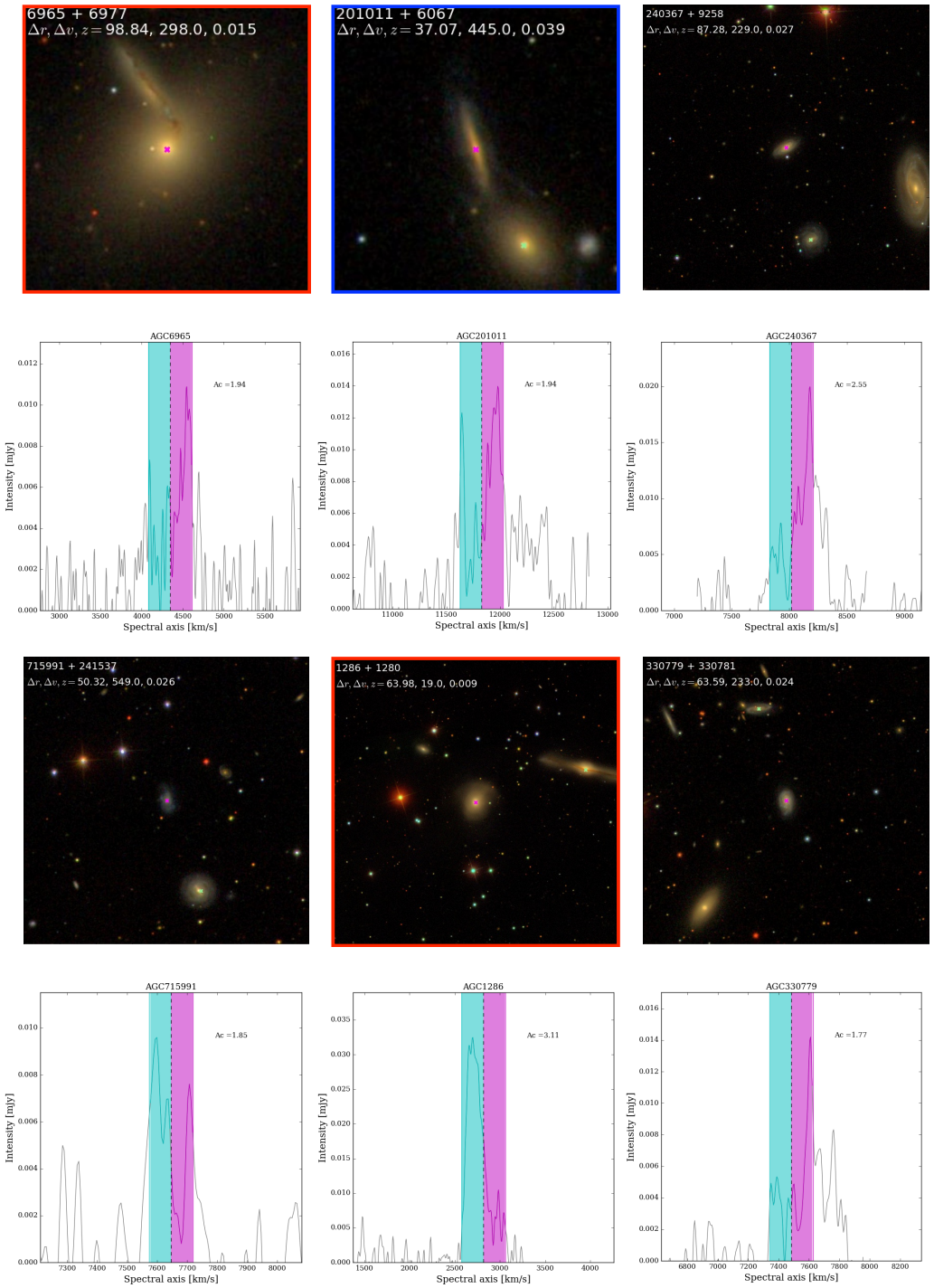
6965 + 6977
Δr, Δv, z = 98.84, 298.0, 0.015
201011 + 6067
Δr, Δv, z = 37.07, 445.0, 0.039
240367 + 9258
Δr, Δv, z = 87.28, 229.0, 0.027
AGC6965
Ac =1.94
AGC201011
Ac =1.94
AGC240367
Ac =2.55
Intensity [mJy]
Spectral axis [km/s]
715991 + 241537
Δr, Δv, z = 50.32, 549.0, 0.026
1286 + 1280
Δr, Δv, z = 63.98, 19.0, 0.009
330779 + 330781
Δr, Δv, z = 63.59, 233.0, 0.024
AGC715991
Ac =1.85
AGC1286
Ac =3.11
AGC330779
Ac =1.77

Figure 4.13: Optical images and HI profiles of some of the most asymmetric (A_c>1.75) galaxies in our pair sample that appear to be currently merging, or in a group. From left to right in panel 1: optical cutouts of the merging pairs AGC6965/6977, AGC201011/6067, and the potential group AGC240367/9258, with their corresponding HI profiles shown below them in panel 2. From left to right in panel 3: the potential groups AGC715991/241537, AGC1286/1280, and AGC330779/330781, with their corresponding HI profiles shown below in panel 4. Red borders indicate the target galaxy (magenta cross) is gas-poor, and the blue border indicates gas-richness. Turquoise and pink shading in the HI profiles indicate the extent of the left and right velocity horns respectively.

4.4 Discussion

By invoking the use of the AMIGA local number density (η) and tidal influence (Q) parameters, galaxy morphologies, and HI profile asymmetries to further characterize our pair sample galaxies, we start to differentiate between the high and low HI deficiency tails of the pair sample deficiency distribution in Bok et al. (2020) as arising from different sub-populations in the sample, and associated with different dynamics. In Figures 4.3 and 4.4 we see that the low deficiency (gas-rich) tail of the distribution corresponds to higher tidal influence (Q) values and lower number densities (η) in general compared to the HI deficient population, however note that these differences are not statistically significant when we compare their means (Q_{mean} = -1.9 ±0.96 and η_{mean} = 1.9 ±0.66 for the gas rich sample (DEF<-0.25), versus Q_{mean} = -2.8 ±1.02 η_{mean} = 2.1 ±0.67 for the gas poor sample (DEF>0.25)). This suggests a local environment in which the target galaxies have a few (low η) relatively large (high Q) neighbours. The mean η value of the most deficient galaxies (DEF>0.4), in fact, coincides with that of Karachentseva (1973)'s isolated triples sample (Figure 4.4). Simulations of merging galaxies show that the merger process is capable of elevating the cold-dense gas content in both primaries and secondaries (Moreno et al. 2020) by way of gravitational torques, and observations of merging/recently merged galaxies show that these galaxies are indeed gas-rich compared to control samples (Ellison et al. 2018). Our results indicate the possible presence of a sub-sample of currently merging/recently merged galaxies in our pair sample, who are gas rich (i.e. with low HI deficiencies) as a result of their merger activity, which we infer from their large Q values (Q_{mean} = -1.9). We note that the deficiency distribution of the irregular galaxy population is also shifted to lower deficiencies compared to both the dominant spiral and small elliptical/S0 galaxy populations (see Figure 4.6), strengthening the argument for a merging sub-sample if we attribute the disturbed, irregular morphologies to merger activity, which is plausible given the coincidence of high Q values. The link between merger activity and disturbed optical morphologies is indeed well documented in the literature (Patton et al. 2005, De Propris et al. 2007, Ellison et al. 2010). The largest HI profile asymmetries (A_c>1.75)

in our pair sample are also associated with Q values strictly larger than -2.5 (see top panel of Figure 4.12), and we put forward that the link is likely causal. Sulentic et al. (2006) found a similar link between high Q values and optically distorted galaxy morphologies.

On the other hand, the high deficiency tail of the pair sample distribution appears to arise from a different set of circumstances. As we see in Figures 4.3 and 4.4, the most deficient galaxies in the sample live on average in more densely populated environments relative to the low deficiency (gas-rich) sample ($\eta_{\rm mean}$=2.1 versus $\eta_{\rm mean}$ = 1.9, respectively). They are also subject to smaller tidal forces on average ($Q_{\rm mean}$ = -2.8 versus -1.9). This suggests a local environment of relatively many, but smaller companions, compared to the gas-rich sample η-Q environment, more akin to a group environment than a merger-pair environment. If these galaxies are indeed living in gravitationally-bound groups, their deficiency in HI can be understood as a consequence of the group environment, which Hess & Wilcots (2013) demonstrate will produce increasingly HI deficient central cores as optical membership increases. Interestingly, the confirmed groups in our sample (those that are part of the Lim et al. (2017) galaxy group catalogue), do not appear to be particularly deficient in HI compared to the rest of the sample, nor does their group membership (N) seem to trend with deficiency. Looking to morphology again (Figure 4.6), the small population of early-type galaxies in the pair sample live almost exclusively in the positive deficiency wing of the deficiency distribution, with a mean deficiency significantly higher than both the spiral and irregular galaxy populations ($\rm DEF_{mean}$ = 0.26, -0.11, and -0.27 for the E/S0, spiral, and irregular galaxy populations respectively). Solanes et al. (2001) also found early-type galaxies to be HI deficient relative to later-types in their study. The presence of early-type galaxies in our pair sample (and relative absence of early-type galaxies in our isolated sample) suggests that morphology is likely contributing to the broadening of the pair sample deficiency distribution towards high HI deficiencies relative to the isolated sample deficiency distribution.

In addition to a broadened deficiency distribution, our pair sample also has a larger low SF/quiescent population relative to the isolated galaxy sample (see Figure 3.6 in Bok et al. (2020)/chapter 3). Upon examination of the HI content of these galaxies, two sub-populations emerged: a low stellar mass/gas-rich population, and a high mass/gas-poor population. The distinctly different gas and mass properties of these two populations suggest different pathways to their quenching. In Figure 4.7 we colour code the SFMS by star formation efficiency (SFE) and find that the low SFR galaxies in both the pair and isolated samples all have similarly low SFEs, implicating SFE as an important pathway to quenching regardless of environment, stellar mass, and gas content.

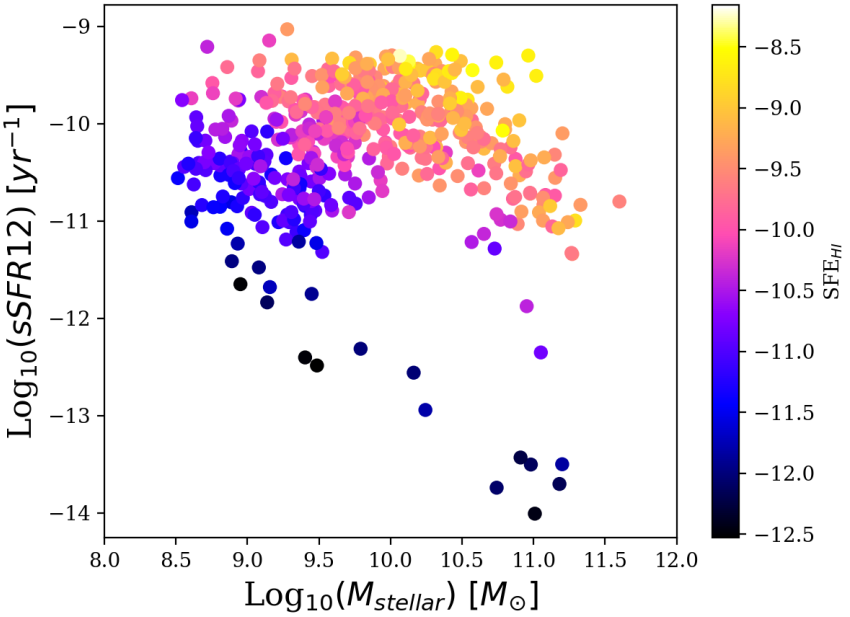

Figure 4.14: Specific star formation (log10(SFR/M★)) versus stellar mass, colour coded by SFE (SFR/M_{HI}). Here we note that our low SFR/SFE populations, previously identified as either low mass and gas rich or high mass and gas poor, can also be separated in sSFR. Both populations have low sSFRs with respect to the main SF sample, however the low mass population is relatively more active than the high mass population.

In Figure 4.14 we plot the specific SFRs (sSFR = SFR/$M_\star$) for our pair galaxies as a function of their stellar mass, and indicate their SFE as colour. Here we note that the low SFR, and low SFE populations previously categorized as either low mass and gas rich, or high mass and gas poor, are additionally separate in their specific star formation rates. While both populations have low sSFR's relative to the main SF population, the low mass galaxies have higher sSFRs (on average) compared to the high mass group (i.e. both populations are under-performing for their weight in terms of SF, and this is more pronounced in the high mass group. Low SFRs and sSFRs in the high mass/gas-poor population can plausibly be explained as driven by the consumption fuel (hence gas-poor) into stars (high stellar mass). With gas reserves depleted, continued SF is unsustainable, and these galaxies can be described as (fast approaching) fully quenched. The low mass population, on the other hand, with their extensive gas reservoirs, may continue to build up their stellar mass via slow and inefficient SF for many years to come, and might then build enough mass to become more efficient star formers. Low SFEs in this population are potentially the result of merger activity, which Moreno et al.

(2020) showed could undermine SF in galaxies with cold-dense gas reservoirs. The ultimate fate of these galaxies may simply be slow death by fuel consumption, or perhaps external processes may intervene and alter their SF journeys, just as external processes may have already undermined their SF by impeding SFE. The fact that we see an increased frequency of low SFE galaxies in the pair sample relative to our isolated sample is potentially the result of merger induced turbulence in the pair sample, which Ellison et al. (2018) propose can reduce SFE, and thereby hinder effective SF. Angular momentum, which is large in large gas disks (high gas fraction galaxies) (Obreschkow et al. 2016), may also be contributing to the low SF in the gas rich population by providing resistance to collapse along the axis of rotation.

Our HI profile analysis revealed our pair sample to have a significantly higher fraction of asymmetric profiles (35% with A_c> 1.26) compared to previous samples in the literature, where a similar flux ratio was used to quantify profile asymmetry in less densely populated (isolated and field) environments (i.e. 9%,9%,17%,18% with A_c> 1.26 in the Espada et al. (2011), Riccardo Giovanelli and Martha P. Haynes (1988), Matthews et al. (1998) and Bok et al. (2019) samples respectively). We attribute this strong signal in asymmetry in our pair sample to the close pair environment, in which tidal interactions are likely at play. Our pair sample also has a higher fraction of asymmetric profiles compared to the pair sample used in Bok et al. (2019), in which 27% (versus 35%) of the HI profiles were classified as asymmetric. The key differences between the two pair samples are the gas-rich requirements of the pair members used in this study (M_{HI}>10^9 $M_\odot$), as well as the allowance of additional companions (more densely populated environments) in the 2020 sample. Examining our profile asymmetries as function of the AMIGA environment parameters reveals no clear trend of increasing asymmetry with density of environment (η), or tidal strength (Q). We also find no evidence to suggest that group size (N) influences the degree of asymmetry when we specifically look at the asymmetry measurements for the Lim et al. (2017) groups in our pair sample as a function of N. The majority of the group galaxies, in fact, do not measure a significant profile asymmetry (only 13% with A_c> 1.26). Our results show no signal of asymmetry being enhanced in groups relative to close pairs, nor between more densely populated environments (as per the AMIGA environment parameters) and close pairs. Similar asymmetry values are found for a broad range of environments, and conversely, particular environments (e.g. small groups) produce a variety of A_c values, ranging from symmetric to highly symmetric. While we certainly see an enhanced frequency of asymmetry in close pair galaxies relative to isolated galaxies, from which we may infer potential merger activity between close companions, the asymmetry value alone cannot be used to distinguish the close pair environment from more densely populated environments.

With regards to gas-content, the deficiency distributions of the asymmetric and symmetric populations are qualitatively similar in shape (see Figure 4.11). Using the two-sample Kolmogorov-Smirnov test to statistically compare the asymmetric and symmetric deficiency distributions, we find that the samples are indeed not significantly different (D = 0.013, p-value = 0.091). Watts et al. (2021) present similar findings in their recent study of the relationship between HI profile asymmetry and gas content. Using the same flux ratio to quantify HI profile asymmetry as the one used in this paper, they find no systematic differences in the HI content of asymmetric and symmetric galaxies. *Our findings here, and those of Watts et al. (2021), indicate the limitations of HI profile asymmetries in communicating their origins.* Such an endeavour may be better suited to cosmological-hydrodynamical galaxy evolution simulations, which Watts et al. (2020) have already shown capable of providing valuable insight into the potential drivers of asymmetry in HI profiles, specifically how a particular asymmetry can arise from multiple physical processes.

4.5 Summary

- We compute the AMIGA environment parameters η and Q for our pair member galaxies and find that our pair members occupy a broad region on the $\eta - Q$ plane, inclusive of triples, groups, and clusters, and distinctly separate from the isolated galaxy population (AMIGA galaxies). We find weak trends of decreasing(/increasing) $Q(/\eta)$ with increasing deficiency

- We visually classify our pair member morphologies and find the sample to consist largely of spiral galaxies (68%), with irregulars and elliptical/S0 galaxies making up 17% and 5% of the sample respectively. Our visual classification scheme is in good agreement with the MIR morphology diagnostics presented for the pair members in Bok et al. (2020) (*WISE* colour-colour diagram and B/T radial profile decomposition measurements).

- We examine HI morphology on the SFMS and show that the low SF galaxies in the pair sample (below the SFMS) are dominated by early-type morphologies, and that these galaxies are shifted towards higher HI deficiencies, contributing to the broadening of the pair sample deficiency distribution to the right.

- We present the star-formation efficiencies for both samples on the SFMS and find that regardless of environment, stellar mass, and HI content, galaxies that have migrated off the SFMS are extremely inefficient at forming stars, with low specific star formation rates. In general SFE increases along the SFMS in both samples, and when we look at the mean SFEs per stellar mass bin we find a turnover in SFE at $\sim 10^{10.25}$ $M_{\odot}$(just before, and

perhaps driving the SFMS turnover at $\sim 10^{10.5}$ $M_{\odot}$), after which the pair sample SFE declines more quickly.

- We compute the HI profile asymmetries of the pair sample using a standard flux ratio, and find a significantly higher rate of high profile asymmetries (with $A_c > 1.26$) compared to samples in less dense environments in the literature. However, we find no evidence of the degree of profile asymmetry increasing with density of environment within our pair sample when we examine asymmetry as a function of η, Q, and group size (N) for the galaxy groups in our sample. We also find no trends between profile asymmetry and HI deficiency.

In this chapter we invoke various galaxy properties derived from optical, radio, and MIR data to investigate potential pathways for the observed trends we find for HI deficiency and galaxy location on the SFMS as a function of environment. While we provide plausible scenarios with the data in hand, inferring potential mechanisms for accretion, gas removal, and quenching, as well as merger activity, from quantities such as HI deficiency, HI profile asymmetry, galaxy morphology (optical and MIR), and the AMIGA isolation parameters (η and Q), the next generation of radio surveys with SKA1-MID are expected to provide direct evidence of accretion, as well as disentangle various gas removal mechanisms, by probing the intergalactic medium (IGM)/intragroup medium in unprecedented detail. State of the art simulations that incorporate more accurate astrophysical processes into their routines, i.e. Moreno et al. (2021)'s FIRE2 simulations, will provide important context for these next-generation observations.

Acknowledgements

This work is based on the research supported in part by the National Research Foundation of South Africa (Grant Numbers UID: 101099 and 111745). JB additionally acknowledges support from the DST-NRF Professional Development Programme (PDP), and the University of Cape Town. MC is a recipient of an Australian Research Council Future Fellowship (project number FT170100273) funded by the Australian Government. THJ acknowledges funding from the National Research Foundation under the Research Career Advancement and South African Research Chair Initiative programs, respectively. We acknowledge the work of the entire ALFALFA team for observing, flagging and performing signal extraction. MGJ is supported by a Juan de la Cierva formación fellowship (FJCI-2016-29685) from the Spanish Ministerio de Ciencia, Innovacion y Universidades (MCIU). MGJ also acknowledges support from the grants AYA2015-65973-C3-1- R (MINECO/FEDER, UE) and RTI2018-096228-B-C31 (MCIU). This work has been supported by the State Agency for Research of the Spanish MCIU through the 'Centro de Excelencia Severo Ochoa' award to the Instituto de Astrofísica de

Andalucía (SEV-2017-0709). This publication makes use of data products from the Wide-field Infrared Survey Explorer, which is a joint project of the University of California, Los Angeles, and the Jet Propulsion Laboratory/California Institute of Technology, funded by the National Aeronautics and Space Administration. This work also utilizes data from Arecibo Legacy Fast ALFA (ALFALFA) survey data set obtained with the Arecibo L-band Feed Array (ALFA) on the Arecibo 305m telescope. Arecibo Observatory is part of the National Astronomy and Ionosphere Center, which is operated by Cornell University under Cooperative Agreement with the U.S. National Science Foundation. Funding for the SDSS and SDSS-II has been provided by the Alfred P. Sloan Foundation, the Participating Institutions, the National Science Foundation, the U.S. Department of Energy, the National Aeronautics and Space Administration, the Japanese Monbukagakusho, the Max Planck Society, and the Higher Education Funding Council for England. The SDSS Web Site is http://www.sdss.org/. In addition, we make use of data from the Sloan Digital Sky Survey (SDSS DR7). The SDSS is managed by the Astrophysical Research Consortium for the Participating Institutions. The Participating Institutions are the American Museum of Natural History, Astrophysical Institute Potsdam, University of Basel, University of Cambridge, Case Western Reserve University, University of Chicago, Drexel University, Fermilab, the Institute for Advanced Study, the Japan Participation Group, Johns Hopkins University, the Joint Institute for Nuclear Astrophysics, the Kavli Institute for Particle Astrophysics and Cosmology, the Korean Scientist Group, the Chinese Academy of Sciences (LAMOST), Los Alamos National Laboratory, the Max-Planck-Institute for Astronomy (MPIA), the Max-Planck-Institute for Astrophysics (MPA), New Mexico State University, Ohio State University, University of Pittsburgh, University of Portsmouth, Princeton University, the United States Naval Observatory, and the University of Washington.

Chapter 5

Conclusions

In this thesis I investigated the roles of galaxy environment and HI content (gas fraction, HI deficiency, and SFE(HI)) in driving galaxy evolution (star formation and galaxy morphology) by collating publicly available data in the optical (SDSS) and radio (ALFALFA/AMIGA) wavelengths, with new MIR imaging data and source characterization from *WISE*. I contrasted the distributions of various galaxy properties as a function of environment (close pair galaxies versus isolated galaxies), and postulated possible pathways to my results by conducting a multi-wavelength analysis of the trends.

By taking care to establish a baseline for secular evolution, I gauged the impact of close/merger companions on both star formation activity, and HI content in galaxies. The identification of galaxy environment was addressed in Chapter 2 where I examined the plausibility of using HI profile asymmetries to trace merger activity in lieu of HI maps. This work is particularly pertinent at high redshifts where resolution is too poor for resolved imaging. I then turned to the MIR galaxy main sequence to study the role of HI content in dictating galaxy location on the SFMS in the local Universe, and thus in both enhancing and suppressing star formation, as well as in the build-up of stellar mass. I solicit galaxy morphology (visual optical morphologies, and MIR colours and B/T ratios), the AMIGA isolation parameters η (local number density) and Q (tidal influence), star formation efficiency, and HI profile asymmetries to investigate trends in the HI deficiency distributions of paired and isolated galaxies.

5.1 Exploring galaxy environment as a driver of HI quantities

5.1.1 HI profile asymmetries

I began my study of the relationship between galaxy environment and HI content in Chapter 2 (published in Bok et al. (2019)) with an investigation into the proposition that merger activity causes HI profiles to become asymmetric. By quantifying and contrasting the distribution of HI profile asymmetries of a sample of close pair galaxies with a control sample of isolated galaxies (both drawn from the ALFALFA α40 catalogue), I explored the possibility of using HI profile asymmetries to trace merger activity. The most discernible feature between the two distributions is a longer tail in the pair asymmetry distribution extending towards high asymmetries. A statistically significant measure of this difference is provided by the k-sample Anderson-Darling (A-D) test (Scholz & Stephens (1987)). Bootstrap re-sampling my isolated galaxy sample 10000 times, I measured a mean A-D test statistic between the pair and isolated samples of A^2 =12.18, with a mean p-value = 0.0002, and therefore rejected the null hypothesis that they are drawn from the same distribution at the 1% level. With the pair and isolated galaxies matched in redshift, well matched in u-r colour and SNR, and confusion ruled out as having a significant impact on my results by simulations, I attributed the enhanced frequency of high asymmetries in the pair sample to environment, and concluded that merger activity is most likely responsible for the measured difference in HI profile asymmetries between our pair and isolated sample. This work provided the first quantitative look into HI profile asymmetries in contrasting environments for large samples of paired and isolated galaxies, and showed that the asymmetry distributions of close pair and isolated galaxies are statistically, and significantly different.

5.1.2 HI deficiency

In Chapter 3 (published in Bok et al. (2020)) I shifted my focus from the aesthetics of the HI profile (in response to environmental influence) to its content. I derived for the first time an HI scaling relation for isolated galaxies using *WISE* W1 (3.4μm)-derived host stellar masses, and thereby established a baseline predictor of HI content that can be used to assess the impact of environment on HI content when compared with samples of galaxies in different environments. By using the most reliably isolated sample of galaxies (AMIGA) to derive the HI scaling relation, we ensure the best possible description of HI content that has been free from external influence for at least the past 3 Myr. The scaling relation is presented here again

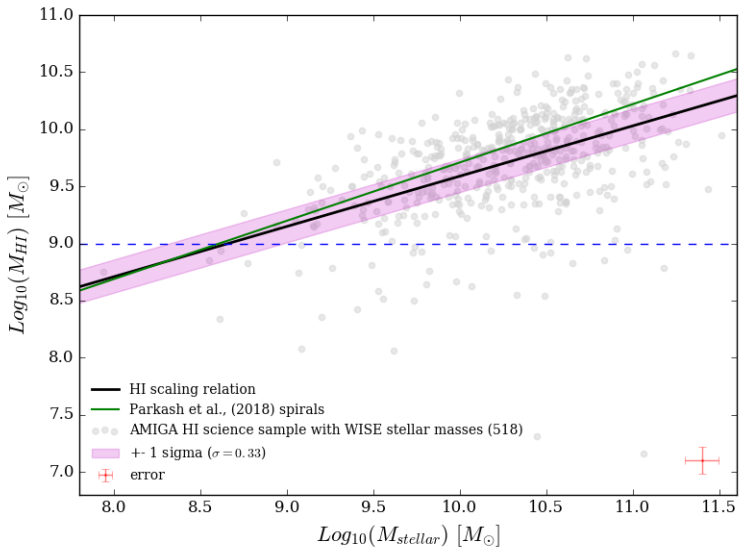

Figure 5.1: The HI scaling relation (solid black line) for the AMIGA HI science sample galaxies (gray points) with the 1σ region shaded in pink. The relation is described by the equation $\mathrm{Log_{10}(M_{HI})[M_\odot]} = 0.44 \times \mathrm{Log_{10}(M_\star)[M_\odot]} + 5.19$, σ= 0.33. The dark green line indicates the Parkash et al. (2018) HI scaling relation for spiral galaxies, and the dashed blue line marks the HI mass cut applied to both our isolated and pair samples ($\mathrm{M_{HI}} > 10^9\ \mathrm{M_\odot}$). Galaxies below this line are not included in the AMIGA-*WISE* sample.

in Figure 5.1 as an important result that may be used widely in future studies to identify, and investigate, anomalous HI content.

I used this relation to compute the HI deficiencies of my pair sample galaxies (the expected HI content given their stellar masses), and found that the deficiency distribution is broadened to both high (i.e. less HI content than expected) and low (i.e. more HI content than expected) deficiencies compared to the narrower distribution of the isolated galaxy sample (σ_{pairs} = 0.34 versus $\sigma_{isolated}$ = 0.28). From the literature we know that different galaxy environments impact HI content differently; the cluster and galaxy group environments appear to produce HI deficient galaxies, while merger activity in galaxy pairs appears to augment HI supplies. Since there is a higher frequency of both high and low deficiency galaxies present in my pair sample, I explored the inference of a broader local environment in my pair sample, which is not ruled out by my selection criteria, by quantifying the local environments around each of my pair galaxy members in a more descriptive manner. I presented the local number density (η) in the vicinity of each galaxy, as well as an estimate of the tidal strength (Q) exerted on each galaxy by neighbours, and found that my pair sample does indeed contain galaxies in a broad range of local environments.

By looking at HI deficiency as a function of these environment parameters I was able to differentiate between the high and low HI deficiency tails of the pair sample deficiency distribution (see figure 3.11) as arising from different sub-populations in the sample, and associated with different physics. The low deficiency (gas-rich) tail of the distribution corresponds to higher tidal influence (Q) values, and lower number densities (η) in general (see Figures 4.3 and 4.4) compared to the HI deficient population. This suggests a local environment in which the target galaxies have a few (low η) relatively large (high Q) neighbours. Simulations of merging galaxies show that the merger process is capable of elevating the HI content in both primaries and secondaries (Moreno et al. 2020) by way of gravitational torques, and observations of merging/recently merged galaxies show that these galaxies are indeed gas-rich (Ellison et al. 2018), seem to sit higher on the SFMS, and would be considered actively star-forming/IR bright, compared to control samples. These results indicate the possible presence of a sub-sample of currently merging/recently merged galaxies in the B20 sample, which are gas rich (i.e. with low HI deficiencies) as a result of their merger activity, which is inferred from their large Q values.

The high deficiency tail of the pair sample distribution appears to arise from a different set of environmental conditions. Based on their mean η value, the most deficient galaxies in the sample live on average in more densely populated environments relative to the low deficiency (gas-rich) sample (see Figures 4.3 and 4.4), they are also subject to smaller tidal forces (lower mean Q) on average. This suggests a local environment of relatively many, but smaller companions, compared to the gas-rich sample η-Q environment, more akin to a group environment than a merger-pair environment. If these galaxies are indeed living in gravitationally-bound groups, their deficiency in HI can be understood as a consequence of the group environment, which Hess & Wilcots (2013) demonstrate will produce increasingly deficient central cores as optical membership increases. Interestingly, the confirmed groups in my sample (those that are part of the Lim et al. (2017) galaxy group catalogue), do not appear to be particularly deficient in HI compared to the rest of the sample, nor does their group membership (N) seem to trend with deficiency as was found by Hess & Wilcots (2013), except perhaps for the larger groups (N>4), of which we have too few in our sample to make any categoric statements.

Since the extreme case of a close pair environment did indeed show a signal in HI profile asymmetry, in Chapter 4 I extended upon the work done in Chapter 2 by exploring how different environments, quantified by the AMIGA isolation parameters (η and Q), impact HI profile asymmetries. Using the same metric to quantify profile asymmetry as was used in Chapter 2 for my original close pair sample (hereafter referred to as B19), I found that the

Table 5.1: HI profile asymmetry measurements from the literature

Galaxy sample	size	A_c >1.26	error
HI refined subsample (Espada et al., 2011)	166	9%	2.2%
Haynes et al., 1988	104	9%	2.8%
Matthews et al., 1998	30	17%	6.8%
HI isolated sample (Bok et al. ,2019)	304	18%	2.2%
HI optical pair sample (Bok et al., 2019)	304	27%	2.6%
HI pair members (Bok et al., 2020)	**347**	**35%**	**2.6%**

asymmetry distribution of the Bok et al. (2020) pair sample (hereafter B20) is qualitatively similar to that of the B19 sample, with an extended tail towards high asymmetries akin to that of the B19 distribution. Quantitatively, the B20 sample has a significantly larger fraction of high profile asymmetries (35% with $A_c > 1.26$) compared to previous samples in less densely populated environments from the literature (see table 5.1). I find no correlation between profile asymmetry and the AMIGA isolation parameters η and Q measured for B20, despite their values indicating a broad range of environments present (isolated pairs, triples, and groups). Similarly, I find no correlation between group membership and asymmetry for those galaxies in the B20 sample identified as groups in the Lim et al. (2017) galaxy group catalogue, which may simply reflect the limited sample size we have of groups with N>4.

My work on profile asymmetries as a function of galaxy environment suggests that while high profile asymmetries may be used to infer potential merger activity, they cannot be used to distinguish isolated mergers from those that reside in more densely populated environments. While imaging techniques might provide a more robust measure of merger activity, HI profile asymmetries provide an alternative that can already be applied to large samples of galaxies. Furthermore, in the absence of imaging data at high redshifts, employing HI profile asymmetries as an indicator of merger activity can allow us to estimate merger activity in the early Universe (soon to be probed in HI with SKA), and test galaxy evolution models. Nevertheless, caution is merited when using single-dish HI profiles for classification and drawing of samples since they do not appear to have the fidelity to differentiate local tidal activity.

5.2 Probing star formation with HI content

When we speak of galaxy evolution, essentially what we are interested in are the processes by which galaxies build up their stellar mass content, and transition from being actively star-forming to quiescent (which roughly correlates with a morphological transition from late to early types). The rate at which galaxies form stars (SFR) is therefore incredibly important for

galaxy evolution, as well as those mechanisms/processes driving SF. HI provides the fuel for SF, it is the prerequisite for the formation of stars. There are, however, many additional factors that require consideration when forming a complete picture for galaxy evolution. For example, how efficiently galaxies convert gas into stars, what particular conditions are conducive to efficient SF or hinder SF, what mechanisms act to deplete galaxies of their fuel (and therefore obstruct SF), and how galaxies replenish their gas reservoirs, as we know is necessary to sustain current SFRs.

I presented the first *WISE* MIR SFR-M$\star$ sequences (star-forming main sequence/SFMS) for isolated and paired galaxies In Chapter 3. With HI content additionally encoded on the SFMS I was able to explore specifically how HI content might be driving the star formation evolution of galaxies in both isolated and more densely populated environments.

5.2.1 The MIR SFMS

The galaxy SFMS (star-forming main sequence) is an incredibly useful diagnostic for identifying instances of both enhanced SF and suppressed SF, which correspond to galaxies that have migrated both upward (starbursts) and downward (quenched) of the SFMS respectively. By additionally looking at HI content on the SFMS we are able to probe its role in driving galaxy location on the SFMS. Any inference we make from a galaxy's location on the SFMS is only as valuable as the SFRs and stellar masses we use are accurate. Interacting spiral galaxies (wet mergers) are inherently dusty. UV/optical SFR tracers would suffer severe extinction in such an environment, as well as introduce significant uncertainty into the measurements. Infrared space telescope, *WISE*, which is sensitive to the evolved stellar population, ISM processes and dust distribution, is particularly well-suited to measuring accurate and reliable stellar masses and SFRs in interacting galaxies, and therefore most appropriate for this study. For a detailed review of the various SFR tracers, as well as the performance of the *WISE* tracers, see §1.4.1.

Our SFMS study revealed a number of important differences between galaxy evolution in isolated environments and more densely populated environments. The difference measured in SFMS scatter ($\sigma_{\rm AMIGA} = 0.37$ versus $\sigma_{\rm PAIRS} = 0.55$) suggests that galaxies in isolation behave relatively predictably, while galaxies that are subject to the potential external influence of one or more close neighbours adopt a more stochastic behaviour.

The pair sample also exhibits an increased frequency of low SF (quiescent) galaxies, which are identified as those galaxies that have fallen well below the SFMS. Examining HI deficiency on the SFMS revealed the low SF galaxies in both samples can be categorized as being either low mass and gas rich, or high mass and gas poor. A likely scenario for the quenching of the latter population of galaxies is simply consumption of fuel. As neutral

hydrogen is converted to stars via molecular gas, the HI content of the galaxy decreases while the stellar mass content increases, thus producing high stellar mass galaxies with depleted gas fractions. The increased frequency of quenched galaxies as stellar mass increases we observe is consistent with the findings of Cluver et al. (2020), who make the same observation for samples of field and grouped galaxies from the Galaxy and Mass Assembly survey (GAMA) with *WISE* photometry, and attribute this result to mass quenching. Mass quenching refers to quenching via internal processes such as AGN feedback, or starvation (i.e. secular evolution). Based on the locations of the small populations of AGN on the SFMS in both the pair and isolated samples (see Figure 3.6), AGN activity was ruled out as a quenching mechanism. Starvation is thus a more likely pathway to quenching in our high mass populations.

Looking at the morphologies of the high mass, gas-poor, low SF galaxies, which are early type based on my visual classification and bulgy according to MIR B/T ratios, suggests a possible morphological quenching scenario. In this scenario the formation of a bulge stabilizes the disk against the gravitational collapse necessary for SF to occur (Bluck et al. 2014). Cook et al. (2019), however, find little evidence to suggest that the presence of a large bulge can alter the gas disk, and cautions interpreting the link between large bulges and quenched galaxies as causal. They suggest quenching processes are more likely occur at the source of in-flowing gas.

The lower mass, low SFR galaxies are disk dominated/late type in morphology, gas rich, with low HI deficiencies (excess HI), suggesting an alternative quenching mechanism in the low stellar mass regime. While the fuel for SF is abundant, the column density of the HI gas may be insufficient to ignite SF. Large angular momentum may also be acting as a support mechanism against collapse (necessary for SF), and thus contributing to the low levels of SF measured in these galaxies-Obreschkow et al. (2016) showed that high atomic gas fraction galaxies have large angular momentum. The lack of SF in these galaxies might also be as a result of gravitational shock heating of their gas (Liu & Cen 2017). Alternatively, these galaxies have simply yet to reach the SFMS.

5.2.2 Star formation efficiency on the SFMS

Quiescence in the high mass/gas-poor population can plausibly be explained as driven by the consumption fuel (hence gas-poor) into stars (high stellar mass). Fuel insufficiency, however, cannot explain the low SFRs in the low mass population, where the fuel for SF is abundant. While HI content is clearly important in moving galaxies along the SFMS, it does not necessarily account for the distance travelled by galaxies above and below it. Since gas rich galaxies can be found below the SFMS, and HI deficient galaxies above it, the efficiency of converting gas into stars is an important quantity to consider.

By colour coding the SFMS with SFE (see Figure 4.7), it becomes clear that the deficit in SF in the low mass gas-rich galaxy population is associated with very inefficient SF, and low sSFRs (see Figure 4.14). This result is in line with Moreno et al. (2021)'s simulations of interacting galaxies, which showed low SFEs to undermine SFRs in galaxies with cold-dense gas reservoirs. Moreno et al. (2021), however, calculate SFE using molecular hydrogen rather than atomic, and thus a direct comparison is not possible. In fact, low SFR galaxies in both the pair and isolated samples all have low SFEs (and sSFRs), implicating SFE as an important pathway to quenching regardless of environment, stellar mass, and gas content. The fact that we see an increased frequency of low SFE galaxies in the pair sample may be the result of merger induced turbulence in the pair sample. Ellison et al. (2018) suggest that post-merger quenching is not the result of gas-exhaustion, but rather the result of increased turbulence impeding efficient SF.

The relationship between HI deficiency and SFE is examined in Figure 4.9, where gas-fraction is additionally encoded as colour. Both samples demonstrate a subtle trend of increasing SFE with increasing deficiency, and decreasing gas fraction, suggesting efficient star formation depletes galaxies of their gas reservoirs. A small population of low SFE, HI deficient galaxies, with depleted gas fractions, perhaps marks a later stage in the cycle in which previous high SFE has depleted gas content, and in turn caused SFE to plummet.

5.3 Concluding statement

Ultimately, this thesis demonstrates that publicly and readily available data in the optical (SDSS), radio (ALFALFA), and mid-infrared (*WISE*), when incorporated into a cohesive multi-wavelength study, has enormous utility in characterizing the nature of our Universe. Using quantities derived from various data sets (e.g. HI deficiency, HI profile asymmetry, galaxy morphology (optical and MIR), and η & Q), we are able to infer potential quenching and accretion events, and postulate the potential mechanisms driving such events. With SKA1-MID we expect our understanding of the various gas-removal and gas-infusing mechanisms driving galaxy evolution in different environments to be significantly upgraded from our current understanding. With greatly improved resolution at low and intermediate redshifts we anticipate direct observational evidence of cold gas accretion, as well as substantial clarification on the role of the various gas removal mechanisms in different galaxy environments. Large volumes of high quality HI data are about to become available out to unprecedented redshifts, which will allow us to extend the analysis outlined in this thesis to large samples of galaxies, and across cosmic time. This thesis provides a road-map for the type of science we can expect to do with

the incoming next-generation data, as well as how to optimize it, to further our understanding of galaxy evolution. While observational data is certainly the backbone of astronomy, in lieu of the ability to conduct traditional scientific experiments, simulations have, and will continue, to provide important context, as well as generate knowledge beyond what can be inferred from observations alone. It is prudent that observational and theoretical astronomers continue to work closely together in their shared pursuit of informed answers to the questions that established the very basis for astronomy in the first place: Where do we come from, and where are we going?

Bibliography

Abadi M. G., Moore B., Bower R. G., 1999, Monthly Notices of the Royal Astronomical Society, 308, 947

Abazajian K. N. et al., 2009, ApJS, 182, 543

Abell G. O., 1958, ApJS, 3, 211

Acosta-Pulido J. A. et al.,, 2015, The Spanish Square Kilometre Array White Book

Argudo-Fernández M. et al., 2013, A&A, 560, A9

Audcent-Ross F. M. et al., 2018, MNRAS, 480, 119

Baldry I. K., Balogh M. L., Bower R., Glazebrook K., Nichol R. C., 2004, in Allen R. E., Nanopoulos D. V., Pope C. N., eds, American Institute of Physics Conference Series Vol. 743, The New Cosmology: Conference on Strings and Cosmology. pp 106–119

Baldwin J. E., Lynden-Bell D., Sancisi R., 1980, MNRAS, 193, 313

Balogh M. L., Baldry I. K., Nichol R., Miller C., Bower R., Glazebrook K., 2004, ApJ, 615, L101

Balogh M. L., Morris S. L., 2000, MNRAS, 318, 703

Balogh M. L., Morris S. L., Yee H. K. C., Carlberg R. G., Ellingson E., 1997, ApJ, 488, L75

Bamford S. P. et al., 2009, MNRAS, 393, 1324

Barnes D. G. et al., 2001, MNRAS, 322, 486

Barnes J. E., 1988, ApJ, 331, 699

Barnes J. E., 1992, ApJ, 393, 484

Barrera-Ballesteros J. K. et al., 2015, A&A, 582, A21

Behroozi P. S., Wechsler R. H., Conroy C., 2013, ApJ, 770, 57

Binney J., Dehnen W., Bertelli G., 2000, MNRAS, 318, 658

Binney J. J., 2000, in Combes F., Mamon G. A., Charmandaris V., eds, Astronomical Society of the Pacific Conference Series Vol. 197, Dynamics of Galaxies: from the Early Universe to the Present. p. 107

Bitsakis T. et al., 2019, MNRAS, 483, 370

Bluck A. F. L., Ellison S. L., Patton D. R., Simard L., Mendel J. T., Teimoorinia H., Moreno J., Starkenburg E., 2014, arXiv e-prints, p. arXiv:1412.3862

Bluck A. F. L. et al., 2016, MNRAS, 462, 2559

Bok J., Blyth S. L., Gilbank D. G., Elson E. C., 2019, MNRAS, 484, 582

Bok J., Skelton R. E., Cluver M. E., Jarrett T. H., Jones M. G., Verdes-Montenegro L., 2020, MNRAS

Borgani S., Kravtsov A., 2011, Advanced Science Letters, 4, 204

Borthakur S., Yun M. S., Verdes-Montenegro L., 2010, ApJ, 710, 385

Boselli A., Fossati M., Gavazzi G., Ciesla L., Buat V., Boissier S., Hughes T. M., 2015, A&A, 579, A102

Bouché N. et al., 2010, The Astrophysical Journal, 718, 1001

Bournaud F., Combes F., Jog C. J., Puerari I., 2005, Astronomy and Astrophysics, 438, 507

Bradford J. D., Geha M. C., Blanton M. R., 2015, ApJ, 809, 146

Brown M. J. I., Jarrett T. H., Cluver M. E., 2014, , 31, e049

Buta R. J. et al., 2019, MNRAS, 488, 2175

Calzetti D., 2013, Star Formation Rate Indicators. p. 419

Calzetti D. et al., 2007, ApJ, 666, 870

Calzetti D. et al., 2010, ApJ, 714, 1256

Cao C. et al., 2016, ApJS, 222, 16

Casasola V., Hunt L., Combes F., Garcia-Burillo S., 2015, VizieR Online Data Catalog, pp J/A+A/577/A135

Catinella B. et al., 2010, Monthly Notices of the Royal Astronomical Society, 403, 683

Chamaraux P., Balkowski C., Gerard E., 1980, A&A, 83, 38

Chung A., van Gorkom J. H., Kenney J. D. P., Crowl H., Vollmer B., 2009, AJ, 138, 1741

Cicone C. et al., 2014, A&A, 562, A21

Cluver M. E. et al., 2011, in American Astronomical Society Meeting Abstracts #218. p. 119.05

Cluver M. E., Jarrett T. H., Dale D. A., Smith J. D. T., August T., Brown M. J. I., 2017, ApJ, 850, 68

Cluver M. E. et al., 2014, ApJ, 782, 90

Cluver M. E. et al., 2020, ApJ, 898, 20

Cochrane R. K., Best P. N., 2018, MNRAS, 480, 864

Conselice C. J., 2003, ApJS, 147, 1

Cook R. H. W., Cortese L., Catinella B., Robotham A., 2019, MNRAS, 490, 4060

Cortese L., Catinella B., Boissier S., Boselli A., Heinis S., 2011, MNRAS, 415, 1797

Cortese L., Catinella B., Smith R., 2021, arXiv e-prints, p. arXiv:2104.02193

Dahari O., 1984, AJ, 89, 966

Davies J. I. et al., 2017, PASP, 129, 044102

de Blok W. J. G. et al.,, 2017, An Overview of the MHONGOOSE Survey: Observing Nearby Galaxies with MeerKAT

De Propris R., Conselice C. J., Liske J., Driver S. P., Patton D. R., Graham A. W., Allen P. D., 2007, ApJ, 666, 212

Dénes H., Kilborn V. A., Koribalski B. S., 2014, MNRAS, 444, 667

Devereux N. A., Young J. S., 1991, ApJ, 371, 515

Dressler A., 1980, ApJ, 236, 351

Durbala A., Sulentic J. W., Buta R., Verdes-Montenegro L., 2008, MNRAS, 390, 881

Elbaz D. et al., 2011, A&A, 533, A119

Ellison S. L., Catinella B., Cortese L., 2018, MNRAS, 478, 3447

Ellison S. L., Patton D. R., Simard L., McConnachie A. W., Baldry I. K., Mendel J. T., 2010, MNRAS, 407, 1514

Elson E. C., Blyth S. L., Baker A. J., 2016, MNRAS, 460, 4366

Espada D., Verdes-Montenegro L., Huchtmeier W. K., Sulentic J., Verley S., Leon S., Sabater J., 2011, A&A, 532, A117

Fernández Lorenzo M., Sulentic J., Verdes-Montenegro L., Argudo-Fernández M., 2013, MNRAS, 434, 325

Fernández Lorenzo M., Sulentic J., Verdes-Montenegro L., Ruiz J. E., Sabater J., Sánchez S., 2012, A&A, 540, A47

Fraternali F., 2017, in Fox A., Davé R., eds, Astrophysics and Space Science Library Vol. 430, Gas Accretion onto Galaxies. p. 323

Fujita Y., Nagashima M., 1999, ApJ, 516, 619

Giavalisco M. et al., 2004, ApJ, 600, L93

Giese N., van der Hulst T., Serra P., Oosterloo T., 2016, MNRAS, 461, 1656

Giovanelli R., Haynes M. P., 1985, ApJ, 292, 404

Giovanelli R. et al., 2005, AJ, 130, 2598

Gunn J. E., Gott J. Richard I., 1972, ApJ, 176, 1

Hani M. H., Sparre M., Ellison S. L., Torrey P., Vogelsberger M., 2018, MNRAS, 475, 1160

Haynes M. P., Giovanelli R., 1984, AJ, 89, 758

Haynes M. P. et al., 2018, ApJ, 861, 49

Haynes M. P. et al., 2011, AJ, 142, 170

Haynes M. P., van Zee L., Hogg D. E., Roberts M. S., Maddalena R. J., 1998, AJ, 115, 62

Hess K. M., Cluver M. E., Yahya S., Leisman L., Serra P., Lucero D. M., Passmoor S. S., Carignan C., 2017, MNRAS, 464, 957

Hess K. M., Wilcots E. M., 2013, AJ, 146, 124

Hibbard J. E., Yun M. S., 1999, AJ, 118, 162

Hickson P., 1982, ApJ, 255, 382

Holwerda B. W., Pirzkal N., de Blok W. J. G., Bouchard A., Blyth S.-L., van der Heyden K. J., 2011, MNRAS, 416, 2437

Hopkins P. F. et al., 2010, ApJ, 715, 202

Inoue A. K., Hirashita H., Kamaya H., 2000, AJ, 120, 2415

Jarrett T. H., Cluver M. E., Brown M. J. I., Dale D. A., Tsai C. W., Masci F., 2019, ApJS, 245, 25

Jarrett T. H. et al., 2011, ApJ, 735, 112

Jarrett T. H., Helou G., Van Buren D., Valjavec E., Condon J. J., 1999, AJ, 118, 2132

Jarrett T. H. et al., 2012, AJ, 144, 68

Jarrett T. H. et al., 2013, AJ, 145, 6

Jog C. J., Combes F., 2009, Physics Reports, 471, 75

Jones M. G. et al., 2018, A&A, 609, A17

Karachentseva V. E., 1973, Astrof. Issledovanija Byu. Spec. Ast. Obs.; Vol. 8; Page 3-49, 8

Kauffmann G. et al., 2003, MNRAS, 341, 33

Kelson D. D., 2014, arXiv e-prints, p. arXiv:1406.5191

Kelvin L. S. et al., 2014, MNRAS, 439, 1245

Kennicutt Robert C. J. et al., 2009, ApJ, 703, 1672

Kessler M. F. et al., 1996, A&A, 500, 493

Kilborn V. A., Forbes D. A., Barnes D. G., Koribalski B. S., Brough S., Kern K., 2009, MNRAS, 400, 1962

Koribalski B., Dickey J. M., 2004, MNRAS, 348, 1255

Koribalski B. S. et al., 2020, Astrophysics and Space Science, 365

Koribalski B. S. et al., 2018, MNRAS, 478, 1611

Kormendy J., Kennicutt Robert C. J., 2004, ARA&A, 42, 603

Kornreich D. A., Haynes M. P., Lovelace R. V. E., van Zee L., 2000, AJ, 120, 139

Kornreich D. A., Lovelace R. V. E., Haynes M. P., 2002, ApJ, 580, 705

Larson R. B., Tinsley B. M., Caldwell C. N., 1980, ApJ, 237, 692

Lee N. et al., 2015, The Astrophysical Journal, 801, 80

Leon S. et al., 2008, A&A, 485, 475

Leroy A. K., Walter F., Brinks E., Bigiel F., de Blok W. J. G., Madore B., Thornley M. D., 2008, AJ, 136, 2782

Lim S. H., Mo H. J., Lu Y., Wang H., Yang X., 2017, MNRAS, 470, 2982

Lisenfeld U. et al., 2007, in Combes F., Palouš J., eds, IAU Symposium Vol. 235, Galaxy Evolution across the Hubble Time. pp 219–219

Liu J., Cen R., 2017, arXiv e-prints, p. arXiv:1701.00866

Lotz J. M., Primack J., Madau P., 2004, AJ, 128, 163

Maddox N. et al., 2021, A&A, 646, A35

Martig M., Bournaud F., Teyssier R., Dekel A., 2009, ApJ, 707, 250

Matthews L. D., van Driel W., Gallagher III J. S., 1998, AJ, 116, 1169

McNamara B. R., Nulsen P. E. J., 2007, ARA&A, 45, 117

McNamara B. R., Wise M. W., David L. P., Nulsen P. E. J., Sarazin C. L., 2000, in AAS/High Energy Astrophysics Division #5. p. 1201

McPartland C., Sanders D. B., Kewley L. J., Leslie S. K., 2018, MNRAS, 482, 129

Mihos J. C., Harding P., Feldmeier J., Morrison H., 2005, ApJ, 631, L41

Mihos J. C., Hernquist L., 1996, ApJ, 464, 641

Moon J.-S., An S.-H., Yoon S.-J., 2019, ApJ, 882, 14

Moore B., Katz N., Lake G., Dressler A., Oemler A., 1995, Nature, Volume 379, Issue 6566, pp. 613-616 (1996)., 379, 613

Moore B., Lake G., Katz N., 1998, ApJ, 495, 139

Moore B., Lake G., Quinn T., Stadel J., 1999, MNRAS, 304, 465

Moreno J. et al., 2020, Monthly Notices of the Royal Astronomical Society

Moreno J. et al., 2021, MNRAS, 503, 3113

Morselli L., Popesso P., Cibinel A., Oesch P. A., Montes M., Atek H., Illingworth G. D., Holden B., 2018, arXiv e-prints

Mundy C. J., Conselice C. J., Duncan K. J., Almaini O., Häußler B., Hartley W. G., 2017, MNRAS, 470, 3507

Naluminsa E., Elson E. C., Jarrett T. H., 2021, MNRAS, 502, 5711

Noeske K. G. et al., 2007, The Astrophysical Journal, 660, L43

Noguchi M., Ishibashi S., 1986, MNRAS, 219, 305

Nulsen P. E. J., 1982, MNRAS, 198, 1007

Obreschkow D., Glazebrook K., Kilborn V., Lutz K., 2016, ApJ, 824, L26

Obreschkow D., Meyer M., 2014, eprint arXiv:1406.0966

Parkash V., Brown M. J. I., Jarrett T. H., Bonne N. J., 2018, ApJ, 864, 40

Patton D. R., Carlberg R. G., Marzke R. O., Pritchet C. J., da Costa L. N., Pellegrini P. S., 2000, ApJ, 536, 153

Patton D. R., Grant J. K., Simard L., Pritchet C. J., Carlberg R. G., Borne K. D., 2005, The Astronomical Journal, 130, 2043

Patton D. R., Pritchet C. J., Yee H. K. C., Carlberg R. G., Ellingson E., 1996, ApJ, 90, 334

Patton D. R., Qamar F. D., Ellison S. L., Bluck A. F. L., Simard L., Mendel J. T., Moreno J., Torrey P., 2016, MNRAS, 461, 2589

Pearson W. J. et al., 2019, arXiv e-prints, p. arXiv:1908.10115

Peng C. Y., Ho L. C., Impey C. D., Rix H.-W., 2010, AJ, 139, 2097

Peng Y., Maiolino R., Cochrane R., 2015, Nature, Volume 521, Issue 7551, pp. 192-195 (2015)., 521, 192

Pilbratt G. L. et al., 2010, A&A, 518, L1

Planck Collaboration et al., 2016, A&A, 594, A1

Popping A., Meyer M., Staveley-Smith L., Obreschkow D., Jozsa G., Pisano D. J., 2015, in Advancing Astrophysics with the Square Kilometre Array (AASKA14). p. 132

Prochaska J. X., Wolfe A. M., 2009, ApJ, 696, 1543

Rasmussen J., Ponman T. J., Verdes-Montenegro L., Yun M. S., Borthakur S., 2008, MNRAS, 388, 1245

Reichard T. A., Heckman T. M., Rudnick G., Brinchmann J., Kauffmann G., 2008, ApJ, 677, 186

Rhee J., 2020, in The Build-Up of Galaxies through Multiple Tracers and Facilities. p. 18

Riccardo Giovanelli and Martha P. Haynes, 1988, Extragalacyic Neutral Hydrogen

Richter O.-G., Sancisi R., 1994, A&A, 290

Rieke G. H., Alonso-Herrero A., Weiner B. J., Pérez-González P. G., Blaylock M., Donley J. L., Marcillac D., 2009, ApJ, 692, 556

Robotham A., Obreschkow D., 2015, Hyper-Fit: Fitting Linear Models to Multidimensional Data with Multivariate Gaussian Uncertainties

Robotham A. S. G. et al., 2014, MNRAS, 444, 3986

Rodighiero G. et al., 2011, ApJ, 739, L40

Sabater J., Leon S., Verdes-Montenegro L., Lisenfeld U., Sulentic J., Verley S., 2008, A&A, 486, 73

Sabater J., Verdes-Montenegro L., Leon S., Sulentic J., Lisenfeld U., Verley S., 2011, in Zapatero Osorio M. R., Gorgas J., Maíz Apellániz J., Pardo J. R., Gil de Paz A., eds, Highlights of Spanish Astrophysics VI. pp 399–399

Saintonge A. et al., 2016, MNRAS, 462, 1749

Sancisi R., Fraternali F., Oosterloo T., van der Hulst T., 2008, , 15, 189

Sanders D. B., Scoville N. Z., Young J. S., Soifer B. T., Schloerb F. P., Rice W. L., Danielson G. E., 1986, ApJ, 305, L45

Schade D., Lilly S. J., Crampton D., Hammer F., Le Fevre O., Tresse L., 1995, ApJ, 451, L1

Schawinski K. et al., 2014, MNRAS, 440, 889

Schiminovich D. et al., 2010, MNRAS, 408, 919

Scholz F. W., Stephens M. A., 1987, Journal of the American Statistical Association, 82, 918

Schreiber C. et al., 2015, A&A, 575, A74

Scott T. C., Brinks E., Cortese L., Boselli A., Bravo-Alfaro H., 2018, MNRAS, 475, 4648

Serra P. et al., 2013, MNRAS, 428, 370

Solanes J. M., Giovanelli R., Haynes M. P., 1996, ApJ, 461, 609

Solanes J. M., Manrique A., García-Gómez C., González-Casado G., Giovanelli R., Haynes M. P., 2001, ApJ, 548, 97

Solomon P. M., Sage L. J., 1988, ApJ, 334, 613

Speagle J. S., Steinhardt C. L., Capak P. L., Silverman J. D., 2014, ApJS, 214, 15

Steinhauser D., Schindler S., Springel V., 2016, Astronomy Astrophysics, 591, A51

Strateva I. et al., 2001, AJ, 122, 1861

Strauss M. A. et al., 2002, AJ, 124, 1810

Sulentic J. W. et al., 2006, A&A, 449, 937

Swaters R. A., Schoenmakers R. H. M., Sancisi R., van Albada T. S., 1999, MNRAS, 304, 330

Tacconi L. J. et al., 2018, ApJ, 853, 179

Tacconi L. J., Genzel R., Tecza M., Gallimore J. F., Downes D., Scoville N. Z., 1999, ApJ, 524, 732

Tacconi L. J. et al., 2013, ApJ, 768, 74

Tifft W. G., Huchtmeier W. K., 1990, , 84, 47

Tinsley B. M., Larson R. B., 1979, MNRAS, 186, 503

Toomre A., 1977, ARA&A, 15, 437

Toribio M. C., Solanes J. M., Giovanelli R., Haynes M. P., Masters K. L., 2011a, ApJ, 732, 92

Toribio M. C., Solanes J. M., Giovanelli R., Haynes M. P., Masters K. L., 2011b, ApJ, 732, 92

Twarog B. A., 1980, ApJ, 242, 242

van der Hulst J. M., van Albada T. S., Sancisi R., 2001, in Hibbard J. E., Rupen M., van Gorkom J. H., eds, Astronomical Society of the Pacific Conference Series Vol. 240, Gas and Galaxy Evolution. p. 451

van Eymeren J., Jütte E., Jog C. J., Stein Y., Dettmar R.-J., 2011, A&A, 530, A30

Verdes-Montenegro L., Sulentic J., Lisenfeld U., Leon S., Espada D., Garcia E., Sabater J., Verley S., 2005, Astronomy and Astrophysics, Volume 436, Issue 2, June III 2005, pp.443-455, 436, 443

Verdes-Montenegro L., Yun M. S., Williams B. A., Huchtmeier W. K., del Olmo A., Perea J., 2001, in Hibbard J. E., Rupen M., van Gorkom J. H., eds, Astronomical Society of the Pacific Conference Series Vol. 240, Gas and Galaxy Evolution. p. 193

Verheijen M., Oosterloo T., Heald G., van Cappellen W., 2009, in Panoramic Radio Astronomy: Wide-field 1-2 GHz Research on Galaxy Evolution. p. 10

Verley S. et al., 2007a, Astronomy and Astrophysics, 472, 121

Verley S. et al., 2007b, Astronomy and Astrophysics, 470, 505

Walter F., Brinks E., de Blok W. J. G., Bigiel F., Kennicutt Robert C. J., Thornley M. D., Leroy A., 2008, AJ, 136, 2563

Wang E., Kong X., Pan Z., 2018, ApJ, 865, 49

Watts A. B., Catinella B., Cortese L., Power C., Ellison S. L., 2021, MNRAS

Watts A. B., Power C., Catinella B., Cortese L., Stevens A. R. H., 2020, MNRAS, 499, 5205

Werner M. W. et al., 2004, ApJS, 154, 1

Westmeier T., Braun R., Koribalski B. S., 2011, MNRAS, 410, 2217

Whitaker K. E. et al., 2015, The Astrophysical Journal, 811, L12

White S. D. M., Rees M. J., 1978, MNRAS, 183, 341

Wilcots E. M., Prescott M. K. M., 2004, AJ, 127, 1900

Wright E. L. et al., 2010, AJ, 140, 1868

Wu H., Cao C., Hao C.-N., Liu F.-S., Wang J.-L., Xia X.-Y., Deng Z.-G., Young C. K.-S., 2005, ApJ, 632, L79

Xu C. K. et al., 2010, in American Astronomical Society Meeting Abstracts #216. p. 307.03

Xu C. K. et al., 2012, ApJ, 760, 72

Yamashita T. et al., 2017, ApJ, 844, 96

Yang X., Mo H. J., van den Bosch F. C., Pasquali A., Li C., Barden M., 2007, ApJ, 671, 153

Young J. S., 1999, ApJ, 514, L87

Young J. S., Schloerb F. P., Kenney J. D., Lord S. D., 1986, ApJ, 304, 443

Zhu Y.-N., Wu H., Cao C., Li H.-N., 2008, ApJ, 686, 155

Zwaan M. A., van der Hulst J. M., Briggs F. H., Verheijen M. A. W., Ryan-Weber E. V., 2005, MNRAS, 364, 1467